Earth-Science Reviews 214 (2021) 103508

Contents lists available at ScienceDirect

Earth-Science Reviews

journal homepage: www.elsevier.com/locate/earscirev

Towards interactive global paleogeographic maps, new reconstructions at 60, 40 and 20 Ma

F. Poblete [a,b,*], G. Dupont-Nivet [a,c], A. Licht [d], D.J.J. van Hinsbergen [e], P. Roperch [a], M. G. Mihalynuk [f], S.T. Johnston [g], F. Guillocheau [a], G. Baby [a], F. Fluteau [h], C. Robin [a], T.J. M. van der Linden [e,i], D. Ruiz [c], M.L.J. Baatsen [j]

[a] Géosciences Rennes, UMR CNRS 6118, Rennes, 35042 Rennes Cedex, France
[b] Departamento de Geología, Facultad de Ciencias Físicas y Matemáticas, Universidad de Chile, Chile
[c] Universität Potsdam, Institute of Geoscience, 14476 Potsdam, Germany
[d] Centre Européen de Recherche et d'Enseignement des Géosciences de l'Environnement (Cerege), UMR CNRS 7330, 13545 Aix-en-Provence, France
[e] Department of Earth Sciences, Utrecht University, Princetonlaan 8a, 3584 CB, Utrecht, the Netherlands
[f] British Columbia Geological Survey, Vancouver, Canada
[g] Department of Earth and Atmospheric Sciences, University of Alberta, Canada
[h] Université de Paris, Institut de physique du globe de Paris, CNRS, F-75005 Paris, France
[i] Thomas van der Linden – LinGeo, Berlin, Germany
[j] IMAU, Utrecht University, Princetonplein 5, 3584CC Utrecht, the Netherlands

ARTICLE INFO

Keywords:
Paleogeographic maps
Paleoelevation
Cenozoic
Eocene-Oligocene transition
Tibetan-Himalayan orogen
paleoclimate

ABSTRACT

Paleogeographic maps are essential tools for understanding Earth system dynamics. They provide boundary conditions for climate and geodynamic modelling, for analysing surface processes and biotic interactions. However, the temporal and spatial distribution of key features such as seaways and mountain belts that govern climate changes and biotic interchange differ between various paleogeographies that require regular updates with new data and models. We developed a reproducible and systematic approach to paleogeographic reconstruction and provide a set of worldwide Cenozoic paleogeographic maps at 60, 40 and 20 Ma. We followed a six-stage methodology that integrates an extensive review of geological data into a coherent plate tectonic model using the open source software GPlates. (1) We generated a global plate kinematic model, and reconstructed intensely-deformed plate boundaries using a review of structural, paleomagnetic and other geologic data in six key regions: the Andes, the North American Cordillera, the Scotia Arc, Africa, the Mediterranean region and the Tibetan-Himalayan collision zone. (2) We modified previously published paleobathymetry in several regions where continental and oceanic crust overlap due to differences in the plate models. (3) We then defined paleoshorelines using updated fossil and geologic databases to locate the terrestrial to marine transition. (4) We applied isostatic compensation in polar regions and global eustatic sea level adjustments. (5) Paleoelevations were estimated using a broad range of data including thermochronology and stable isotopes, combined with paleobotanical (mostly pollen and leaf physiognomy), structural and geomorphological data. We address ongoing controversies on the mechanisms and chronology of India-Asia collision by providing alternate reconstructions for each time slice. We finally discuss the implications of our reconstructions on the Cenozoic evolution of continental weatherability and review methodological limitations and potential improvements. Future addition of new data, tools and reconstructions can be accommodated through a dedicated interactive website tool (https://map.paleoenvironment.eu/) that enables users to interactively upload and download data and compare with other models, and generate their own plots. Our aim is to regularly update the models presented here with new data as they become available.

* Corresponding author at: Departamento de Geología, Universidad de Chile, Plaza Ercilla 803, Santiago Zip code: 8370450, Región Metropolitana, Chile.
E-mail address: ferpoble@uchile.cl (F. Poblete).

https://doi.org/10.1016/j.earscirev.2021.103508
Received 21 May 2020; Received in revised form 30 December 2020; Accepted 4 January 2021
Available online 8 January 2021
0012-8252/© 2021 Elsevier B.V. All rights reserved.

1. Introduction

Paleogeographic reconstructions relay the current understanding of geodynamic and plate tectonic processes that have shaped Earth's surface, influencing global climate and biotic evolution. Plate tectonics control the opening and closure of ocean gateways, modulating the development or decline of ocean currents, influencing water mass and heat transport between the oceans and the heat exchange between the ocean and the atmosphere (e.g. Barker, 2001; Munday et al., 2015; Scher et al., 2015). Collision and rifting generate mountain ranges providing rain-shadows, diverting trade and anti-trade winds, or as elevated temperature source modulating atmospheric circulation cells and monsoons (e.g. Ehlers and Poulsen, 2009; Licht et al., 2017; Si and Ding, 2013; Wheeler et al., 2016). Geodynamic and surface processes also play a fundamental role in the carbon cycle through modulation of CO_2 emissions, through atmospheric CO_2-consuming metamorphic or silicate weathering reactions, or through organic carbon sequestration with delivery of erosional nutrient to marine domains of high primary productivity (e.g. Berner and Kothavala, 2001; Goddéris et al., 2014; Karl and Trenberth, 2003; Larsen et al., 2014; Lasaga et al., 1985; Royer et al., 2004; Stephens et al., 2012; Sternai et al., 2014). In addition, the long-recognized impact of continental break-up, drift and collision on the radiation of species (e.g. Clyde et al., 2003; Dalziel et al., 2013; Wegener, 1929), has, owing to the increasing utilization of phylogenetic approaches, developed more recently into fields of research on understanding of the interplay between biotic evolution, climate and paleogeography (e.g. Lieberman, 2003).

This study focuses on the Cenozoic era for which reconstructing past environmental conditions has become crucial to constrain and calibrate model predictions of future climate and biodiversity changes. Indeed, continuously rising modern CO_2 levels necessitate exploration of deeper time to find analogous conditions and global response to high atmospheric CO_2 concentration scenarios (e.g. Karl and Trenberth, 2003; Lunt et al., 2017; Trenberth et al., 2009). It is critical to test these models by simulating paleoclimates in periods with high CO_2 concentrations (Baatsen et al., 2016; Baatsen et al., 2020) for which paleogeographic maps provide the necessary boundary conditions. The most recent greenhouse period was during Paleocene to Eocene times with 2× to 5× times preindustrial pCO_2 levels (i.e. 560–1400 ppm; Anagnostou et al., 2016; Heureux and Rickaby, 2015). After reaching maximum temperatures during the Early Eocene Climate Optimum (~ 53–52 Ma), gradual cooling from greenhouse to icehouse conditions reached a threshold at the Eocene-Oligocene Transition (EOT, ~34 Ma; Zachos et al., 2001). Earth's climate changed abruptly with dramatic impacts around the globe: ice expansion in Antarctica, increasing aridity of continent interiors, drop in sea surface temperatures at high latitudes, and changes in atmospheric and oceanic circulation (Dupont-Nivet et al., 2007; Liu et al., 2009; Zachos and Kump, 2005).

The causes of the EOT and the longer-term fall into the Icehouse remain debated (e.g. Li and Elderfield, 2013). One explanation for the EOT invokes development of the Antarctic Circumpolar Current (ACC) that isolated the Antarctic Continent. The onset of the ACC is linked to the opening of the Drake Passage and the Tasman seaway during the Eocene, development of the Antarctic ice sheet, drop in CO_2 levels, and changes in ocean circulation (Barker, 2001; Barker and Burrell, 1977; Gill and Bryan, 1971; Kennett et al., 1975; Scher et al., 2015). Alternative models suggest that the EOT is related to diminishing global CO_2 atmospheric concentration during the Eocene, reaching threshold conditions for the development of the full Antarctic ice sheet at the EOT (e.g. DeConto and Pollard, 2003). An uncontested cause of dwindling atmospheric CO_2 during the Eocene remains elusive (e.g. Caves et al., 2016). Increase of continental weathering and denudation associated with global and Tibetan-Himalayan mountain uplift has been proposed (e.g. Hay et al., 2002; Herman et al., 2013; Raymo and Ruddiman, 1992; Schildgen et al., 2018; Shields and Mills, 2017), along with increased terrestrial and marine organic carbon burial due to enhanced runoff and sediment transport into the deep ocean (e.g. France-Lanord and Derry, 1997; Galy et al., 2015; Galy et al., 2007). Other mechanisms include: contribution of arc volcanism to the CO_2 budget (Hoareau et al., 2015; Sternai et al., 2020), weathering of specific volcanic provinces such as ophiolite belts, island arcs (Jagoutz et al., 2016; Macdonald et al., 2019) and large igneous provinces (Kent and Muttoni, 2008; Lefebvre et al., 2013) at low latitudes, or decreasing global oceanic spreading and subduction rates (e.g. Lefebvre et al., 2013; van der Meer et al., 2014). A critical unknown on the long-term CO_2 budget is the respective contribution of weathering of various elevated regions compared to the alteration in lowlands during sediment transport with long residence time (e.g. Lefebvre et al., 2013; Caves-Rugenstein et al., 2019; van der Meer et al., 2014). Orogenesis along the North and South American Cordillera and along the Neo-Tethys subduction zones from the Mediterranean region to SE Asia, has been particularly important in driving Cenozoic climate evolution. To test these mechanisms, reproducible, systematic, and data-informed Cenozoic paleogeographic reconstructions have been essential (Baatsen et al., 2016; Blakey, 2011; Golonka et al., 2006; Herold et al., 2014; Scotese, 2001; Scotese and Golonka, 1997).

Exponential increases in computational power has made atmospheric general circulation models more accessible to the earth science community. Meanwhile, those models have improved, better simulating natural climate complexity, including atmosphere-ocean-sea ice-vegetation coupling, and they can be run at twice the resolution of early model generations. In addition, the variability of data that they can be input has also grown dramatically, including paleogeographic information, making reconstructions fundamentally relevant in the climate model space (Barron and Washington, 1984; DeConto and Pollard, 2003; Frigola et al., 2018; Huber and Sloan, 2001; Otto-Bliesner et al., 2002; Scotese and McKerrow, 1990; Sewall and Sloan, 2006; Sloan and Barron, 1992). Paleogeographic reconstruction involves a comprehensive search for evidence of past elevations, ocean depths, continental locations, ice sheet extents, and vegetation types in a specific time period (Blakey and Ranney, 2017; Scotese and Wright, 2018). These data are integrated to build a singular or suites of global reconstructions that are necessarily limited in the scope of data types and geographic coverage despite huge efforts (e.g. Bice et al., 1998; Fluteau et al., 1999; Hay and Wold, 1998; Markwick and Valdes, 2004; Sewall et al., 2000). It is a time-consuming and technically complex task, requiring both GIS expertise and the collaboration of scientists with specific geological and paleontological knowledge. This knowledge is not easily transferred into paleogeographic maps that need recurrent updates with incorporation of newer data sets. Thus, while climate models rapidly grow more sophisticated, paleogeographic reconstruction updates lag behind.

As part of a large collaborative effort between geologists and climate modellers, we present here a set of worldwide Cenozoic paleo-digital elevation models (paleoDEM) at 60, 40 and 20 Ma, to be used as boundary condition maps for the scientific community. Our paleotopographic reconstruction efforts have focused mainly on the review of geological literature and datasets to describe the evolution of six tectonically active regions during the Cenozoic (Fig. 1): 1) the Andes, 2) the North American Cordillera, 3) the Scotia Arc, 4) the Mediterranean region 5) the Tibetan-Himalayan collision zone, 6) Africa. We specifically account for the paleotopographic evolution of mountain ranges, the evolution of continental margins in response to terrane and microcontinent accretion and land-sea distribution. These three time slices at 60, 40 and 20 Ma aim to cover part of the Cenozoic and include the greenhouse to icehouse transition. They complement well paleogeographic maps published previously (e.g Herold et al., 2014, at 55 Ma; Baatsen et al., 2016, at 38 Ma; Ruiz et al., 2020) allowing for comparison of different interpretations of paletopographies, gateways and land sea distributions depending on various tectonic scenarios of major features such the Indo-Asia collision.

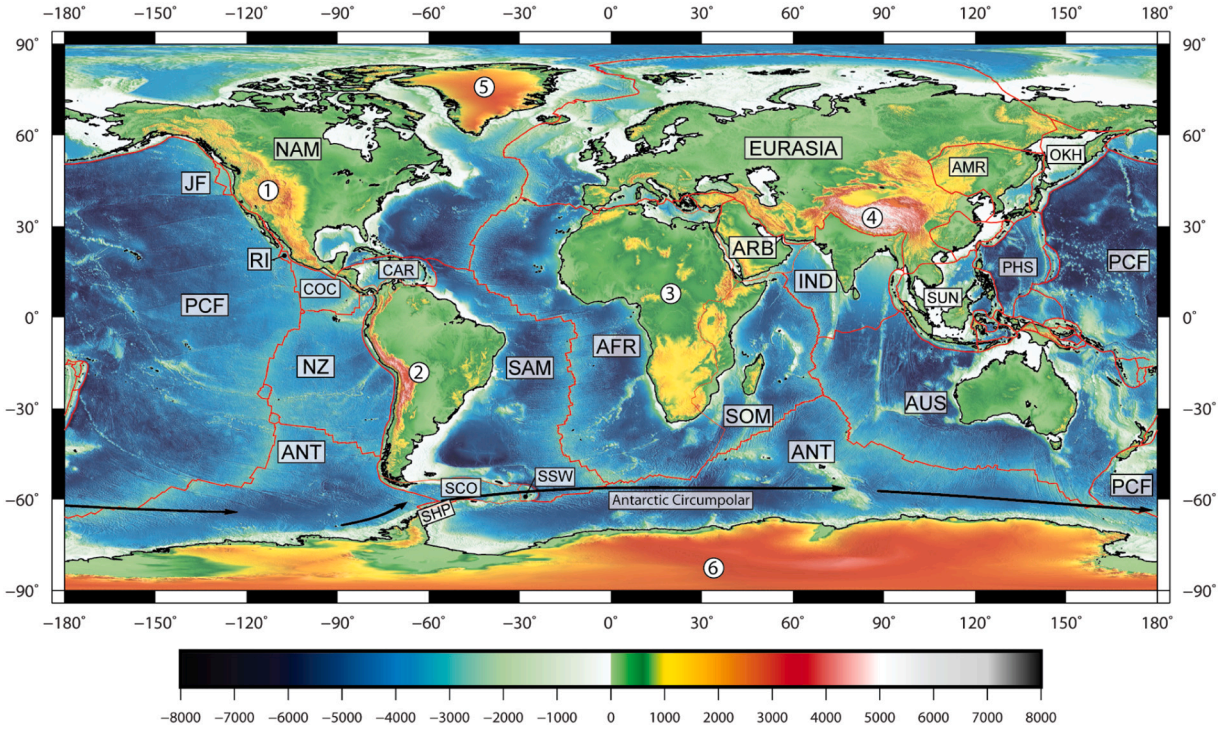

Fig. 1. Physiography of the world. Red lines show the present plate boundaries. Main plates are: AFR, African Plate; ANT, Antarctic Plate; ARB, Arabian Plate; AUS, Australian Plate; AMR, Amur Plate; CAR, Caribbean Plate; COC, Cocos Plate; EURASIA, Eurasian Plate; IND, Indian Plate; JF, Juan de Fuca Plate; NAM, North American Plate; NZ, Nazca Plate; OKH, Okhotsk Plate; PCF, Pacific Plate; PHS, Philippines Sea Plate; RI, Rivera Plate; SAM, South American Plate; SCO, Scotia Plate; SHP, South Shetland Plate; SOM, Somalian Plate; SSW, South Sandwich Plate; SUN, Sunda Plate. 1, North American Cordillera; 2, The Andes Cordillera; 3, African Topography; 4, Tibetan-Himalayan Orogen; 4–5, Greenland and Antarctic ice sheet (Modified from Bird, 2003). (For interpretation of the references to colour in this figure legend, the reader is referred to the web version of this article.)

2. Methodology

Paleogeographic reconstruction requires integration of paleobathymetric, paleotopographic, and paleoshoreline data into a coherent and self-consistent plate tectonic model. We based our method essentially on that described by Baatsen et al., (2016) with some modifications, notably the integration of new kinematic and geological data sets.

Integration of disparate datasets was achieved using a combination of the Generic Mapping Tools (GMT) software (Wessel et al., 2013) to generate and modify paleobathymetric, paleotopographic, and paleoshoreline elements, and the open source software GPlates (www.GPlates.org; Boyden et al., 2011) to move these elements using an internally consistent plate rotation model. We also used a GIS software (such as QGIS or Global Mapper) as a bridge between GMT and GPlates, and for the creation of polygonal overlays (masks) for the manipulation of spatial databases. GMT provides a multiplatform open source collection of several tools that allow performing mathematical operations between raster grids, the interaction between vector masks and raster grid files, and several interpolation algorithms among other functions. GMT allowed generating and manipulating Network Common Data Format (netCDF) or similar file types for climate models requiring globally gridded elevation data (Herold et al., 2014). In the following subsections, we explain the successive steps that we undertook to develop our paleogeographic maps, following four key elements: (1) the plate tectonic model; (2) the paleobathymetry of the ocean crust; (3) paleoshorelines, and (4) the paleotopography (see also supplementary data).

2.1. Plate tectonic model

The fundamental framework of any paleogeographic map is the plate tectonic model that provides: (1) the kinematic model that describes relative motions between various tectonic blocks expressed as rotation parameters (latitude, longitude, angle); and (2) the global reference frame for the plate circuit that can be either based on paleomagnetic data assuming a geocentric axial dipole (for paleoclimatic or biological purposes) or based on hotspot tracks assuming a fixed hotspot assumption or moving mantle (for geodynamic purposes; Boyden et al., 2011; van Hinsbergen et al., 2015b). In our reconstructions using GPlates, rotations of tectonic plates are expressed relative to South Africa so that changing global reference frames can be accomplished by simply changing the motion of South Africa (Torsvik et al., 2008) with respect to the preferred global reference frame. We use the paleomagnetic reference frame from Torsvik et al. (2012) although growing evidence suggests that this reference frame may be less robust for the Eocene than for the Paleocene time (Westerweel et al., 2019).

As per Baatsen et al. (2016), the global plate rotation model provided by Seton et al., (2012) is used as a first-order reconstruction of the main plates. We then modified this original model by integrating with GPlates a selection of previously published regional plate models providing detailed reconstructions of various orogenic zones (Fig. 2) including the Andes and the Caribbean (a, b and c in Fig. 2i, Arriagada et al., 2008, 2013; Boschman et al., 2014; Eagles and Jokat, 2014; Poblete et al., 2011, 2014, 2016; Schepers et al., 2017), the North American Cordillera (d, and e in Fig. 2i, Henderson et al., 2014; McQuarrie and Wernicke, 2005), the Mediterranean and Anatolia (f in Fig. 2i, Gürer and Van Hinsbergen, 2019; van Hinsbergen et al., 2020; van Hinsbergen et al., 2014; van Hinsbergen and Schmid, 2012), the Arabia-Eurasia and Tibetan-Himalayan collision zones (g, h in Fig. 2.i, McQuarrie and van Hinsbergen, 2013; van Hinsbergen et al., 2019), and finally the Banda Arc zone (I in Fig. 2.i, Spakman and Hall, 2010; Tate et al., 2015, 2017). The combination of these models is referred to as the "Poblete rotation model" which extends back to 60 Ma and is provided in the supplementary data. In the N, NW, and SW Pacific regions we used the original plate model of Seton et al. (2012) without incorporating more recent

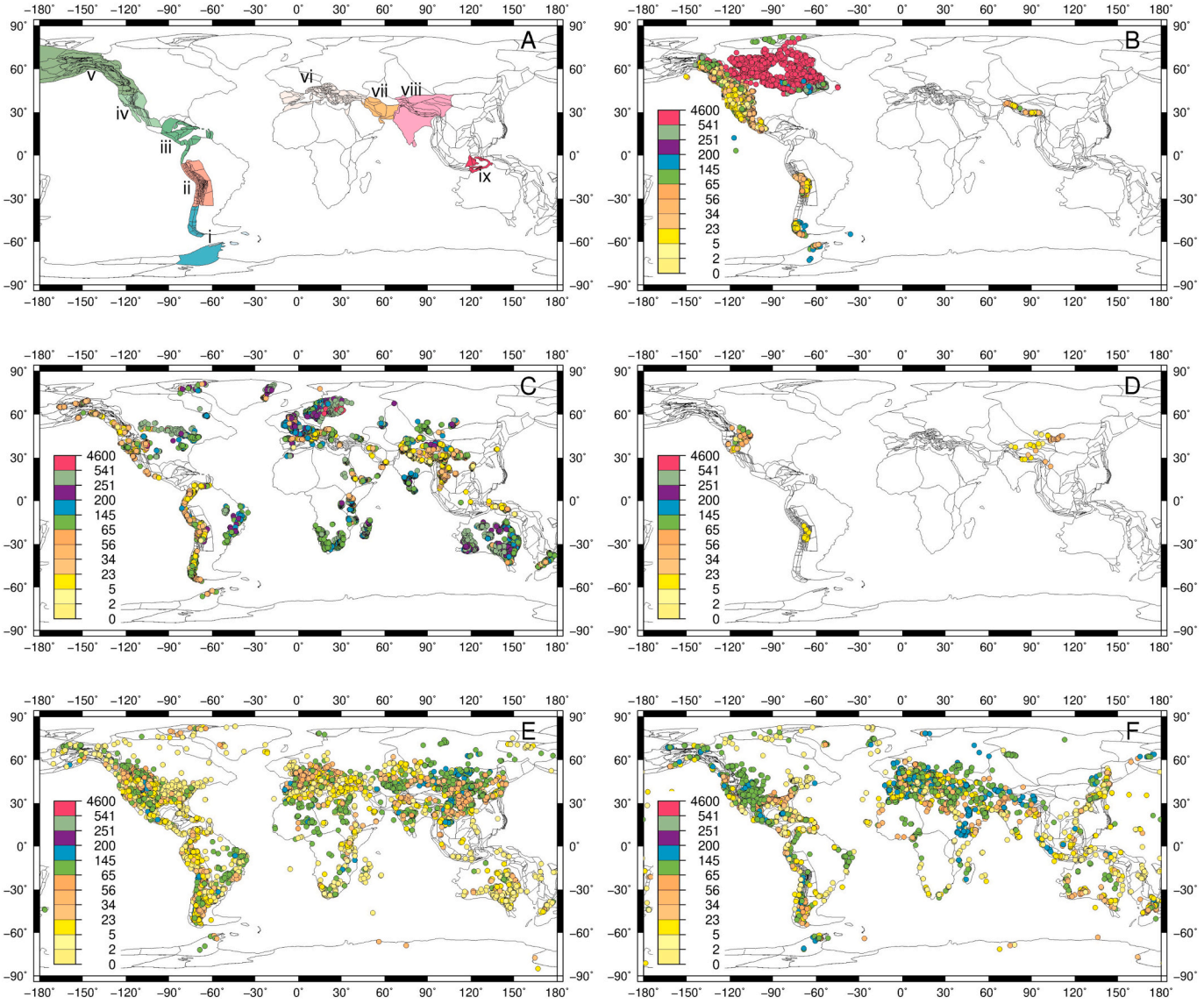

Fig. 2. Compilation of the different tectonic models and entire database integrated in GPlates. A) Compilation of tectonic models used in our reconstructions. i-ix are the location of the tectonic models (see section II.1 "Plate tectonic models" for more information). B) K/Ar, $^{39}Ar/^{40}Ar$ and U—Pb Geochronology compilation of magmatic rocks (Breitsprecher and Mortensen, 2004; Chapman and Kapp, 2017; Trumbull et al., 2006; http://www.navdat.org, Hervé et al., 2007, among others); the vertical colour scale is of time in Ma. C) Compilation of thermochronological data (Herman et al., 2013; this study). D) Paleoelevation compilation (Botsyun et al., 2016; Chamberlain et al., 2012; this study). E) and F) terrestrial and marine fossil database (www.paleobiodb.org, time span of data 160–0 Ma).

modifications addressing the complex subduction and deformation histories of the area, including the accretion of several terranes which are not depicted in our reconstructions (Domeier et al., 2017; Vaes et al., 2019; Van de Lagemaat et al., 2018).

Small continental blocks in orogenic regions are often depicted using polylines instead of polygons in previous reconstructions using GPlates, which simplifies changing their shape through time; or topological lines (Gurnis et al., 2018) which can be used to show lithospheric deformation parameters. A polygon overlay is the standard method used to "cut" raster topography in the process of creating paleotopography (see "Paleotopography" below). Müller et al. (2019) presented a global plate model where plate deformation is explicitly shown; however, this model cannot be used as a starting point for our approach because the deformed area is not constrained by static polygons and the topography cannot be cut and restored to past positions. We therefore created, for each considered age step, static polygon shapes that match as much as possible the lines in the original tectonic models and derived rotations for each of these static polygons using GPlates. For example, in the Basin and Range we developed a simplified version of McQuarrie and Wernicke (2005) while in the Central Andes we used the tectonic model of Arriagada et al. (2008).

2.2. Paleobathymetry

To reconstruct the paleobathymetry we used the digital grids provided by Müller et al. (2008a) and available at http://www.earthbyte.org. These files are ASCII files in 1 Myr intervals and in the format of longitude, latitude, age, depth-to-basement and bathymetry. We extracted the paleobathymetry column from the original file in Müller et al. (2008a) and converted the ASCII file into a netCDF grid with a resolution of 6 min (GMT command xyz2grd). Combining the paleobathymetry reconstructions of Müller et al. (2008a) with our deformed continental polygons generated some overlaps. We erased these overlaps by cutting the paleobathymetry using a mask of the continental ocean boundaries (COBs, Seton et al., 2012), which correspond to the limit between the continental and oceanic crust. In the particular case of the

Greater Indian Basin (van Hinsbergen et al., 2012) we use the general depth-age relationship (Baatsen et al., 2016) to convert a set of created isochrons, by considering symmetric spreading between 120 and 60 Ma, into paleobathymetry; in the case of the Neo-Tethys we represented microcontinental blocks as submerged plateaus shown by the tectonic models (see sections IV to VI). We have also combined our paleotopographies at 60, 40 and 20 Ma, with the recently published paleobathymetry from Straume et al. (2020) (see supplementary data).

2.3. Paleoshoreline

Defining paleoshoreline maps is a crucial step in the construction of paleogeographic maps. Previous compilations (e.g. Heine et al., 2015), produced a set of Cretaceous and Cenozoic paleoshoreline maps from the two global paleogeographic atlases of Smith et al. (2004) and Golonka et al. (2006). We used the paleoshoreline maps from Golonka et al. (2006), based on their better global consistency as noted by Heine et al. (2015). Heine et al. (2015) provided each atlas as a shapefile in present day coordinates. In order to restore the paleoshoreline through time we have integrated these paleoshorelines in GPlates by dividing the shorelines into polygons, following the tectonic blocks defined in our plate tectonic model. At each time slice, we have then modified these paleoshorelines according to marine vs. terrestrial fossil data reported from www.paleobiodb.org. In some of the reconstructed regions, we have further constrained paleoshorelines, by comparing it with depositional environments (i.e. marine vs. terrestrial sediments) of the age at the time of the reconstruction provided by regional geological maps (e.g. Akhmetiev, 2007; Barrier et al., 2018; Caminos and González, 1997; Dercourt et al., 2000; Gómez et al., 2015; Kaya et al., 2019; Olivero and Malumián, 2008; Scotese et al., 1988; Sempere et al., 1997; SERNAGEOMIN, 2003; Slattery et al., 2015; Swezey, 2009; Thiéblemont et al., 2016). Note that large lakes are not taken into account in our reconstructions. Resulting updated paleoshorelines are available in the supplementary data.

2.4. Paleotopography

2.4.1. Datasets

Paleotopographic datasets were integrated in GPlates (Fig. 2ii, iii, iv, v, vi; supplementary data) and include quantitative (stable isotopic, paleobotanical) and qualitative (thermochronologic, geochronologic, and geologic) data.

Analysis of stable oxygen isotope ratios in paleosols can be used to quantitatively estimate past elevation changes (e.g. Poage and Chamberlain, 2002; Quade et al., 2015; Rowley et al., 2001). Stable isotope paleoaltimetry is a mature technique based on the fractionation of oxygen isotopes in an air-cell with elevation gain (Botsyun et al., 2016; Rowley and Garzione, 2007). Here we supplement such paleoaltimetry with estimates based on paleoflora and palynological data. Biotic paleoaltimetry relies on identifying past elevation and temperature based on nearest living relatives, or on paleoenvironmental data obtained from fossil plant physiognomy (Gregory-Wodzicki, 2000; Hoorn et al., 2012; Spicer, 2018; Utescher et al., 2014). The accuracy of these approaches varies depending on the orogen and are discussed for each region in Part III.

Quantitative thermochronologic methods record the thermal evolution of rocks based on estimating the time elapsed since the rock cooled below the closure temperature of various radio-isotopic systems (Lisker et al., 2009; Peyton and Carrapa, 2013; Reiners and Brandon, 2006). At a given geothermal gradient, temperatures are then converted to depth such that the age and rate of exhumation of a rock (rock uplift) through the closure temperature can be estimated. Thermochronology does directly not constrain surface paleoelevation; however, its integration with geomorphological and structural data (for example, with the extent of planation surfaces and tectonic activity) can be used to qualitatively estimate surface paleoelevations (e.g Carrapa and DeCelles, 2015; Japsen et al., 2012a; Rohrmann et al., 2012). We relied mostly on the database compiled by Herman et al. (2013) with additional thermochronological studies in various regions. When possible, we sought additional geomorphic information through inspection of the original publications and/or in additional references to better constrain paleoelevation estimates. Finally, we used an extensive compilation of geochronological data of igneous rocks that do not provide direct paleoelevation estimates but cover wide regions with no paleotopographic information. When associated with petrological and structural data, this compilation allowed us to reconstruct the location and magmatic style of past volcanic arcs, for which we made inferences on the elevation based on modern analogues. For example, geochronological and isotopic data from igneous rocks in southern Lhasa (Wen et al., 2008; Zhu et al., 2011) and Central Andes (Haschke et al., 2006) indicate the presence of a narrow and rectilinear Andean-type arc during late Cretaceous-Paleogene times. As there is no paleoaltimetry data for these two arcs, we attributed them paleoelevation similar to modern Andean-type arcs (with values around 500 to 2500 m) taking into account the tectonic setting and paleoelevation evolution.

2.4.2. Isostatic compensation in polar regions and global eustatic sea level adjustments

We considered a simplified model in which the topography at the poles only depends on the presence, extent, and thickness of ice sheets and their associated isostatic effects. We first created a modified modern topography for Greenhouse conditions (without ice-sheet; 60 and 40 Ma) by compensating isostatically the loss of the ice masses in Greenland, as done in Baatsen et al. (2016). Several recent studies have shown that additional vertical motion is induced on the margins of Greenland when glacial erosion is considered (Medvedev et al., 2018; Straume et al., 2020). The free-ice isostatic compensation used here should thus be considered as a first order approach of Greenland's paleotopography (a combination of our paleotopography at 60 Ma and 40 Ma, with the recent published Greenland paleotopography from Straume et al. (2020) can be found in the supplementary data). To obtain the topography for Icehouse conditions in Antarctica (with ice-sheets; 20 Ma), we used the same ice thickness as today, although we allowed the areal extension of the ice-sheets to vary (see section IV.3.1). The chronology of ice-sheet development in Greenland is debated (Bernard et al., 2016; Coxall et al., 2005; DeConto et al., 2008; Lear et al., 2008; Liu et al., 2009); we thus model no Greenland ice at 60 and 40 Ma and an ice sheet similar to today at 20 Ma.

Finally, we adjusted the topography for sea level changes using the eustatic sea-level curve of Müller et al. (2008b) so that the past topographies are given with respect to paleo-sea levels: +94.7 m at 60 Ma., +73.3 m at 40 Ma and + 65.7 m at 20 Ma.

2.4.3. Topographic modifications

The next step was to reconstruct topographic data from their modern location to their paleogeographic location at a given age. This was achieved using GPlates to cut the modern topography using the polygons of tectonic blocks (as defined in section II.1 and Fig. 2A) and rotate these blocks including their topography at the desired time and position. Then, we exported this data into a netCDF file.

The following steps were applied to modify the topography of all regions and are illustrated in fig. 3 for South America. (A) The first step was to create a mask with "1" values inside the COB (the boundary between the oceanic and continental crust, Seton et la., 2012) and "NaN" values outside those limits, such that multiplying or dividing topographic values of any map with the mask values only yields values for locations within the COB. (B) We then used a surface interpolation implemented in GMT (Fig. 3B, "blockmean" and "surface" commands in GMT) to correct the gaps that arose from restoring shortening between individual polygons. (C) Then, we separated land and sea regions by creating a mask using paleoshorelines modified with updated fossil and geological data (blue line in Fig. 3C), which resulted in two areas, one

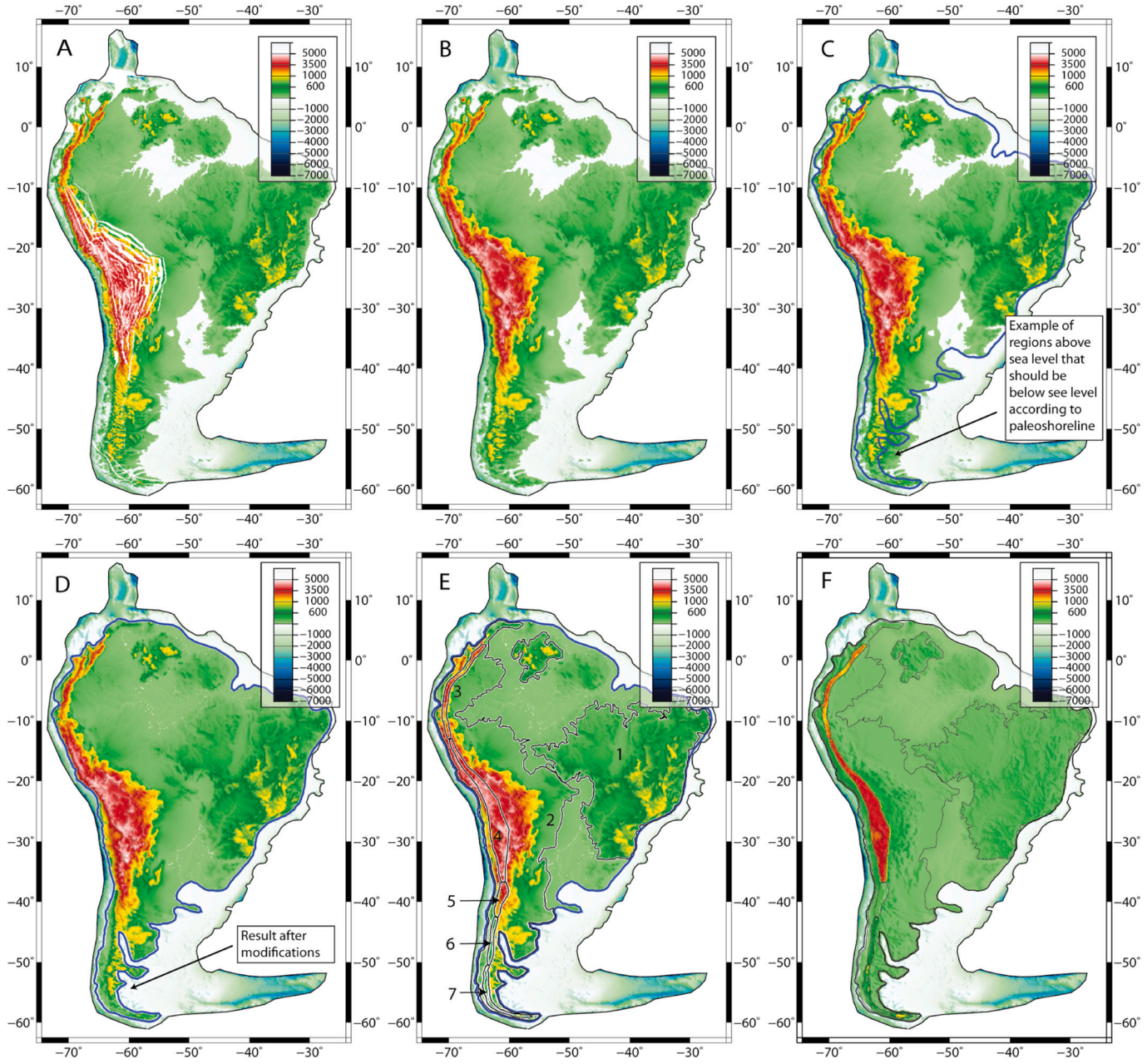

Fig. 3. Procedure for the topographic modification. (A) reconstructed South America at 40 Ma, black line denoted the COB; (B) resulting topography after fillings gaps; (C—D) first transformations in regions located seaward and landward of the paleoshoreline (blue thick line); E) highlight individual masks (1–7) used to reconstruct the paleotopography; (F) final result. For more details, see text and supplementary data. (For interpretation of the references to colour in this figure legend, the reader is referred to the web version of this article.)

that should be below sea level and one that should be above sea level (Fig. 3C). All emerged regions located seaward of the paleoshoreline (Fig. 3C) were transformed to end up below sea level using a linear equation defined by the initial minimum and maximum altitude (Zmin and Zmax) of these areas (obtained by using the 'grdinfo' command in GMT) and the final minimum and maximum altitude (Z'min and Z'max) defined by the user (see next step). Z values that were already below sea level are not modified. We used the same procedure for the region landward the paleoshoreline. We obtained a paleotopography in which all the values seaward/landward the paleoshoreline are below/above sea level, but with no major changes in the topography (Fig. 3D). (D) The next step was to modify the values above sea level according to geological constraints. To do that we first defined a set of masks in areas that were required to be modified with respect to the present day topography (Fig. 3E, numbers 1 to 7). It is important to notice that the mask covered a much wider area than the data used to constrain paleoaltimetry, and in such masked areas there is a high degree of uncertainty (see section IV.2 for a discussion). To modify the topography over each region, we interpolated linearly between the initial minimum and maximum altitude (Z min and Zmax) and the final altitudes (Z'max and Z'min), defined by our review of paleotopographic datasets, resulting in a linear equation in the form

$$Z' = f(Z) = A + m^{*}Z$$

in which Z represents any initial altitude value in the selected region and $Z'$is the final altitude at that point. m is defined by (Z'max-Z'min) / (Zmax-Zmin) and A by solving the equation for$Z$max and Z'max (or Zmin and Z'min).

2.4.4. Final blend and change of reference frame

As stated above, our reconstructions are based on the rotation file of Seton et al. (2012) which uses the moving Indo-Atlantic hotspot reference frame of O'Neill et al. (2005) as an absolute reference frame. Various global mantle reference frames (e.g. Doubrovine et al., 2012; Torsvik et al., 2008; van der Meer et al., 2010) as well as paleomagnetic reference frames (e.g. Besse and Courtillot, 2002; Kent and Irving, 2010; Torsvik et al., 2012) are available and users may want to switch between frames. For instance, a paleomagnetic reference frame is appropriate for climate reconstructions since it includes true polar wander (Torsvik et al., 2012; van Hinsbergen et al., 2015a, 2015b). Switching between frames (Boyden et al., 2011; van Hinsbergen et al., 2015a, 2015b) is straightforward, since our GPlates reconstructions are all relative to southern Africa and changing the global reconstruction between frames only requires application of a global reference frame correction using the GMT command "grdrotation" (see supplementary data).

3. Paleogeographic reconstructions at 60, 40 and 20 Ma

We focused our work on the main cordilleras, critical zones for paleoclimate models. Other areas received less attention: Australia, Southeast Asia, the western Pacific rim, the Caribbean region, the Mediterranean region, and the NW Pacific and Aleutian basin. For these regions, we used recent tectonic models that were corrected for the paleoshorelines, but the regional paleotopography is mostly based on modern topography (see supplementary data for major data sources and masks used at each reconstruction time). Cenozoic paleogeographic history is marked by the formation of three main orogens: the Himalayan-Alpine system along the Eurasian Plate, and the Andes and the North American Cordillera along the western margins of the americas. The Tibetan-Himalayan orogen and the Central Andes now include the highest plateaus on Earth, with elevations reaching more than 4000 m (Fig. 1). The Cenozoic also witnessed several episodes of oceanic gateway opening and closure, which exerted a major control on oceanic currents (Barker, 2001; Straume et al., 2020; Ladant et al., 2014, 2020). In particular, the connection between the Atlantic, Pacific and Indian parts of the Southern Ocean, through the Drake Passage (across the Scotia Arc) and the Tasman Gateway, allowed the development of the Antarctic Circumpolar and Subpolar currents (e.g. Barker and Thomas, 2004; Ladant et al., 2014; Lagabrielle et al., 2009; Scher et al., 2015; Williams et al., 2019). The formation of other gateways and straits had an important impact on past global climate, such as the Panama, Bering and Turgai Straits, and the Indonesian passage (Akhmetiev et al., 2012; Ladant et a., 2014; 2020; Lunt et al., 2008; Montes et al., 2015; Straume et al., 2020). We integrated these changes in a set of paleo Digital Elevation Models (DEMs) at 60, 40 and 20 Ma. These paleoDEMs (see supplementary data) are presented in three different reference frames: a paleomagnetic reference frame (Fig. 4, 5 and 6; Torsvik et al., 2012), a moving Atlantic hotspot (O'Neill et al., 2005), and a global moving hotspot reference frame (GMHRF, Doubrovine et al., 2012), as appropriate for paleoclimate or geodynamic studies respectively (van Hinsbergen et al., 2015a, 2015b). In the following sections, we review and discuss the tectonic setting of selected regions that underwent changes in the Cenozoic widely perceived as critical for global climate. We focused sequentially at 60 Ma, 40 Ma and 20 Ma on the Andes and the Scotia Arc, the Western North American Cordillera, the African and Brazilian shields and the Tibetan-Himalayan orogeny in which we developed different paleogeographies taking into account different models. We also explain how we dealt with ice caps on Antarctic and Greenland and we review the main modifications of paleoshorelines.

3.1. South America

South American Cenozoic tectonics are dominated by the build-up of the Andean cordillera in contrast with the limited evolution of the Brazilian shield. The Andean Cordillera can be followed uninterruptedly

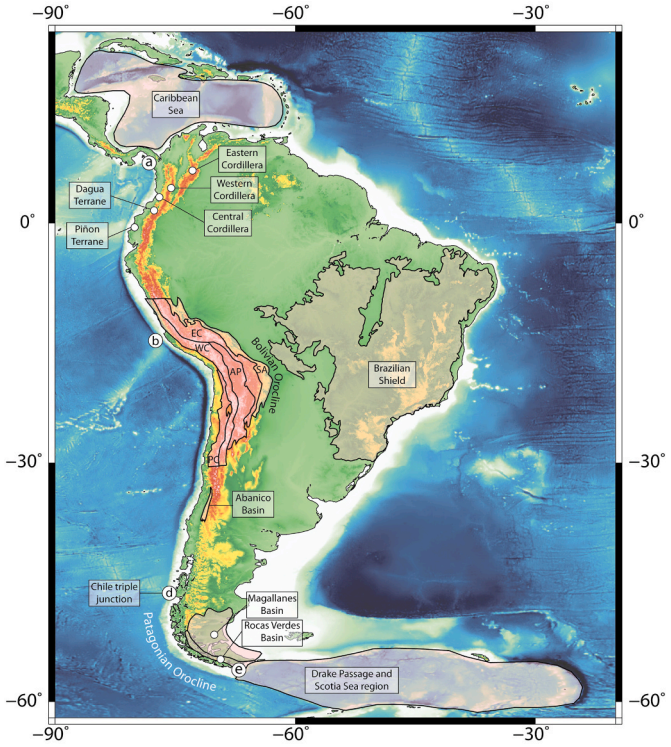

Fig. 4. Physiography of South America. a-b, Northern Andes segment; b-c Central Andes segment; c-d Southern Andes segment; d-e Austral Andes segment. PC, Precordillera; WC, Western Cordillera; AP, Altiplano Puna; EC, Eastern Cordillera; SA: Sub Andes. (Modified from Mpodozis et al., 2005; Poblete et al., 2016; Tassara and Yáñez, 2003;).

from the Caribbean Sea to the Drake Passage, where the Scotia Arc marks the consumptive plate boundary between southernmost Andes and the northern tip of the Antarctic Peninsula (Fig. 4, Dalziel et al., 2013). On a continental scale, the most outstanding feature of the Andean Cordillera are changes in its orientation that define the Bolivian and the Patagonian oroclines (Fig. 4, Arriagada et al., 2008; Carey, 1958; Isacks, 1988; Poblete et al., 2014; Rapalini, 2007). The Nazca Plate subducts beneath the western margin of central South America along most of its length. Along its northern margin, the South American Plate is juxtaposed with the Caribbean Plate (north) along a contact dominated by strike-slip and reverse faulting (Meschede and Frisch, 1998; Müller et al., 1999; Pindell and Dewey, 1982; Pindell and Kennan, 2001). Offshore of southern Chile, the Chile triple junction (Fig. 4) marks the northernmost point of the Antarctic Plate, where it subducts below Patagonian. From the Strait of Magellan, southmost Chile, to the Antarctic Peninsula, the Antarctic Plate is in contact with the Scotia Plate along both convergent and transform plate boundaries.

3.1.1. South America 60 Ma

From Peru to Colombia, the northwestern Andes include a collage of accreted terranes. For example, the Dagua and Piñon Terranes (Fig. 4), are thought to be pieces of an oceanic plateau, the Caribbean Large Igneous Province (CLIP), which collided in the Late Cretaceous (Pindell and Kennan, 2009; Ramos, 2009; Roperch et al., 1987; Villagómez and Spikings, 2013). Uplift and exhumation of the continental margin is attributed to this accretionary event (Villagómez and Spikings, 2013). In the Central Andes, shortening, basin inversion, and normal convergence have been documented during the Late Cretaceous-early Paleocene (Amilibia et al., 2008; Charrier et al., 2013; Henríquez et al., 2018; Herrera et al., 2017; Martínez et al., 2020, 2013; Sempere et al., 1997). This pulse of deformation was accompanied by calc-alkaline magmatism, suggestive of subduction-related arc petrogenesis (Trumbull et al.,

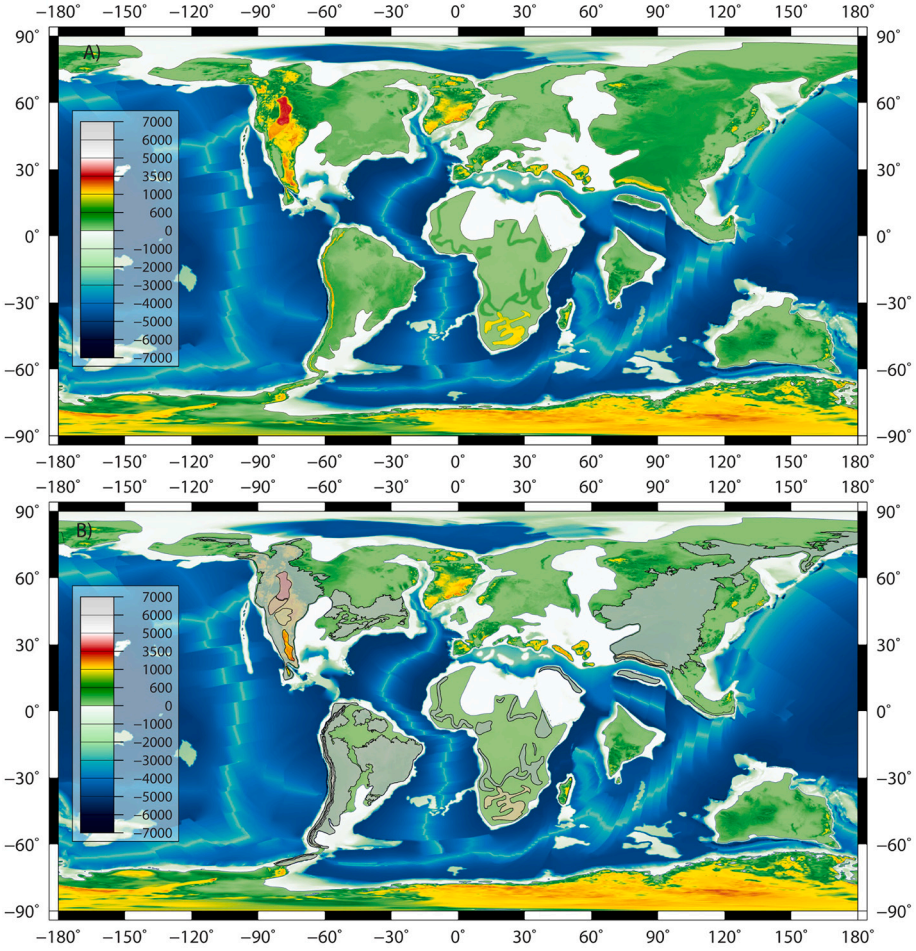

Fig. 5. (A) Paleogeographic reconstruction at 60 Ma. (B) Shaded regions show the location of modified regions (for more details see supplementary data).

2006). Both deformation and calc-alkaline magmatism were focused in the Precordillera and Western Cordillera (Fig. 4), and only began to migrate to the east during the Eocene (Canavan et al., 2014; Carrapa and DeCelles, 2015; Garzione et al., 2014; Leier et al., 2013; Quade et al., 2015; Trumbull et al., 2006). Tectonic restoration of the Bolivian Orocline suggests that its construction began during the middle Eocene and the margin was more linear before that time (Arriagada et al., 2008; Eichelberger and McQuarrie, 2015; Roperch et al., 2006; Schepers et al., 2017). In the Southern Andes, low temperature thermochronology and field observations show that orogenic growth, associated with slab shallowing and arc migration, occurred between 100 and 60 Ma (Echaurren et al., 2016; Folguera et al., 2015). Further South, in the Fuegian Andes, closure of the Rocas Verdes Basin during the Cretaceous has been related to differential shortening and bending due to rigid block rotation around a vertical axis (Betka et al., 2015; Cunningham et al., 1991; Dalziel et al., 1973; Poblete et al., 2014, 2016; Rapalini et al., 2016). The closure of the Rocas Verdes Basin resulted in the collision of the Patagonian batholith against South America with the Río Chico Arch acting as a buttress (Calderón et al., 2012, 2007; Klepeis et al., 2010; Poblete et al., 2016; Torres Carbonell et al., 2016, 2014; Torres Carbonell and Olivero, 2019; Torres García et al., 2020) and in the thickening of the crust of Cordillera Darwin on the north western Scotia plate (Klepeis et al., 2010). In particular, deformation in the Cordillera Darwin was accompanied by denudation and uplift during Late Cretaceous-Early Paleocene (Gombosi et al., 2009; Kohn et al., 1993; Maloney et al., 2011; Nelson, 1982), creating a barrier that acted as a drainage divided since the Late Cretaceous (Barbeau et al., 2009). There are no direct paleoelevation constraints in the Andes for the Late Cretaceous-Early Cenozoic, but evidence for shortening and calc-alkaline magmatism (Bruce et al., 1991; Hervé et al., 2007) is consistent with the presence of a rectilinear volcanic-dominated mountain range along the Pacific subduction margin, although probably narrower and lower than the modern Cordillera. Based on these considerations, we modeled paleoaltitudes at 2000 m for the northern and central Andes that decreased to the south, except in Cordillera Darwin where we suggest that it already formed a topographic high at that time, with a proposed elevation of 2000 m (Fig. 5).

For the Brazilian shield, thermochronological studies in different sectors of the Atlantic coast concluded that its current relief is the results of a series of cooling phases that took place between the Upper Cretaceous and late Neogene (e.g. Cogné et al., 2012, 2011; Japsen et al., 2012a; Karl et al., 2013). These studies suggest the eastern South American margin stood at altitudes not higher than 400 m, instead of 1000 m or higher as it is today in some areas. We thus used maximum altitudes of ~400 m, unchanged for our 60, 40, and 20 Ma reconstructions.

For paleoshorelines, an epicontinental sea incursion along the eastern edge of the Andes is indicated by geological and fossil data from 84 to 60 Ma (Sempere et al., 1997) but after 60 Ma that sea retreated from the northern part of South America (Gómez et al., 2015; Malumián and Ramos, 1984; Sempere et al., 1997). We have chosen to modify the paleoshoreline from Golonka et al. (2006) in the northern part of South America by eliminating the sea reentrant in the western Amazonas that was mostly gone by 60 Ma. In the area of the Scotia Arc region, we have adapted the paleoshorelines presented by Eagles and Jokat (2014).

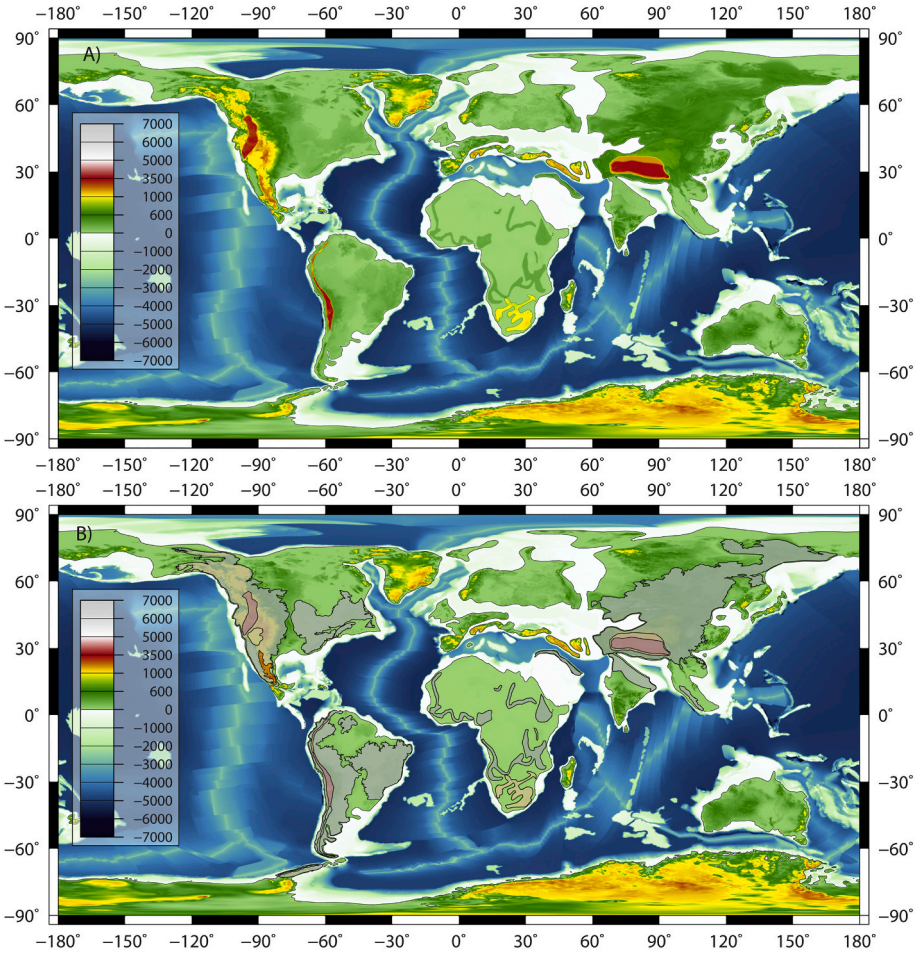

Fig. 6. (A) Paleogeographic reconstruction at 40 Ma. (B) Shaded regions show the location of modified regions (for more details see supplementary data).

3.1.2. South America 40 Ma

Thermochronological data indicates a second pulse of uplift in the middle Eocene which led to the onset of growth of the Western-Central Cordillera system (Villagómez and Spikings, 2013). This exhumation event is also recognized in the Ecuadorian Cordillera between 45 and 30 Ma (Spikings et al., 2010) and in the central Andes, where heterogeneous uplift gave rise to high altitudes in the Precordillera and Western Cordillera before 50 Ma and in the Puna Plateau by 35 Ma (Carrapa and DeCelles, 2015). Uplift is synchronous with shortening and basin inversion during the Incaic phase of the Andean orogeny (Charrier et al., 2009) and with the beginning of the rotation in the Bolivian Orocline (Arriagada et al., 2008). In the southern Central Andes, extension related to the Abanico Basin (Fig. 4) began by 40 Ma, suggesting that this region had a low elevation (Charrier et al., 2007). Further south, similar extension along the eastern side of the Cordillera is attributed to slab roll-back (Echaurren et al., 2016). In the Fuegian Andes, however, internal thickening and exhumation (Betka et al., 2015; Fosdick et al., 2011; Klepeis et al., 2010) indicates that shortening and contraction continued throughout the Eocene. Geochronological compilation of igneous rocks in the Central Andes (Trumbull et al., 2006) shows that the region was a magmatically active volcanic arc (Pindell and Tabbutt, 1995).

Paleoelevation data in the Cordillera are restricted to the Central Andes (Fig. 2D and supplementary data). There are, however, conflicting interpretations of these datasets, with two contrasting models. One model requires significant uplift only during the Miocene (~15 Ma), related to the latest stage of Bolivian Orocline development (Garzione et al., 2006; Gregory-Wodzicki, 2000), whereas a second model entails significant paleorelief in the Central Andes by 35 Ma with elevations higher than 4000 m (Canavan et al., 2014; Carrapa and DeCelles, 2015; Hartley, 2003; Quade et al., 2015). Paleoelevation data from fossil leaf physiognomy and oxygen isotopic values have been interpreted to show that the Eastern Cordillera and the Altiplano Plateau were rapidly uplifted during the Miocene (Garzione et al., 2006, 2014; Ghosh, 2006; Gregory-Wodzicki, 2000; Rowley and Garzione, 2007). However, these studies do not consider climatic variations during the interval of study (Ehlers and Poulsen, 2009) and may underestimate the paleoelevation. Paleoelevations corrected for climatic effects suggest a plateau elevation of ca. 3 km since at least 25 Ma (Ehlers and Poulsen, 2009). Moreover, paleoaltimetry studies in the area of the Puna Plateau and Western Cordillera, suggest that these regions (including the western side of the Altiplano Plateau) were already elevated at 35 Ma (Canavan et al., 2014; Quade et al., 2015). In the Brazilian region, thermochronological data do not indicate any major topographic change (Cogné et al., 2012; Japsen et al., 2012a).

We thus depict orogenic growth of the Andes at 40 Ma with a high degree of along strike variability (Fig. 6). We propose that the northern Andes were narrow, with maximum elevations around 3000 m, while the deformation front in the Central Andes was already farther east, in response to increasing elevation and width, and displaying a plateau-like configuration with maximum elevations reaching around 4000 m. Immediately to the south, a depression is related to the development of the extensional Abanico Basin (Charrier et al., 2007, 2009). In the Southern and Austral Andes, the Cordillera gained again in elevation, although with lower elevations than in the Central and Northern Andes (around 2000 m).

We adapted the paleoshoreline presented by Eagles and Jokat (2014) for the Scotia Arc region, similar to the 60 Ma reconstruction. We also made minor modifications to the reference paleoshorelines of Golonka et al. (2006) for consistency with marine and terrestrial fossil data.

3.1.3. South America 20 Ma

Thermochronological data do not show evidence of Oligocene exhumation in the Western and Central Cordillera of the Northern Andes (Villagómez and Spikings, 2013). However, in the Eastern Cordillera of Colombia, thermochronological and structural data suggest rapid orogenic propagation, basin inversion and shortening related to a plate reorganization and a related increase of plate convergence during early Miocene (Mora et al., 2013; Parra et al., 2009, 2012; Spikings et al., 2010). In the Central Andes, paleoelevation data show that surface uplift in the Eastern Cordillera had already started during the Oligocene (Quade et al., 2015) in agreement with thermochronological data (Carrapa and DeCelles, 2015) and the Eocene-Oligocene construction of the Bolivian Orocline showing shortening in the Eastern Cordillera (Arriagada et al., 2008; McQuarrie et al., 2008). The Subandean zone only deformed after the mid-Miocene (Arriagada et al., 2008; Quade et al., 2015). In the Southern Andes, extension was ongoing in the early Miocene (around 19 Ma), with orogenic contraction starting in the middle Miocene (Echaurren et al., 2016). By contrast, contraction was still active in the Austral Andes, with eastward migration of the deformation front (Alvarez-Marrón et al., 1993; Fosdick et al., 2011; Klepeis et al., 2010). We thus propose a Northern and Central Andes forming a wider mountain chain with elevations around 4000 m for the highest peaks in these regions. For the Southern and Austral Andes, we kept paleoelevation similar to the previous 40 Ma reconstruction (Fig. 6). Paleoshorelines are the same as the reference paleoshorelines from Golonka et al. (2006), with only minor local modifications (Fig. 7).

3.2. North America

North American Cenozoic tectonic evolution is dominated by orogenic build-up and demise along the Western Cordillera orogenic belt, extending from Alaska in the north, to Central America in the south. It is characterized by an alternation of subduction and transform contacts between the North American Plate, the Pacific Plate and relicts of the conjugate Farallon Plate (Juan de Fuca, Gorda, Rivera, Cocos, Nazca; Fig. 1). The western margin of North America can be divided into several morphological units, among them: The Sierra Nevada, Cascades and Coast Belt mountains along the coast; the Basin and Range region and the Colorado Plateau; the Rocky Mountains, Alaskan and St. Elias Ranges (Fig. 8, Chamberlain et al., 2012; Fenneman, 1931; Mathews, 1991, 1986; Ordonez, 1936).

3.2.1. North American 60 Ma

The Intermontane and Insular superterranes located westboard of the North American Cordillera traveled northward relative to North America during the late Cretaceous, but by how much is subject of a long-standing debate. Structural geological estimates give no more than ~700–900 km (e.g. Gabrielse et al., 2006), whereas paleomagnetic (Enkin et al., 2006; Kent and Irving, 2010) and detrital zircon (Garver and Davidson, 2015) data suggest >2000 to 3200 km of coastwise translation, placing British Columbia (BC) adjacent to Baja California -

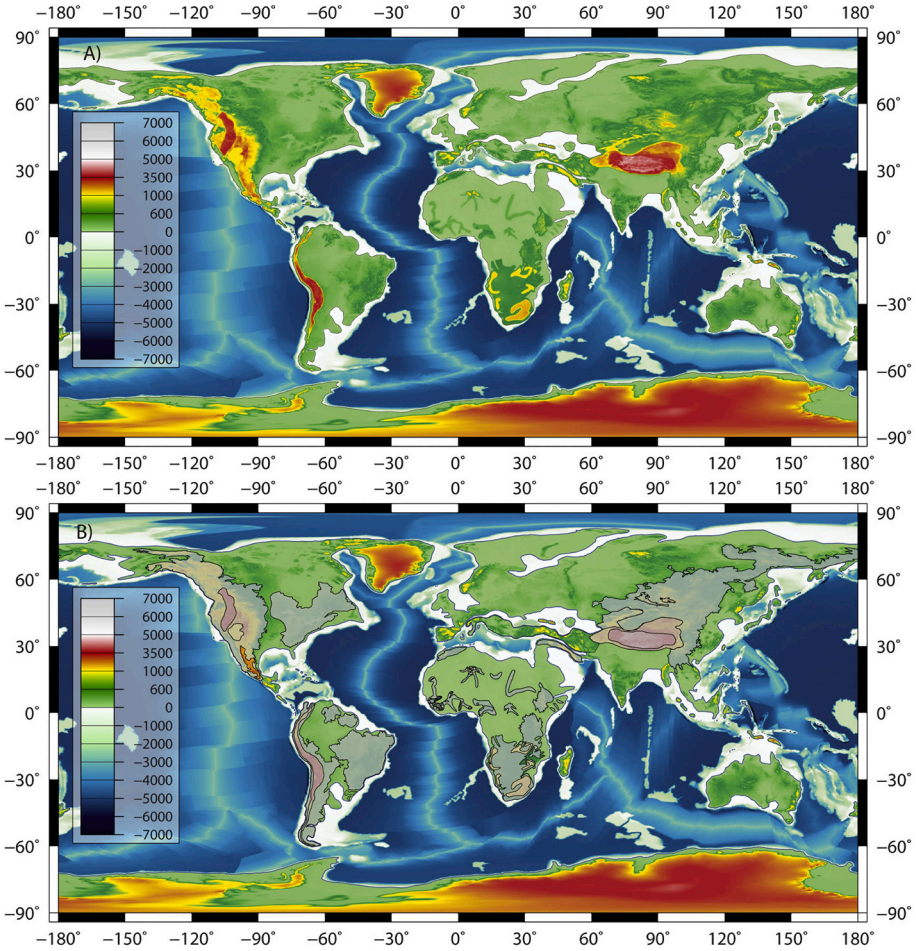

Fig. 7. (A) Paleogeographic reconstruction at 20 Ma. (B) Shaded regions show the location of modified regions (for more details see supplementary data).

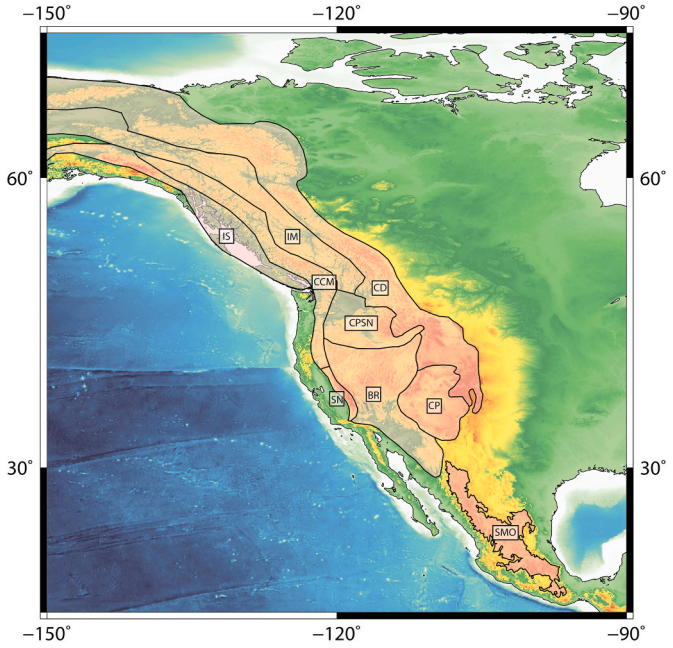

Fig. 8. Physiography of North America SMO, Sierra Madre Oriental; SN, Sierra Nevada; BR, Basin and Range; CP, Colorado Plateau; CCM, Coastal Domain and Cascades Mountains; CPSN, Columbian Plateau and Snake River plain; IS, Insular Domain; IM, Intermontane domain; CD, Continental Domain including the Rocky Mountains. (Modified from Chamberlain et al., 2012; Colpron et al., 2007; Silberling et al., 1992).

the so called "baja-BC" hypothesis (Irving et al., 1985). This dilemma has tantalized geologists for decades (Beck et al., 1981; Butler et al., 1989; Cowan, 1994; Irving and Archibald, 1990; Umhoefer, 1987). However, the blocks were essentially in place at 60 Ma (Cather et al., 2012; Coney, 1972; Dickinson and Snyder, 1978; English and Johnston, 2004; Ziegler et al., 1985). Post-60 Ma motion on major faults accounts for only a few hundreds of kilometers (Gabrielse et al., 2006), and are generally irresolvable using paleomagnetic methods (Enkin et al., 2006). The Laramide Orogeny, is a broad orogenic event responsible for the uplift of the Rocky Mountains, Sierra Madre and Laramide blocks (Armstrong, 1968; Coney, 1972, 1976; Copeland et al., 2017; Haxel et al., 1984). Major impacts of this orogeny on paleogeography includes the reactivation of the Rocky Mountains, the formation of a high plateau in central Nevada, called the "Nevadoplano" (analogous to the Altiplano in Bolivia), and the final regression of the Western Interior Seaway (Cather et al., 2012; DeCelles, 2004; Ziegler et al., 1985). Paleoelevation studies suggest a high Cordillera in the southern part of the Canadian Rocky Mountains (Chamberlain et al., 2012 and references therein; Mulch et al., 2007); elevations are thought to have been much lower further south in the Cordillera (Cather et al., 2012; Lechler et al., 2013; Licht et al., 2017), though past crustal thickness suggests that a 3 km high plateau may have extended as far south as northern Mexico in the latest Cretaceous (Chapman et al., 2020). We opted for a reconstruction that displays a North American Cordillera with the highest elevations in the Canadian Rocky Mountains at around 4000 m and decreasing elevation southward, reaching 2000 m in Nevada and around 800 m in Mexico (Fig. 5). Elevations in Sierra Madre were not modified.

For North American paleoshorelines, we used a modified version of Slattery et al. (2015) other minor modifications to the reference paleoshorelines of Golonka et al. (2006) were constrained by marine and terrestrial fossil data provided from the paleobiodb.org.

3.2.2. North American 40 Ma

The Laramide Orogeny was completed at ca. 40 Ma (Coney, 1976; Coney, 1972; Copeland et al., 2017; English and Johnston, 2004; Henderson et al., 2014). Paleoelevation data suggest that the surface uplift was at its maximum expression and that the Nevadoplano reached elevations near 4000 m with a latitudinal extension of around 2500 km (Chamberlain et al., 2012; Fan and Dettman, 2009; Lechler et al., 2013; Sjostrom et al., 2006). To the southwest, contrasting models for the evolution of the Sierra Nevada mountains propose that elevations were attained either recently or in the early Cenozoic. Revised geomorphological observations have, however, shown that the Sierra Nevada has been at high elevations at least since the Eocene in agreement with stable isotope data (Gabet, 2014; Mix et al., 2016; Mulch et al., 2006). The high elevation in the Nevadoplano and Sierra Nevada contrast with elevations in the Colorado Plateau where stable isotopes are compatible with paleoelevations of around 1000 m (Cather et al., 2012; Licht et al., 2017). To the north, limited fission-track data suggest that the Coast Belt attained average elevations of ~2500 m that persisted until ~6 Ma (Densmore et al., 2007).

We thus propose a topographic reconstruction for which the Nevadoplano dominates the landscape of western North America with a north-south extent of ~2500 km and paleoelevations as high as 4000 m (Fig. 6). It also includes a modern-like Sierra Nevada and a Colorado Plateau at lower elevation, with altitudes around 1000 m, surrounded by mountains to the west, north and east. Paleoshorelines were reconstructed from the reference paleoshorelines from Golonka et al. (2006).

3.2.3. North America 20 Ma

A major change in the tectonic regime of Western North America took place during the Early Miocene with initial subduction of the Pacific-Farallon ridge and formation of the Mendocino triple junction (Atwater, 1970; Furlong and Schwartz, 2004; Silver, 1971). Northward migration of the Mendocino triple junction marks the long-term diachronous demise of the Farallon subduction zone, replaced by a new transform margin, part of which forms the modern-day San Andreas Fault (Atwater, 1970; Furlong and Schwartz, 2004; Silver, 1971). As North America rode over the growing slab window, a combination of thermal softening and coupling with the north-moving Pacific plate resulted in extension and formation of the Basin and Range province, starting ca. 36 Ma, with the most important pulse of deformation occurring after the mid Miocene (~14 Ma; McQuarrie and Wernicke, 2005).

Despite ongoing extension in the Basin and Range province, paleoelevation data suggests that during the Oligocene the Nevadoplano was still present from Central Nevada to Southern Canada (Chamberlain et al., 2012 and references therein), extending up to the Sierra Nevada (Chamberlain et al., 2012; Gabet, 2014; Wheeler et al., 2016). Paleoelevation estimates for the Colorado Plateau are debated ranging from elevations as high as today (e.g. Flowers et al., 2008) to less than 1000 m during the Oligocene (Sahagian et al., 2002). We opted for elevations similar to the 40 Ma paleotopography for the Nevadoplano and Colorado Plateaus, i.e., 4500 m and 1000 m, due to the lack of conclusive data showing significant topography change between 40 and 20 Ma (Fig. 7). Like previously, paleoshorelines were reconstructed from the reference paleoshorelines from Golonka et al. (2006).

3.3. Africa

The African realm, including Madagascar, comprises three major plates: The African-Nubian Plate, the Africa-Somalian Plate, and the Arabian Plate (Fig. 1; Bird, 2003; Stamps et al., 2018). These plates are surrounded by spreading ridges or rifts, except for the northern border of the African and Arabian plates, where they subduct below the Eurasian Plate (Bird, 2003; Müller et al., 2016). Bimodal elevation distributions characterize the African topography (Fig. 9, Burke and Gunnell, 2008; Dauteuil et al., 2009) with high relief (900–1100 m) corresponding to domes, large plateaus (Kalahari, East African and Ethiopian Dome and Cameroon, Darfur, Tibesti, Hoggar and the Atlas, Guillocheau et al., 2018) and elevated passive continental margins (Japsen et al., 2012b),

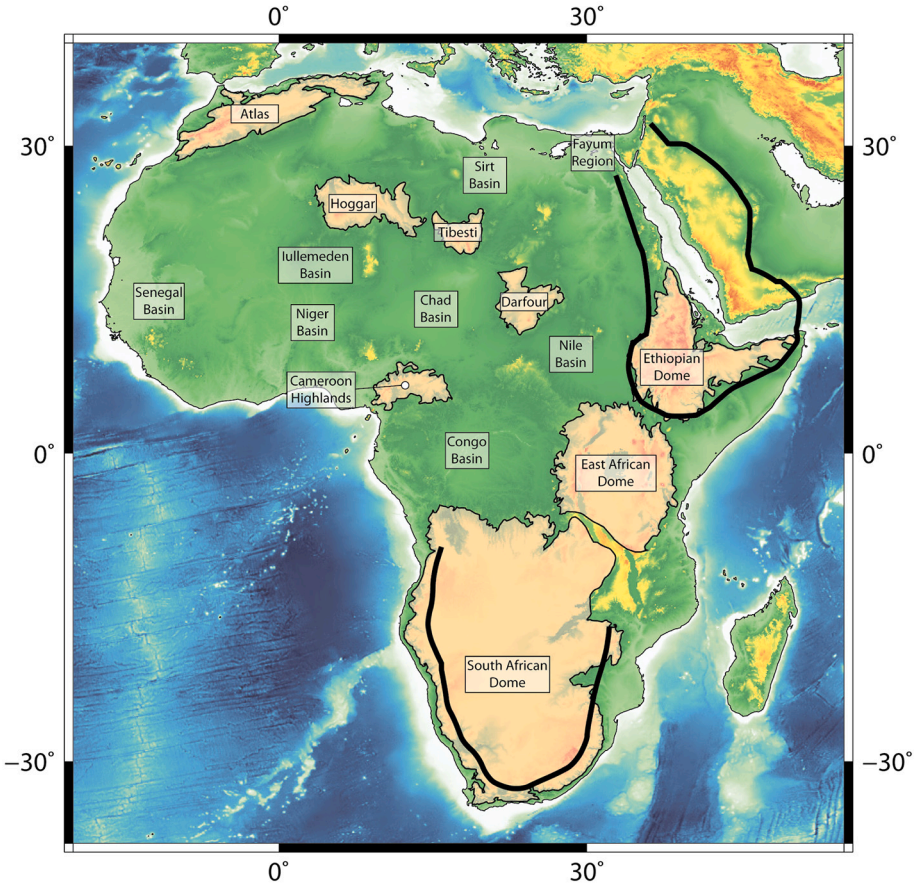

Fig. 9. Physiography of Africa. Thick black lines represent elevated passive margins. (Modified Burke and Gunnell, 2008).

and low relief regions (300–400 m) corresponding to the Sahara and the Congo Basin (Guillocheau et al., 2015) where most of the drainage basins are located (Senegal, Niger, Chad, Nile, Congo, among others, Burke and Gunnell, 2008). High relief regions have been argued to be related to isostatic compensation (Bechtel et al., 1987; Brown and Girdler, 1980) or dynamic topography related to vertical stresses generated by mantle flow (Burke and Gunnell, 2008; Gurnis, 1990; Lithgow-Bertelloni and Silver, 1998). New data, however, support the idea that the topographic evolution of the African surface is the result of a coupled interaction between mantle dynamic, lithospheric deformation and passive continental margin processes (Braun, 2010; Dauteuil et al., 2009; Guillocheau et al., 2018; Japsen et al., 2012b).

3.3.1. *Africa 60 Ma*

Elevated, passive continental margins (Japsen et al., 2012b) are a characteristic feature of the African continent that were first suggested to be long-lasting relict topographic features (Ollier and Pain, 1997; Weissel and Karner, 1989). Apatite fission track thermochronology, however, has revealed a more complex history in which denudation and surface uplift occurred long after break-up (Beauvais and Chardon, 2013; Gallagher and Brown, 1999; Tinker et al., 2008; Wildman et al., 2017).

The only area at 60 Ma in Africa with clear evidence for high topography is the southernmost part of the South African Plateau (or Kalahari Plateau), remnant of a late Cretaceous relief (Baby et al., 2020, 2018b, 2018a). Planation surfaces (etchplains and pediplains), used as geomorphological markers to identify vertical movements related to dynamic topography, indicate that during the late Paleocene-mid Eocene, an African-scale weathering surface (etchplain) known as the African Surface (Burke and Gunnell, 2008 for a review) was almost flat, with a faint drainage divide in central Africa (Guillocheau et al., 2018). In northern Africa (Sahara) this etchplain was flooded by the sea during Late Paleocene times (Berggren and Hollister, 1974; Ye et al., 2017), confirming a flat topography near sea level. We thus propose a reconstruction with very low elevations on the African continent at 60 Ma (Fig. 5), including near sea level altitude for northern Africa, a curved drainage divide of elevations lower than 300 m in central Africa, and remnants of an early South African Plateau to the south. Our reconstructed paleoshorelines follow Golonka et al. (2006) with some modifications in northern Africa after Couvreur et al. (submitted).

3.3.2. *Africa 40 Ma*

Thermochronological data and paleogeographic maps (e.g. Burke and Gunnell, 2008) suggest that 40 Ma was the onset of a major change in the paleotopography of Africa that ended around 30 Ma (Fig. 5). For Northern Africa, thermochronological data in the Hoggar Dome (Rougier et al., 2013) indicate that the onset of exhumation occurred during the late Eocene (English et al., 2017), in agreement with Oligocene fluvial sedimentary rocks on top of the modern Hoggar (Rognon et al., 1983). The incipient growth of the Hoggar Dome initiated a divide in northwest Africa (Chardon et al., 2016) that might be extended until the Moroccan Atlas, and likely resulted from basin inversion related to the Europe-African collision responsible for the onset of surface uplift (e.g. Frizon de Lamotte et al., 2009). We thus changed the topography in Northern Africa in the area of the Hoggar Dome, with elevations between 200 m to 500 m (Fig. 6).

At 40 Ma, proposed paleoshorelines for northernmost Africa range between a large epicontinental sea (www.deepmaptimes.com; Blakey, 2008) to a paleoshoreline more similar to that of today (www.scotese.com; Golonka et al., 2006; Smith et al., 2004). Stratigraphic and sedimentological data indicate fluvial and lacustrine environments in the Chad (Genik, 1993) and Sudanese (e.g. Schull, 1988) Rifts and for the

Iullemmeden Basin (Niger-Mali, e.g. Moody, 1997). The shoreline was therefore located northward of the Atlas-Hoggar-Tibesti-Darfur divide. The Late Eocene was a major period of emergence in the South Atlas, in Libya, and in Egypt (e.g. Mebrouk et al., 1997). The shoreline ran from central Tunisia (Merzeraud et al., 2016), through the southern Sirt Basin (Libya, Abouessa et al., 2014) to south Cairo (Fayum region, Underwood et al., 2013).

3.3.3. *Africa 20 Ma*

At 20 Ma, new domes and plateaus were initiated, and remnant topography from the 40–30 Ma uplift phase got more uplifted as a response of long wavelength deformation related to mantle dynamics (Guillocheau et al., 2018). The Southern African Plateau reached its modern elevation (Baby et al., 2018a). The Zambia-Malawi Plateau, East African Dome, Hoggar-Aïr-Tibesti-Darfur cluster, and Cameroon Volcanic Line started reaching significant elevations, attaining their modern elevations in the Late Miocene-Early Pliocene. Geological, thermochronological and structural data shows that the 1500-m high Atlas Mountains started growing in the late Eocene and must have reached significant elevation by the early Miocene (Balestrieri et al., 2009; Frizon de Lamotte et al., 2000; Missenard et al., 2008; Ruiz et al., 2011). We estimate paleoelevations for the Hoggar Dome and the Moroccan Atlas at around 1800 m and 1100 m respectively, and around 900 m for the Cameroon Volcanic Line and the East African dome (Fig. 7). Paleoshorelines are reconstructed following Golonka et al. (2006).

3.4. *Eurasia*

Eurasian Cenozoic tectonics are dominated by the development of the Alpine-Himalayan orogen at the boundary between the Eurasian Plate to the north and the African, Arabia, and Indian plates to the south. This orogen extends from the Mediterranean Sea in the West to the Sunda Arc in the East and is the classic example of an orogen constructed by accretion during continental underthrusting/subduction. In the following we present the paleogeographic evolution associated with the Tibetan-Himalayan orogen, and - more briefly - the Anatolian orogenic belt and the Alpine-Mediterranean region.

3.4.1. *The Tibetan-Himalayan orogen*

The Tibetan-Himalayan orogen (Fig. 1) is composed of various mountain belts and plateaus that resulted from the accretion of continental slivers originating from the northern margin of Gondwana against the southern margin of North China since the late Paleozoic (e.g. Kapp and DeCelles, 2019; Yin and Harrison, 2000). From south to north, the different accreted terranes and geological provinces include India, the Lhasa Terrane (referred here as “Southern Tibet”), the Qiangtang Terrane (referred here as “Central Tibet”), and the Songpan-Ganze accretionary complex overlain by the Hoh-Xil Basin (referred here as “Northern Tibet”). The orogen extends further north into the Qaidam and Tarim Basins, surrounded by the Pamir, Kunlun Shan, Tian Shan, Altyn Shan and Qilian Shan / Nan Shan mountain ranges (Fig. 10).

Tectonic models for the India-Asia collision remain debated. Recent studies have narrowed the age of the collision to ca. 60–55 Ma based on the first input of Asia-derived material in the northernmost preserved continental rocks on the Indian Plate, in the Indian Foreland Basin (e.g. DeCelles et al., 2014; Garzanti, 2019; Garzanti et al., 2018; Hu et al., 2014). This age generates a dramatic difference between the amount of convergence of India and Asia since the collision — around 4000 km since 60 Ma — and the estimated amplitude of shortening in the Tibetan Plateau and Himalaya — totaling around 1500–2000 km (e.g. Dupont-Nivet et al., 2010; van Hinsbergen et al., 2011). Several models have been proposed to account for this mismatch. A first type of models invoke a “Greater India Basin” (Huang et al., 2015; van Hinsbergen et al., 2012, 2019). They propose that a terrane drifted off northern India in the Cretaceous, carrying ahead Greater Himalayan sequences, and was separated from mainland India by a wide oceanic basin. This small terrane collided with Asia at 60–55 Ma; the Greater India oceanic basin then subducted beneath Asia until the final India-Asia collision in the late Oligocene - early Miocene. Another family of models suggest a continuous subduction of the 2400 Km long Greater Indian continental crust below Asia (Ingalls et al., 2016; Searle et al., 2016). Arc collision models propose a first collision of India with an intra-oceanic arc at 60–55 Ma while subduction is kept along the Asian margin until a much later India-Asia collision. Various versions of this arc collision model have been proposed (Aitchison et al., 2007; Gibbons et al., 2015; Guilmette et al., 2012; Hébert et al., 2012; Jagoutz et al., 2015; Müller et al., 2016; Westerweel et al., 2019). These models invoke collision between India and Asia in the Late Eocene to Miocene, depending on the assumed magnitude of intra-Asian shortening. Finally, a set of “classic” models propose removal of continental lithosphere by lateral extrusion of continental blocks, wholesale continental subduction and very high estimates of overriding plate shortening (e.g. Cogné et al., 2013; Guillot et al., 2003; Molnar and Tapponnier, 1975; Replumaz and Tapponnier, 2003).

We propose here reconstructions following the different models. At 60 and 40 Ma, we have computed two different configurations of the Indian paleogeography, whereby we used the GPlates reconstruction of (van Hinsbergen et al., 2011, 2019) as basis: (1) the Greater India Basin model (Fig. 5, 6 and 7 and Fig. 11a; van Hinsbergen et al., 2012), and (2) a fully continental post 58 Ma Greater India collision with Asia, assuming wholesale continental subduction of several 1000s of km (Ingalls et al., 2016; see Fig. 11b). We have also explored the Arc collision model (Müller et al., 2016; Westerweel et al., 2019; see Fig. 11c) and the lateral extrusion model in which the Lhasa block is located further south (Replumaz and Tapponnier, 2003; Fig. 11d).

3.4.1.1. The Tibetan-Himalayan orogen 60 Ma. It has been proposed that topography in Tibet was already important before the India-Asia collision due to topographic build-up from previous terrane accretions and Cordilleran-style orogeny (Murphy et al., 1997), resulting in a high elevation “Lhasaplano” in southern Tibet as early as the Late Cretaceous (e.g. Kapp et al., 2007; Wen et al., 2008). This Lhasaplano would have built-up following increased India-Asia convergence, Gangdese and Kohistan-Ladakh magmatism, shortening and rapid exhumation in the

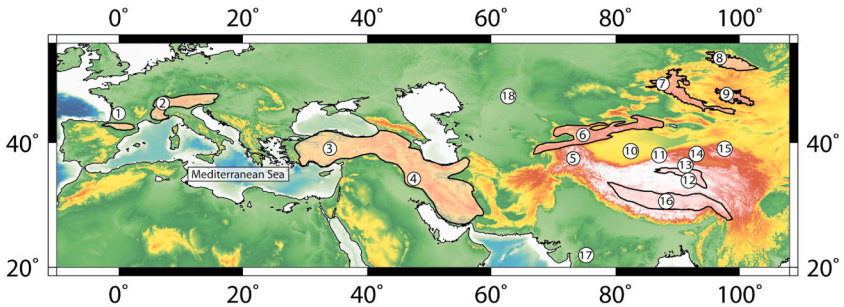

Fig. 10. Physiography of Eurasia. 1, Pyrenees; 2, Alps; 3–4, Anatolian, Zagros and other orogens; 5, Pamir; 6, Tian Shan; 7, Altai-Hangay-Sayan mountains; 7, Altai mountain; 8, Sayan mountain; 9, Hangay mountain; 10, Tarim Basin; 11, Altyn Shan; 12, Hoh Xil Basin; 13, Kunlun Shan; 14, Qaidam Basin; 15, Qilian Shan and Nan Shan; 16, Lhasa Block; 17, Deccan Traps; 18; Turgai Region. (Modified from Choukroune, 1992; Dai et al., 2019; McQuarrie and van Hinsbergen, 2013; Schmid et al., 1996; Yin and Harrison, 2000).

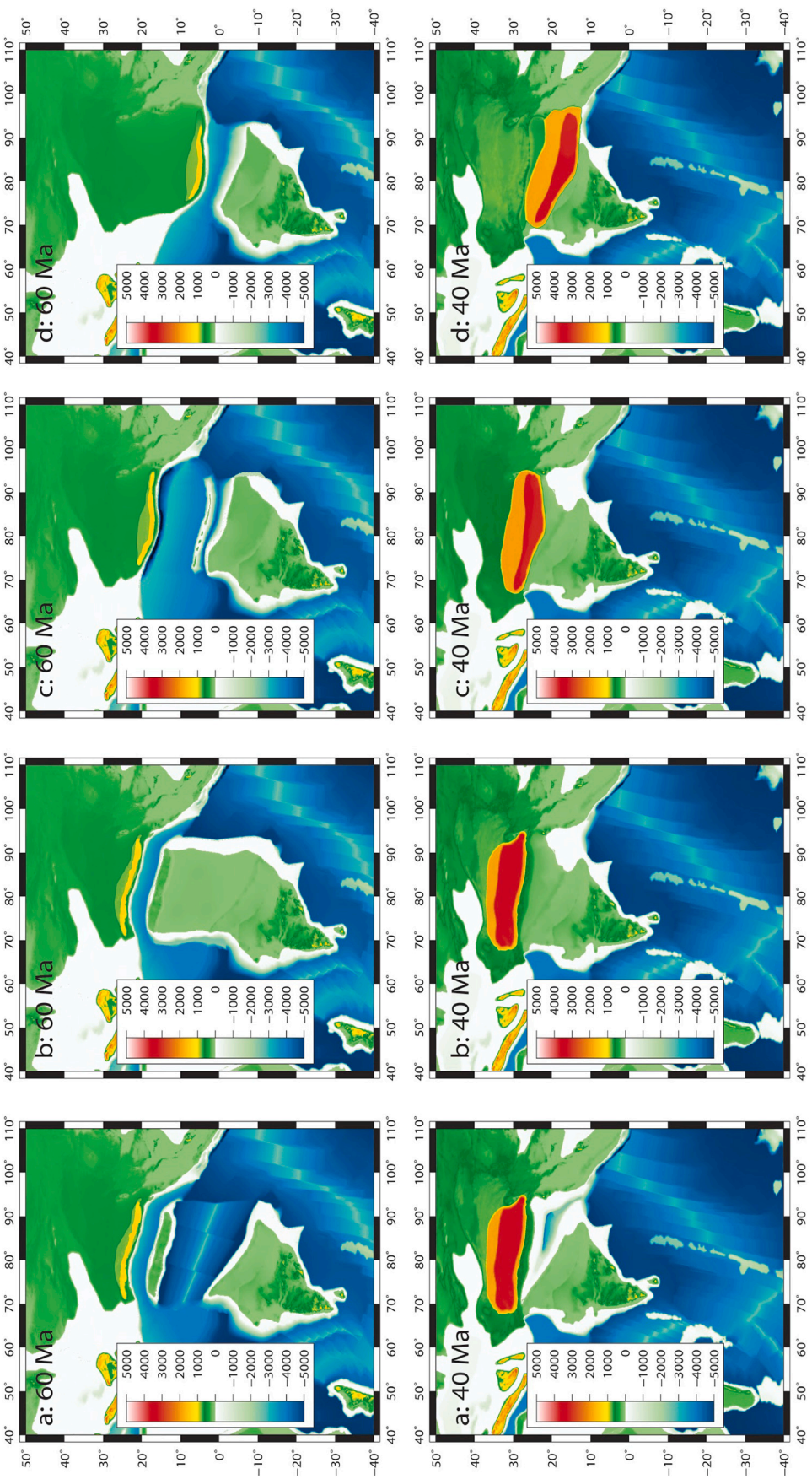

Fig. 11. Indo-Asia collision paleogeographies at 60 and 40 Ma according to various models: a) Double collision, first with an drifted fragment of Greater India, then with India after subduction of the Greater Indian Basin following van Hinsbergen et al. (2012, 2019); (b) Single India-Asia collision assuming collision age ca. 55 Ma; (c) India collision with a Trans-Tethyan arc and then with Asia (e.g. Jagoutz et al., 2015); and (d) India collision with Asia but with Lhasa block located at more southerly paleolatitudes (e.g. Cogné et al., 2013).

northern Lhasa Terrane and Qiangtang Terrane after 80–70 Ma (Chapman and Kapp, 2017; Kapp et al., 2007; Ravikant et al., 2009; Volkmer et al., 2014, p. 201; Wen et al., 2008). Further to the north in Central Tibet, it has been proposed that the Qiangtang Terrane formed a topographic relief since ca. 70 Ma, shedding detritus northward into the nonmarine Hoh-Xil Basin (Li et al., 2018; Staisch et al., 2014, 2016). Thermochronological data suggests that construction of the Central Tibetan Plateau began during the Late Cretaceous forming a conspicuous relief, but it was only later, during the Eocene, that the Tibetan Plateau formed a significant topographic high (e.g. Rohrmann et al., 2012; van der Beek et al., 2009; Wang et al., 2008). In northern Tibet, no major deformation is reported before the collision apart from local events possibly reactivating older structures (Jolivet et al., 2018; Morin et al., 2019; van Hinsbergen et al., 2015a, 2015b).

Paleoaltimetry data has suggested elevations ca. 4.000 m across the Lhasa and Qiangtang terranes near the time of initiation of the collision (e.g. Currie et al., 2016; Ding et al., 2014; Li et al., 2019) with relatively lower elevation to the north in the Hoh-Xil (Cyr et al., 2005; Miao et al., 2016; Polissar et al., 2009) and south in the proto-Himalaya (e.g. Ding et al., 2017; Leary et al., 2017). However, the interpretation of these data is still controversial. The primary nature of Eocene Tibetan oxygen isotopic records is questioned (Quade et al., 2020) and the use of modern isotopic lapse rates for paleoaltimetry estimates might significantly overestimate the actual topography (Botsyun et al., 2019). In addition, some stable isotopic records (Currie et al., 2016) are associated with fossils indicating lower elevation (Su et al., 2019) and their depositional age control has been revised to younger ages (e.g. Deng et al., 2019; Leary et al., 2018). These data overall suggest a more complex topographic development with pre-existing valleys and ranges instead a monotonic progression of plateau uplift (e.g. Laskowski et al., 2019). A precise description of paleotopography remains challenging to produce for this time slice.

Thus, we favored a conservative configuration in our reconstruction at 60 Ma with relatively low elevations (Fig. 5, Fig. 11a), with later, gradual uplift at 40 and 20 Ma, time slices for which pieces of evidence for high topography are more numerous. Our 60 Ma reconstruction displays a contiguous east-west trending volcanic arc located in the southern margin of Asia formed a relatively narrow mountain range at elevations between 500 and 1500 m. In central Tibet we also implemented an incipient plateau with elevations around 700 m. North of this, elevations are reduced to 500 m or less.

3.4.1.2. The Himalayan-Tibetan orogen 40 Ma. Structural evidence points to enhanced development of an elevated Central Tibetan Plateau in the Lhasa and Qiangtang regions during later Paleogene time (e.g. Kapp et al., 2007, 2005; van der Beek et al., 2009; Wang et al., 2014, 2008), although stable isotopic data yield contrasting results either suggesting complex topography combining low and high elevations and/or a more complex hydrological cycle affecting stable isotope paleoaltimetry (e.g. In northern Tibet, in the Hoh-Xil Basin and Kunlun Shan region, geological studies have shown late Eocene basin closure and exhumation, suggesting surface uplift) (Dai et al., 2019; Polissar et al., 2009; Staisch et al., 2016, 2014; Wang et al., 2017). Further north in the Qaidam and Tarim Basin, late Eocene increased subsidence and sea retreat is associated with tectonic activation along the Kunlun Shan (Bosboom et al., 2014b; Cheng et al., 2019; Kaya et al., 2019; Song et al., 2018), but apart from local ranges with elevations (e.g. Hoorn et al., 2012) significant surface uplift of those basins is not expected until later propagation of deformation in the Tian Shan and Qilian Shan in the Miocene (e.g. He et al., 2017; Zuza et al., 2016).

We propose a 40 Ma reconstruction in which South and Central Tibet formed an incipient plateau with intermediate elevations at ca. 3500 m, and a moderate to low elevation paleosurface for Northern Tibet (Fig. 6, Fig. 11a).

3.4.1.3. The Himalayan-Tibetan orogen 20 Ma. Most thermochronology and paleoaltimetry studies indicates that the Central Tibetan Plateau attained high elevations by the early Miocene (e.g. Botsyun et al., 2019; Quade et al., 2011; Rowley and Currie, 2006; Wang et al., 2017). Important changes at this time include the growth of the Himalayas, enhanced since the early Miocene as suggested by a wide range of studies (e.g. Clift et al., 2008; Xu et al., 2018 and references therein), although some local lower elevation basins may have persisted in southern Tibet into the Miocene (e.g. DeCelles et al., 2018; Leary et al., 2017; Wang et al., 2013). To the north of Tibet, exhumation begins (or, in places, resumes) in the Tian Shan, Pamir, Kunlun, Altyn Shan, Qilian Shan, Nan Shan with infilling, uplift and closure of associated intermontane basins (Dai et al., 2019; Dedow et al., 2020; Sobel et al., 2013; Wang et al., 2017; Zuza et al., 2016). We propose a 20 Ma reconstruction with wider and higher Tibetan Plateau than at 40 Ma, with elevations reaching beyond 4000 m. The Tian Shan, Pamir, Kunlun, Nan Shan and Qilian and intermontane basins north of Tibet are modeled at elevations around 1000–1500 m to reflect incipient range uplift before its further development later in the Miocene (Fig. 7).

3.4.2. The central Eurasian proto-Paratethys Sea

The extension of the proto-Paratethys epicontinental sea over Central Eurasia is particularly important for paleoenvironmental and biogeographic reconstructions, including the presence or absence of a N-S trending seaway (the Turgai Strait) that constituted the connection between the Neo-Tethys with the west Siberia interior sea (Akhmetiev et al., 2012) and through this, with the Arctic Ocean (Golonka et al., 2006). Although some paleogeographic maps have suggested that the Turgai Strait was closed at 40 Ma (www.deepmaptimes.com; Blakey, 2008), and terrestrial fossils are (mis?)placed in the strait at this time (Mihlbachler et al., 2004; www.paleobiodb.org). Geological data show three major sea transgressions in the proto-Paratethys in the Paleogene (Bosboom et al., 2017, 2014b, 2014a; Kaya et al., 2019). These studies suggest that the sea did not retreat sufficiently to close the Turgai Strait between the first and most extensive incursion (58–53 Ma) and the second one (46–41 Ma); however, the strait likely closed between the second (46–41 Ma) and the last (39–37 Ma) incursions, and remained closed after 37 Ma. Thus, we provide reconstructions with an open Turgai Strait at 60 Ma and closed at 20 Ma. At 40 Ma, we provide two maps, with an open or closed strait (see supplementary data).

3.4.3. The Alpine-Mediterranean region and the Anatolian and Zagros orogens

Cenozoic interaction between Africa, Iberia and Eurasia resulting in the orogenic growth in the Pyrenean-Alpine chain and basin segmentation and extension in the Mediterranean Sea which lead to the formation of several micro-basins (Choukroune, 1992; Dewey et al., 1989; Schettino and Turco, 2006; van Hinsbergen et al., 2014; Vissers and Meijer, 2012; Ziegler, 1987). Further East, the Anatolian and Zagros orogenic belts (Fig. 8), between the Eastern Mediterranean Sea and the Gulf of Oman, is within the collision zone between Arabia-Nubia to the south and Eurasia to the north (Bird, 2003). The current configuration results from the subduction of the Neotethyan Oceanic crust and collision between the Arabian and African Plates and the Eurasian Plate (Agard et al., 2007; Bird, 2003; Gürer and van Hinsbergen, 2019; Kuscu et al., 2010; McQuarrie and van Hinsbergen, 2013; Mouthereau et al., 2012; Reilinger et al., 2006; van Hinsbergen et al., 2020). The Arabian and Nubian Plates are being underthrusted/subducted below the western Mediterranean, Anatolian, Aegean and Zagros orogens (Bird, 2003; McQuarrie, 2004; Reilinger et al., 2006; van Hinsbergen et al., 2020).

Our paleogeographic reconstructions of these regions are simplified from Barrier et al. (2018) and Popov et al. (2004), and follow the tectonic models of McQuarrie and van Hinsbergen (2013) and van Hinsbergen et al. (van Hinsbergen et al., 2014, 2020). Our paleogeographic reconstructions in this region are mainly restricted to the location of paleoshorelines and do not consider Late Miocene-Pleistocene uplift

(Cosentino et al., 2012; Fernández-Blanco et al., 2019; Öğretmen et al., 2018) which have been proposed to be a responses to lithospheric delamination (Bartol and Govers, 2014; Göğüş et al., 2017), slab breakoff (Portner et al., 2018; Schildgen et al., 2018),and to the arrival of the subducting African margin to the southern Taurides (McPhee et al., 2019).

4. Antarctica and Greenland

4.1. Antarctica and Greenland at 60 Ma and 40 Ma

The common approach to reconstruct past Antarctic landscape before ice-sheet spreading has been to use fossil databases (e.g Lazarus and Caulet, 1993) and correct the present-day topography to account for the isostastic response to the ice mass removal (e.g. DeConto and Pollard, 2003). This approach results in a large part of the Antarctic continent being submarine before the EOT, particularly in West Antarctica (Fig. 12) around the West Antarctic Rift System (e.g. Blakey, 2008; DeConto and Pollard, 2003; Lazarus and Caulet, 1993). However, recent studies have suggested that most of the continent was above sea level before 34 Ma (Hochmuth et al., 2020; Wilson et al., 2012; Wilson and Luyendyk, 2009), by integrating erosion, thermal subsidence, shelf sedimentation and plate tectonic processes. In Antarctica, Hochmuth et al. (2020) presented a paleobathymetry, which could be complemented with the paleotopography from Paxman et al. (2019). However, their combination is made difficult by discrepancies. Paxman et al. (2019) suggests that the Ronne-Filchner and Ross Ice shelf were below sea level at 34 and 23 Ma as well as a sea interior that separates the Antarctic Peninsula from the Ellsworth Whitmore block, while Hochmuth et al. (2020) shows that both ice shelfs as well as the west coast of west Antarctica (Antarctic Peninsula, Turston island and Marie Byrd Land blocks) were above sea level at 34 Ma and the Ronne-Filchner and Ross Ice shelf were still above sea level at 21 Ma. Because of these differences resulting in an artificial internal basins at 34 Ma, we preferred keeping the paleotopography from Wilson et al. (2012). We use this Antarctic paleotopographic reconstruction with minor modifications in the South Shetland Islands to take into account the presence of Cenozoic volcanism, fossilized trees and bird tracks in the archipelago (Birkenmajer and Zastawniak, 1989; Mansilla et al., 2012; Smellie et al., 1984; Torres, 1984) and the history of the Bransfield Strait which was closed at 60 Ma (Galindo-Zaldívar et al., 2014; Pelayo and Wiens, 1989; Solari et al., 2008). For Greenland, we have simply taken into account the isostatic rebound due to ice removal (Fig. 5, Fig. 6). We have also combined our paleotopographies at 60, and 40 Ma, with the recent published Greenland paleotopography from Straume et al. (2020) (see supplementary data).

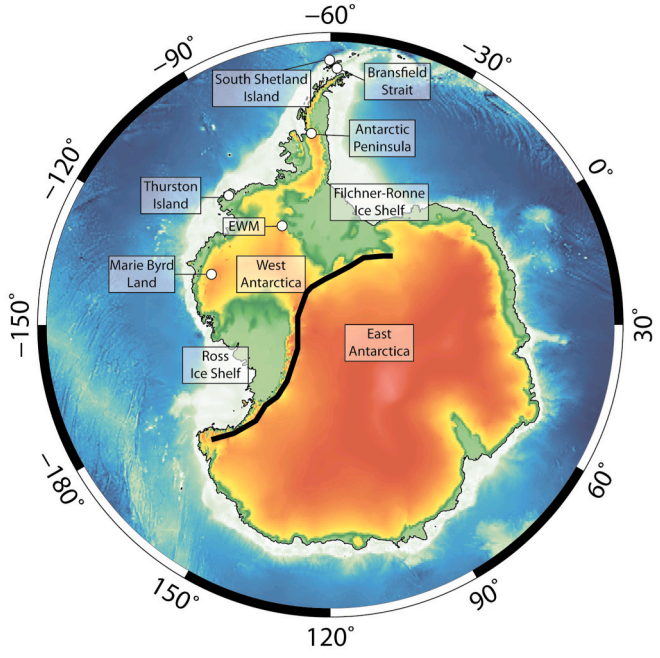

Fig. 12. Physiography of Antarctica. EWM, Ellsworth-Withmore Mountains. Thick black lines represent the Transantarctic Mountains. (Modified from Poblete et al., 2011).

4.2. Antarctica and Greenland 20 Ma

After the spread of Antarctic ice-sheet, and in the absence of data for 20 Ma, we use the current Antarctic topography. We use today's topography for Greenland as well, assuming it was glaciated at 20 Ma. For paleoshorelines, Golonka et al. (2006) suggested at 20 Ma a sea reentrant in the Ross Sea that extended up to 400 km in the interior of the Amundsen-Shackleton Coast. However, thermochronological and sedimentological data show that exhumation of the Transantarctic Mountains started before the Miocene (Fitzgerald, 2002; Olivetti et al., 2013; Zattin et al., 2010, 2014). Moreover, the drop in CO_2 at 23 Ma suggests that cold conditions predominated during the Early Miocene with ice-sheets expanding across the Antarctic continental shelf (McKay et al., 2016). The presence of the Transantarctic Mountains and the extension of the ice-sheet preclude the existence of the sea reentrant proposed by Golonka et al. (2006). In the Scotia Arc we have adapted the paleoshoreline presented by Eagles and Jokat (2014), while in other regions we have adjusted the paleoshoreline to be consistent with the fossil database (Fig. 7, paleobiodb.org). As for 60 and 40 Ma, we have also combined our 20 Ma paleotopography with the recent published Greenland paleotopography from Straume et al. (2020) (see supplementary data).

5. Discussion

5.1. Cenozoic topography, continent weatherability and climate

The most conspicuous result of our paleoreconstructions is a drastic increase in orography associated with the Cenozoic development of major mountain ranges (Fig. 13). The Cenozoic is also marked by one of the most dramatic decrease of atmospheric CO_2 and associated global cooling, starting at the end of the Early Eocene Climatic Optimum ~50 million years ago (Anagnostou et al., 2016; Zachos et al., 2001). Though many factors such as long-term volcanic degassing have been proposed as a driver for CO_2 drawdown over the period (Hoareau et al., 2015), most Cenozoic carbon cycle models require changes in continent and/or sea floor weatherability to explain this drop (Krissansen-Totton and Catling, 2017; Caves-Rugenstein et al., 2019). Two main mechanisms have been proposed to drive the increase of terrestrial weatherability after 50 Ma:

1. Increased fresh minerals exposure by tectonically-driven denudation along the Neo-Tethys margin, particularly in the Himalayas, where monsoonal dynamics enhanced denudation (Raymo and Ruddiman, 1992)
2. The emplacement of weatherable material through the equatorial belt, such as with the drift of the Deccan Taps of India (Kent and Muttoni, 2013) or the obduction of ophiolitic belts and volcanic arc material along the Neo-tethys subduction margin (Jagoutz et al., 2016; Macdonald et al., 2019).

Fig. 13a and b displays the percentage of emerged land (submerged land) and the percentage of emerged land per Myr per 10° latitudinal band. The distribution of emerged land surface significantly changed between 60 and 20 Ma at low latitudes. The northward motion of India redistributed emerged lands from the low southern latitudes to the low

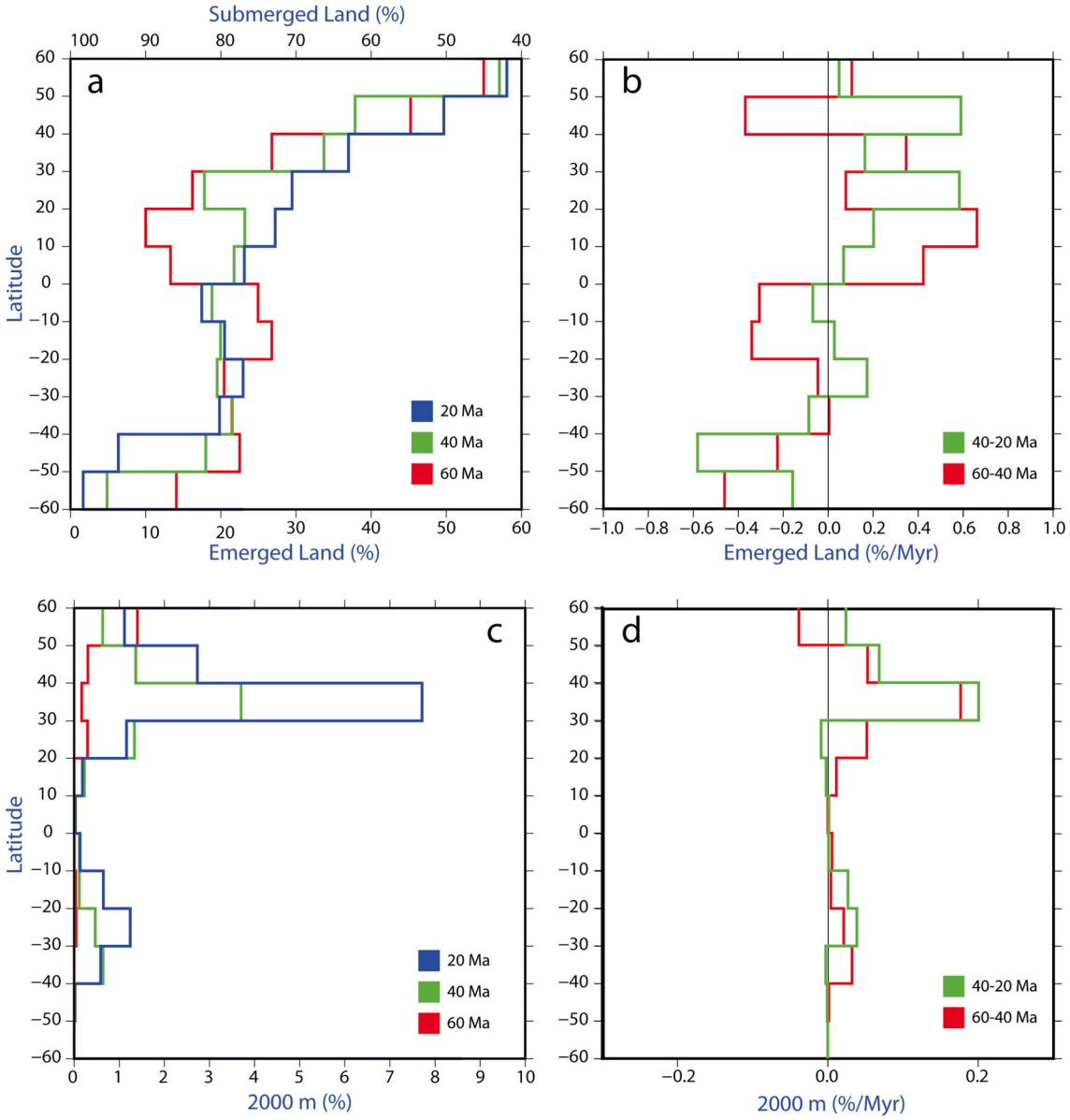

Fig. 13. a-b) Percentage of land above sea level and flux of emerged land (in %/Myr) per 10° latitudinal band c-d) Percentage of land above 2000 m flux of land above 2000 m (in %) binned for each 10° latitude band. Both figures are calculated following the Great India Basin tectonic scenario (see text for discussion).

northern latitudes, between 60 and 40 Ma, which itself should not have had much impact on weathering on the Indian Crust itself; however, the drying of the Northern Indian Seaway during this time window, covering most of North Indian Continental shelf, increased the amount of total land mass at low latitudes (Fig. 13). Two other events significantly increased the amount of emerged areas between 0 and 30°N: the long-term shrinkage of the Paratethys Sea, north of the Neotethyan Subduction zone, and the northward motion of Africa, associated with the retreat of its northern epicontinental seas, between 60 and 20 Ma. During this time window, the surface of emerged land masses increased by 50.4% between 0 and 30°N. This increase alone could have had a significant impact on weathering fluxes without evoking the presence of highly weatherable volcanic and ophiolitic rocks in this latitudinal band.

It is harder to evaluate potential changes of denudation through time with our approach as our model does not have the spatial resolution to reproduce steep gradients – where most denudation occurs at global scale (Larsen et al., 2014). Fig. 13b displays the percentage of areas above 2000 m, and shows a massive increase (90% between 60 Ma and 40 Ma and 42% between 40 Ma and 20 Ma) of high altitude areas between 20 and 40°N during the period of reconstruction. Most of this altitude gain is associated with Tibetan Plateau growth in our reconstruction –a low relief orogen. However, increased uplift at its margin (Himalayas) and birth and growth of surrounding mountains ranges (Pamir, Tian Shan, Kunlun) during this time period can have had a major impact, potentially quantifiable by using our paleogeographic maps with GCM-coupled carbon models like GEOCLIM (Goddéris et al., 2017; Maffre et al., 2018).

5.2. *Limitations and uncertainties*

Limitation and sources of uncertainties in the reconstructions are obviously numerous. They are identified and organized below according to different features involved in the making of a paleogeographic map: 1) plate tectonic models; 2) paleobathymetry; 3) paleoshoreline; and 4) paleotopography.

The basis for any paleogeographic model is the plate tectonic model on which it is based and most reconstructions commonly use a set of rigid tectonic plates (Matthews et al., 2016; Müller et al., 2016; Seton

et al., 2012); this represents a first source of uncertainty because of the lack of rigidity of continental margins (e.g., the Patagonian bend and Bolivian Orocline in the Andes or the Basin and Range extension in North America). Including evolving shapes for plate margins (for example, Müller et al., 2019) adds uncertainties related to the shape restoration process. Latitudinal resolution of paleomagnetic data is around 5°. Uncertainties in shortening calculations have been calculated in the order of 20% in well constrained cross sections (Allmendinger and Judge, 2013; Pueyo et al., 2004). This is particularly critical in the restoration of the Central Andes and South Asian margin, where Cenozoic shortening and deformation have been significant. For example, in the Bolivian Orocline, 400 km of shortening has been calculated near the Arica bend, which led to uncertainties of at least 80 km of this part of the margin. In the case of the south margin of Asia before the Indo-Asia collision, a shortening estimation of around 1000 km has been calculated (van Hinsbergen et al., 2019), which leads to an uncertainty of at least 200 km. Ongoing work in these geodynamically active regions - and many others - consistently generates new data that will potentially improve these restorations (e.g. Boschman et al., 2019; Westerweel et al., 2019).

The paleobathymetry has intrinsic uncertainties due to differences between the observed age and gridded age, estimations of sediment thickness and the age-depth model used (see Müller et al., 2008a for details). The original paleobathymetry, however, does not consider the development of several small basins related to local tectonic features that were manually adjusted. For example, the Greater Indian Basin is not associated with any paleobathymetry estimate in the Müller et al. (2008a) reconstructions; we estimated depths from −5000 to −2600 m in this region, following a depth-age relationship formula (Baatsen et al., 2016). Maximum depths, however, could reach more than −6000 m if we consider other age-depth correlations (e.g. Chung-Hwa et al., 1990).

Determining the ancient paleoshoreline is also an important source of uncertainty. Our approach was to take Golonka et al. (2006) paleoshoreline presented in Heine et al. (2015), and then change it for each period accordingly to margin deformation, the fossil database, and geological data. The first source of errors here is the rotation and restoration of the paleoshorelines to their past position. Shorelines were originally drawn on reconstructed paleogeographies according to a previous kinematic rotation model (Golonka et al., 2006). We repositioned them to present day using another rotation model (Heine et al., 2015), and rotated them again into the desired time-slice (60, 40 and 20 Ma) with our own model. This required re-adjusting the shorelines to follow new continental positions, but also new continental boundaries defined in the rotation model. Another related source of error is that the paleoshorelines of Golonka et al. (2006) have a low temporal resolution because they were reconstructed per geological stage or Epoch. In addition, as pointed out by Heine et al. (2015), the information used for the construction of the different paleoshorelines available are sometimes proprietary, and it is difficult to check afterwards the accuracy of the reconstructions. A dramatic example of uncertainty in past reconstructions are the paleoshorelines of South America, which include a huge sea reentrant until the Eocene in previous reconstructions, although it was likely only present until the middle Maastrichtian (Sempere et al., 1997). Here, we adjusted paleoshorelines for each period of time in which the reconstruction was done.

The ultimate and most difficult task in creating a paleoDEM is evaluating the paleotopography. Stable isotope datasets, although still relatively rare, constitute promising quantitative estimations of paleoelevation. However, stable isotopes are sensitive to temperature changes, moisture source, relative humidity, post-condensational effects, changes in paleoclimate, and may be biased by diagenetic and/or tectonic effects, which results in high variability of results and complicates their interpretation (Botsyun et al., 2016, 2019; Ehlers and Poulsen, 2009; Licht et al., 2017; Rowley and Garzione, 2007). Geological, structural and geochronological data are much more important and widespread, however they only constitute qualitative approximations and cannot be used to directly determine paleoelevation estimations. These limitations are critical to correctly estimate the surface paleoelevation of the three main Cenozoic orogens: The Tibetan-Himalaya, the Andes and the North American Cordillera. As mentioned in the previous sections, in the Tibetan-Himalayan orogen, uncertainties are most important at 60 and 40 Ma with predicted maximum elevations between 1000 m to 4500 m for both periods. In Western North America, the existence of a Nevadoplano at 60 Ma with maximum elevations around 4500 m is better documented, although the southerly extent of the Nevadaplano remains poorly defined and recent work suggests controversial interpretations (see associated section above). There is more consensus that the Andes formed a low elevated range at 60 Ma, but more debate on the more recent evolution.

Finally, the combination of available data makes depicting uncertainties in a quantitative manner impractical. Although we provide means to assess the data we used, quantification of uncertainty remains a future frontier for paleogeographic research.

5.3. Potential improvements and expected progress

Potential improvements should focus on topographic reconstructions that are the biggest source of uncertainty. Our general approach following previous work (Baatsen et al., 2016) has been to rotate modern topography to its past position and modify it according to geological data. This implies that our reconstructions may bear features that should not be there, especially in areas that have not been worked on in detail or that are lacking relevant data. We have concentrated here on the main orogenic regions in the considered timeslices but still left out many that will require updates (e.g. Australia, Southeast Asia, the western Pacific rim, the Caribbean region, the Mediterranean region, and the NW Pacific and Aleutian basin). We hope our effort will spark collaborations with geologist experts in these regions that could provide valuable feedback. To stimulate this exchange we offer the reconstructions through a platform containing interactive paleogeographic tools associated with this publication (https://map.paleoenvironment.eu/). The tool consists currently of interactive maps, which can be zoomed, panned in different projections and downloaded in different formats (image or raster data). It is foreseen to be extended with other tools that aid constructing paleogeographic reconstructions (Ruiz et al., 2020).

In the areas we considered in detail, we generated new topography by simply increasing or decreasing linearly the modern digital elevations models (DEMs), sometimes radically to fully form or obliterate mountain ranges (e.g. in Africa). Resulting topographies usually yield unrealistic relief and drainage patterns, thus limiting the applicability of the reconstructions. This can be improved by developing more advanced tools enabling to generate various types of topographies (basins and mountains) with more realistic drainages based on simple governing physics such as the stream power laws (e.g. Braun and Willett, 2013; Cordonnier et al., 2019; Ruiz-Villanueva et al., 2019). Furthermore, rather than modifying modern DEMs, topographic features may be fully generated based on geodynamic setting and surface processes, in turn constrained by geologic data (e.g. Frigola et al., 2018; Sewall and Sloan, 2006; van der Linden et al., 2020).

As part of a continuous collaborative effort building paleogeographies and associated databases, we foresee that the addition and consideration of more and new data reconstructed to its past position with dedicated reconstruction tools (Baatsen et al., 2016; Ruiz et al., 2020; van der Linden et al., 2020) will certainly help to define more comprehensive, accurate and reliable paleoDEMs. The development and comparison of more reconstructions at different time slices, increasing the resolution in the Cenozoic and going further back in time, will necessarily add relevant data for a continuous and integrative overview of paleotopographies. In particular, the formation of features in the distant past that are potentially preserved 10^7 to 10^8 yrs. such as rift margins and orogenies. Another high potential approach, is using sedimentary budgets to estimate paleoreliefs (e.g. Baby et al., 2020; Roberts

and White, 2010; Yuan et al., 2019). A related aspect is the reconstruction of shelf and deep marine bathymetry and how they were influenced by terrestrial drainages. Considerable progress may be achieved with these additional constraints and tools acknowledging that they also require ground proofing from the sort of data provided in the present study.

6. Conclusion

We produced a set of global Cenozoic paleogeographic maps at 60, 40 and 20 Ma following a systematic approach based on a coherent plate tectonic model. These reconstructions are primarily designed to provide boundary conditions for regional and global climate models to test and explore Cenozoic paleoclimate. In particular, our paleogeographic maps show that emerged land surface areas increased by 30% and shifted from a low- to a high-relief regime in northern low latitudes between 60 and 20 Ma. These two processes are likely significant enough to partly contribute to the Cenozoic atmospheric CO_2 drawdown; our paleogeographic maps, in combination with carbon cycle models, provide key boundary conditions to test these mechanisms.

To take into account current paleogeographic controversies on the Indo-Asia collision, we provide four sets of reconstructions covering different tectonic scenarios at 60 and 40 Ma. Creating different paleoDEMs for competing tectonic models may contribute to resolve controversies by exploring their respective implications on climate, mantle dynamics, or paleobiodiversity that can be tested by field data and models. For example, climate models using various paleoDEM will result in different patterns of Asian monsoons and aridification that can be compared to paleoenvironmental proxy records. Thereby, paleoDEMs may ultimately improve our understanding of the underlying surface and tectonic processes that helped to build the past relief of the Earth.

This work builds on a wealth of previously published paleogeographic maps (e.g., Baatsen et al., 2016; Blakey, 2011; Golonka et al., 2006; Popov et al., 2004; Scotese, 2001; Scotese and Golonka, 1997) and an extensive review of geological constraints, with as a novelty to provide them as a consultable interactive database (https://map.paleoenvironment.eu/). Our global compilation approach is naturally bound to oversee important regions of the world, miss large portions of the literature, key datasets and even methods; we view this effort as another step of a long-term work to improve paleoDEMs through geological time. Paleotopographic maps are necessarily products of a collaborative effort, and these sets of maps are a starting point for future improvements. We plan to achieve this with regular updates on results and methods relayed on an interactive platform that will, hopefully, promote collaborations with regional experts and generate open source paleogeographic resources. We therefore do not consider the resulting paleoDEMs as comprehensive representations but rather as works in progress, especially given that this first publication will be revised and improved as new data comes available.

Declaration of Competing Interest

None.

Acknowledgments

This work was supported by the European Research Council's consolidator grant MAGIC (Monsoons in Asia caused Greenhouse to Icehouse Cooling) no. 649081. We thank Yannick Donnadieu, Pierre Sepulchre and Marc Jolivet for fruitful discussions. Finally, we thank three anonymous reviewers and editor Dr. Fielding for detailed and constructive reviews.

Appendix A. Supplementary data

Supplementary data to this article can be found online at https://doi.org/10.1016/j.earscirev.2021.103508.

References

Abouessa, A., Duringer, P., Schuster, M., Pelletier, J., Rubino, J.-L., 2014. Small-scale sedimentary structures and their implications in recognizing large-scale ancient tidal bedforms. Example from Dur At Talah outcrop, Late Eocene, Sirt Basin, Libya. J. Afr. Earth Sci. 100, 346–364. https://doi.org/10.1016/j.jafrearsci.2014.07.008.

Agard, P., Jolivet, L., Vrielynck, B., Burov, E., Monié, P., 2007. Plate acceleration: the obduction trigger? Earth Planet. Sci. Lett. 258, 428–441. https://doi.org/10.1016/j.epsl.2007.04.002.

Aitchison, J.C., Ali, J.R., Davis, A.M., 2007. When and where did India and Asia collide? J. Geophys. Res. 112, B05423 https://doi.org/10.1029/2006JB004706.

Akhmetiev, M.A., 2007. Paleocene and Eocene floras of Russia and adjacent regions: climatic conditions of their development. Paleontol. J. 41, 1032–1039. https://doi.org/10.1134/S0031030107110020.

Akhmetiev, M.A., Zaporozhets, N.I., Benyamovskiy, V.N., Aleksandrova, G.N., Iakovleva, A.I., Oreshkina, T.V., 2012. The Paleogene history of the Western Siberian seaway-a connection of the Peri-Tethys to the Arctic ocean. Aust. J. Earth Sci. 105.

Allmendinger, R.W., Judge, P., 2013. Stratigraphic uncertainty and errors in shortening from balanced sections in the North American Cordillera. Geol. Soc. Am. Bull. 125, 1569–1579. https://doi.org/10.1130/B30871.1.

Alvarez-Marrón, J., McClay, K., Harambour, S., Rojas, L., Skarmeta, J., 1993. Geometry and evolution of the frontal part of the Magallanes foreland thrust and fold belt (Vicuna area), Tierra del Fuego, southern Chile. AAPG Bull. 77, 1904–1921. https://doi.org/10.1306/BDFF8F74-1718-11D7-8645000102C1865D.

Amilibia, A., Sàbat, F., McClay, K.R., Muñoz, J.A., Roca, E., Chong, G., 2008. The role of inherited tectono-sedimentary architecture in the development of the central Andean mountain belt: insights from the Cordillera de Domeyko. J. Struct. Geol. 30, 1520–1539. https://doi.org/10.1016/j.jsg.2008.08.005.

Anagnostou, E., John, E.H., Edgar, K.M., Foster, G.L., Ridgwell, A., Inglis, G.N., Pancost, R.D., Lunt, D.J., Pearson, P.N., 2016. Changing atmospheric CO2 concentration was the primary driver of early Cenozoic climate. Nature 533, 380–384. https://doi.org/10.1038/nature17423.

Armstrong, R.L., 1968. Sevier orogenic belt in Nevada and Utah. Geol. Soc. Am. Bull. 79, 429–458. https://doi.org/10.1130/0016-7606(1968)79[429:SOBINA]2.0.CO;2.

Arriagada, C., Roperch, P., Mpodozis, C., Cobbold, P.R., 2008. Paleogene building of the Bolivian Orocline: tectonic restoration of the central Andes in 2-D map view. Tectonics 27. https://doi.org/10.1029/2008TC002269 n/a-n/a.

Arriagada, C., Ferrando, R., Córdova, L., Morata, D., Roperch, P., 2013. The Maipo Orocline: a first scale structural feature in the Miocene to Recent geodynamic evolution in the central Chilean Andes. Andean Geol. 40. https://doi.org/10.5027/andgeoV40n3-a02.

Atwater, T., 1970. Implications of plate tectonics for the Cenozoic tectonic evolution of western North America. Geol. Soc. Am. Bull. 81, 3513–3536. https://doi.org/10.1130/0016-7606(1970)81[3513:IOPTFT]2.0.CO;2.

Baatsen, M., Van Hinsbergen, D.J.J., von der Heydt, A.S., Dijkstra, H.A., Sluijs, A., Abels, H.A., Bijl, P.K., 2016. Reconstructing geographical boundary conditions for palaeoclimate modelling during the Cenozoic. Clim. Past 12, 1635–1644. https://doi.org/10.5194/cp-12-1635-2016.

Baatsen, M., von der Heydt, A.S., Huber, M., Kliphuis, M.A., Bijl, P.K., Sluijs, A., Dijkstra, H.A., 2020. The middle-to-late Eocene greenhouse climate, modelled using the CESM 1.0.5. Clim. Past Discuss. 2020, 1–44. https://doi.org/10.5194/cp-2020-29.

Baby, G., Guillocheau, F., Boulogne, C., Robin, C., Dall'Asta, M., 2018a. Uplift history of a transform continental margin revealed by the stratigraphic record: the case of the Agulhas transform margin along the Southern African Plateau. Tectonophysics 731–732, 104–130. https://doi.org/10.1016/j.tecto.2018.03.014.

Baby, G., Guillocheau, F., Morin, J., Ressouche, J., Robin, C., Broucke, O., Dall'Asta, M., 2018b. Post-rift stratigraphic evolution of the Atlantic margin of Namibia and South Africa: implications for the vertical movements of the margin and the uplift history of the South African Plateau. Mar. Pet. Geol. 97, 169–191. https://doi.org/10.1016/j.marpetgeo.2018.06.030.

Baby, G., Guillocheau, F., Braun, J., Robin, C., Dall'Asta, M., 2020. Solid sedimentation rates history of the Southern African continental margins: implications for the uplift history of the South African Plateau. Terra Nova 32, 53–65. https://doi.org/10.1111/ter.12435.

Balestrieri, M.L., Moratti, G., Bigazzi, G., Algouti, A., 2009. Neogene exhumation of the Marrakech High Atlas (Morocco) recorded by apatite fission-track analysis. Terra Nova 21, 75–82. https://doi.org/10.1111/j.1365-3121.2008.00857.x.

Barbeau, D.L., Olivero, E.B., Swanson-Hysell, N.L., Zahid, K.M., Murray, K.E., Gehrels, G. E., 2009. Detrital-zircon geochronology of the eastern Magallanes foreland basin: implications for Eocene kinematics of the northern Scotia Arc and Drake Passage. Earth Planet. Sci. Lett. 284, 489–503. https://doi.org/10.1016/j.epsl.2009.05.014.

Barker, P.F., 2001. Scotia Sea regional tectonic evolution: implications for mantle flow and palaeocirculation. Earth Sci. Rev. 55, 1–39. https://doi.org/10.1016/S0012-8252(01)00055-1.

Barker, P.F., Burrell, J., 1977. The opening of Drake Passage. Mar. Geol. 25, 15–34. https://doi.org/10.1016/0025-3227(77)90045-7.

Barker, P.F., Thomas, E., 2004. Origin, signature and palaeoclimatic influence of the Antarctic Circumpolar Current. Earth Sci. Rev. 66, 143–162. https://doi.org/10.1016/j.earscirev.2003.10.003.

Barrier, E., Vrielynck, B., Brouillet, J., Brunet, M., 2018. Paleotectonic reconstruction of the central tethyan realm. tectonono-sedimentary-palinspastic maps from late Permian to Pliocene. In: CCGM/CGMW, Paris, Atlas of 20.

Barron, E.J., Washington, W.M., 1984. The role of geographic variables in explaining paleoclimates: Results from Cretaceous climate model sensitivity studies. J. Geophys. Res.-Atmos. 89, 1267–1279. https://doi.org/10.1029/JD089iD01p01267.
Bartol, J., Govers, R., 2014. A single cause for uplift of the Central and Eastern Anatolian plateau? Tectonophysics 637, 116–136. https://doi.org/10.1016/j.tecto.2014.10.002.
Beauvais, A., Chardon, D., 2013. Modes, tempo, and spatial variability of Cenozoic cratonic denudation: the West African example. Geochem. Geophys. Geosyst. 14, 1590–1608. https://doi.org/10.1002/ggge.20093.
Bechtel, T.D., Forsyth, D.W., Swain, C.J., 1987. Mechanisms of isostatic compensation in the vicinity of the East African Rift, Kenya. Geophys. J. Int. 90, 445–465. https://doi.org/10.1111/j.1365-246X.1987.tb00734.x.
Beck, M., Burmester, R., Engebretson, D.C., Schoonover, R., 1981. Northward translation of Mesozoic batholiths, western North America: paleomagnetic evidence and tectonic significance. Geofis. Int. 20, 143–162.
Berggren, W.A., Hollister, C.D., 1974. Paleogeography, Paleobiogeography and the History of Circulation in the Atlantic Ocean.
Bernard, T., Steer, P., Gallagher, K., Szulc, A., Whitham, A., Johnson, C., 2016. Evidence for Eocene–Oligocene glaciation in the landscape of the East Greenland margin. Geology 44, 895–898. https://doi.org/10.1130/G38248.1.
Berner, R.A., Kothavala, Z., 2001. GEOCARB III: a revised model of atmospheric CO2 over Phanerozoic time. Am. J. Sci. 301, 182–204. https://doi.org/10.2475/ajs.301.2.182.
Besse, J., Courtillot, V., 2002. Apparent and true polar wander and the geometry of the geomagnetic field over the last 200 Myr: APPARENT AND TRUE POLAR WANDER. J. Geophys. Res. 107 https://doi.org/10.1029/2000JB000050. EPM 6-1-EPM 6–31.
Betka, P., Klepeis, K., Mosher, S., 2015. Along-strike variation in crustal shortening and kinematic evolution of the base of a retroarc fold-and-thrust belt: Magallanes, Chile 53°S-54°S. Geol. Soc. Am. Bull. B31130, 1. https://doi.org/10.1130/B31130.1.
Bice, K.L., Barron, E.J., Peterson, W.H., 1998. Reconstruction of realistic early Eocene paleobathymetry and ocean GCM sensitivity to specified basin configuration. Oxf. Monogr. Geol. Geophys. 39, 227–250.
Bird, P., 2003. An updated digital model of plate boundaries. Geochem. Geophys. Geosyst. 4 https://doi.org/10.1029/2001GC000252.
Birkenmajer, K., Zastawniak, E., 1989. Late Cretaceous-early Tertiary floras of King George Island, West Antarctica: their stratigraphic distribution and palaeoclimatic significance. Geol. Soc. Lond., Spec. Publ. 47, 227–240. https://doi.org/10.1144/GSL.SP.1989.047.01.17.
Blakey, R.C., 2008. Gondwana paleogeography from assembly to breakup—A 500 m.y. odyssey. In: Special Paper 441: Resolving the Late Paleozoic Ice Age in Time and Space. Geological Society of America, pp. 1–28. https://doi.org/10.1130/2008.2441(01.
Blakey, R., 2011. Global paleogeography. NAU Geol.
Blakey, R.C., Ranney, W.D., 2017. Ancient Landscapes of Western North America: A Geologic History with Paleogeographic Maps. Springer. https://doi.org/10.1007/978-3-319-59636-5.
Bosboom, R., Abels, H.A., Hoorn, C., Van den Berg, B.C.J., Guo, Z., Dupont-Nivet, G., 2014a. Aridification in continental Asia after the Middle Eocene Climatic Optimum (MECO). Earth Planet. Sci. Lett. 389, 34–42. https://doi.org/10.1016/j.epsl.2013.12.014.
Bosboom, R., Dupont-Nivet, G., Huang, W., Yang, W., Guo, Z., 2014b. Oligocene clockwise rotations along the eastern Pamir: Tectonic and paleogeographic implications: oligocene clockwise rotations east Pamir. Tectonics 33, 53–66. https://doi.org/10.1002/2013TC003388.
Bosboom, R., Mandic, O., Dupont-Nivet, G., Proust, J.-N., Ormukov, C., Aminov, J., 2017. Late Eocene palaeogeography of the proto-Paratethys Sea in Central Asia (NW China, southern Kyrgyzstan and SW Tajikistan). Geol. Soc. Lond., Spec. Publ. 427, 565–588. https://doi.org/10.1144/SP427.11.
Boschman, L.M., Van Hinsbergen, D.J.J., Torsvik, T.H., Spakman, W., Pindell, J.L., 2014. Kinematic reconstruction of the Caribbean region since the Early Jurassic. Earth Sci. Rev. 138, 102–136. https://doi.org/10.1016/j.earscirev.2014.08.007.
Boschman, L.M., Wiel, E., Flores, K.E., Langereis, C.G., Hinsbergen, D.J.J., 2019. The Caribbean and Farallon plates connected: constraints from stratigraphy and paleomagnetism of the Nicoya Peninsula, Costa Rica. J. Geophys. Res. Solid Earth 124, 6243–6266. https://doi.org/10.1029/2018JB016369.
Botsyun, S., Sepulchre, P., Risi, C., Donnadieu, Y., 2016. Impacts of Tibetan Plateau uplift on atmospheric dynamics and associated precipitation δ 18 O. Clim. Past 12, 1401–1420. https://doi.org/10.5194/cp-12-1401-2016.
Botsyun, S., Sepulchre, P., Donnadieu, Y., Risi, C., Licht, A., Caves Rugenstein, J.K., 2019. Revised paleoaltimetry data show low Tibetan Plateau elevation during the Eocene. Science 363. https://doi.org/10.1126/science.aaq1436 eaaq1436.
Boyden, J.A., Müller, R.D., Gurnis, M., Torsvik, T.H., Clark, J.A., Turner, M., Ivey-Law, H., Watson, R.J., Cannon, J.S., 2011. Next-Generation Plate-Tectonic Reconstructions using GPlates. https://doi.org/10.1017/CBO9780511976308.008.
Braun, J., 2010. The many surface expressions of mantle dynamics. Nat. Geosci. 3, 825–833. https://doi.org/10.1038/ngeo1020.
Braun, J., Willett, S.D., 2013. A very efficient O(n), implicit and parallel method to solve the stream power equation governing fluvial incision and landscape evolution. Geomorphology 180–181, 170–179. https://doi.org/10.1016/j.geomorph.2012.10.008.
Breitsprecher, K., Mortensen, J., 2004. BCAge 2004A-1-a database of isotopic age determinations for rock units from British Columbia. British Columbia Ministry of Energy, Mines and Petroleum Resources Open-File (2004–03).
Brown, C., Girdler, R., 1980. Interpretation of African gravity and its implication for the breakup of the continents. J. Geophys. Res. Solid Earth 85, 6443–6455, 10.1029/JB085iB11p06443.
Bruce, R.M., Nelson, E.P., Weaver, S.G., Lux, D.R., 1991. Temporal and spatial variations in the southern Patagonian batholith; Constraints on magmatic arc development. In: Geological Society of America Special Papers. Geological Society of America, pp. 1–12. https://doi.org/10.1130/SPE265-p1.
Burke, K., Gunnell, Y., 2008. The African Erosion Surface: A Continental-Scale Synthesis of Geomorphology, Tectonics, and Environmental Change over the Past 180 Million Years. Memoir, Geological Society of America.
Butler, R.F., Gehrels, G.E., McClelland, W.C., May, S.R., Klepacki, D., 1989. Discordant paleomagnetic poles from the Canadian Coast Plutonic Complex: regional tilt rather than large-scale displacement? Geology 17, 691–694. https://doi.org/10.1130/0091-7613(1989)017<0691:DPPFTC>2.3.CO;2.
Calderón, M., Fildani, A., Hervé, F., Fanning, C.M., Weislogel, A., Cordani, U., 2007. Late Jurassic bimodal magmatism in the northern sea-floor remnant of the Rocas Verdes basin, southern Patagonian Andes. J. Geol. Soc. 164, 1011–1022. https://doi.org/10.1144/0016-76492006-102.
Calderón, M., Fosdick, J.C., Warren, C., Massonne, H.-J., Fanning, C.M., Cury, L.F., Schwanethal, J., Fonseca, P.E., Galaz, G., Gaytán, D., Hervé, F., 2012. The low-grade Canal de las Montañas Shear Zone and its role in the tectonic emplacement of the Sarmiento Ophiolitic Complex and Late Cretaceous Patagonian Andes orogeny, Chile. Tectonophysics 524–525, 165–185. https://doi.org/10.1016/j.tecto.2011.12.034.
Caminos, R.L., González, P.D., 1997. Mapa Geológico de la República Argentina. Servicio Geológico Minero Argentino, Instituto de Geología y Recursos Minerales.
Canavan, R.R., Carrapa, B., Clementz, M.T., Quade, J., DeCelles, P.G., Schoenbohm, L.M., 2014. Early Cenozoic uplift of the Puna Plateau, Central Andes, based on stable isotope paleoaltimetry of hydrated volcanic glass. Geology 42, 447–450. https://doi.org/10.1130/G35239.1.
Carey, S., 1958. The tectonic approach to continental drift, Continental Drift: A Symposium, 177–355. Hobart, Tasmania.
Carrapa, B., DeCelles, P.G., 2015. Regional exhumation and kinematic history of the central Andes in response to cyclical orogenic processes, in: Geodynamics of a Cordilleran Orogenic System: the Central Andes of Argentina and Northern Chile. Geol. Soc. Am. https://doi.org/10.1130/2015.1212(11.
Cather, S.M., Chapin, C.E., Kelley, S.A., 2012. Diachronous episodes of Cenozoic erosion in southwestern North America and their relationship to surface uplift, paleoclimate, paleodrainage, and paleoaltimetry. Geosphere 8, 1177–1206. https://doi.org/10.1130/GES00801.1.
Caves, J.K., Jost, A.B., Lau, K.V., Maher, K., 2016. Cenozoic carbon cycle imbalances and a variable weathering feedback. Earth Planet. Sci. Lett. 450, 152–163. https://doi.org/10.1016/j.epsl.2016.06.035.
Caves-Rugenstein, J.K.C., Ibarra, D.E., von Blanckenburg, F., 2019. Neogene cooling driven by land surface reactivity rather than increased weathering fluxes. Nature 571, 99–102. https://doi.org/10.1038/s41586-019-1332-y.
Chamberlain, C.P., Mix, H.T., Mulch, A., Hren, M.T., Kent-Corson, M.L., Davis, S.J., Horton, T.W., Graham, S.A., 2012. The Cenozoic climatic and topographic evolution of the western North American Cordillera. Am. J. Sci. 312, 213–262. https://doi.org/10.2475/02.2012.05.
Chapman, J.B., Kapp, P., 2017. Tibetan Magmatism Database. Geochem. Geophys. Geosyst. 18, 4229–4234. https://doi.org/10.1002/2017GC007217.
Chapman, J.B., Greig, R., Haxel, G.B., 2020. Geochemical evidence for an orogenic plateau in the southern U.S. and northern Mexican Cordillera during the Laramide orogeny. Geology 48, 164–168. https://doi.org/10.1130/G47117.1.
Chardon, D., Grimaud, J.-L., Rouby, D., Beauvais, A., Christophoul, F., 2016. Stabilization of large drainage basins over geological time scales: Cenozoic West Africa, hot spot swell growth, and the Niger River. Geochem. Geophys. Geosyst. 17, 1164–1181. https://doi.org/10.1002/2015GC006169.
Charrier, R., Pinto, L., Rodríguez, M.P., 2007. Tectonostratigraphic evolution of the Andean Orogen in Chile. In: The Geology of Chile. Geological Society Special Publication.
Charrier, R., Farías, M., Maksaev, V., 2009. Evolución tectónica, paleogeográfica y metalogénica durante el Cenozoico en los Andes de Chile norte y central e implicaciones para las regiones adyacentes de Bolivia y Argentina. Rev. Asoc. Geol. Argent. 65, 05–35.
Charrier, R., Hérail, G., Pinto, L., García, M., Riquelme, R., Farías, M., Muñoz, N., 2013. Cenozoic tectonic evolution in the Central Andes in northern Chile and west central Bolivia: implications for paleogeographic, magmatic and mountain building evolution. Int. J. Earth Sci. (Geol. Rundsch) 102, 235–264. https://doi.org/10.1007/s00531-012-0801-4.
Cheng, F., Garzione, C.N., Jolivet, M., Guo, Z., Zhang, D., Zhang, C., Zhang, Q., 2019. Initial deformation of the Northern Tibetan Plateau: insights from deposition of the Lulehe formation in the Qaidam Basin. Tectonics 38, 741–766. https://doi.org/10.1029/2018TC005214.
Choukroune, P., 1992. Tectonic evolution of the Pyrenees. Annu. Rev. Earth Planet. Sci. 20, 143–158. https://doi.org/10.1146/annurev.ea.20.050192.001043.
Chung-Hwa, P., Tamaki, K., Kobayashi, K., 1990. Age-depth correlation of the Philippine Sea back-arc basins and other marginal basins in the world. Tectonophysics 181, 351–371.
Clift, P.D., Hodges, K.V., Heslop, D., Hannigan, R., Van Long, H., Calves, G., 2008. Correlation of Himalayan exhumation rates and Asian monsoon intensity. Nat. Geosci. 1, 875–880. https://doi.org/10.1038/ngeo351.
Clyde, W.C., Khan, I.H., Gingerich, P.D., 2003. Stratigraphic response and mammalian dispersal during initial India-Asia collision: evidence from the Ghazij Formation, Balochistan, Pakistan. Geology 31, 1097–1100. https://doi.org/10.1130/G19956.1.
Cogné, N., Gallagher, K., Cobbold, P.R., 2011. Post-rift reactivation of the onshore margin of southeast Brazil: evidence from apatite (U–Th)/He and fission-track data. Earth Planet. Sci. Lett. 309, 118–130. https://doi.org/10.1016/j.epsl.2011.06.025.

Cogné, N., Gallagher, K., Cobbold, P.R., Riccomini, C., Gautheron, C., 2012. Post-breakup tectonics in southeast Brazil from thermochronological data and combined inverse-forward thermal history modeling. J. Geophys. Res. 117 https://doi.org/10.1029/2012JB009340 n/a-n/a.

Cogné, J.-P., Besse, J., Chen, Y., Hankard, F., 2013. A new Late Cretaceous to Present APWP for Asia and its implications for paleomagnetic shallow inclinations in Central Asia and Cenozoic Eurasian plate deformation. Geophys. J. Int. 192, 1000–1024. https://doi.org/10.1093/gji/ggs104.

Colpron, M., Nelson, J., Murphy, D.C., 2007. Northern Cordilleran terranes and their interactions through time. GSA Today 17, 4.

Coney, P.J., 1972. Cordilleran tectonics and North America plate motion. Am. J. Sci. 272, 603–628. https://doi.org/10.2475/ajs.272.7.603.

Coney, P., 1976. Plate tectonics and the Laramide orogeny. In: Tectonics and Mineral Resources of Southwestern North America. New Mexico Geol. Soc. Special Publication, pp. 5–10.

Copeland, P., Currie, C.A., Lawton, T.F., Murphy, M.A., 2017. Location, location, location: the variable lifespan of the Laramide orogeny. Geology 45, 223–226. https://doi.org/10.1130/G38810.1.

Cordonnier, G., Bovy, B., Braun, J., 2019. A Versatile, Linear Complexity Algorithm for Flow Routing in Topographies with Depressions. https://doi.org/10.5194/esurf-2018-81.

Cosentino, D., Schildgen, T.F., Cipollari, P., Faranda, C., Gliozzi, E., Hudackova, N., Lucifora, S., Strecker, M.R., 2012. Late Miocene surface uplift of the southern margin of the Central Anatolian Plateau, Central Taurides, Turkey. Geol. Soc. Am. Bull. 124, 133–145. https://doi.org/10.1130/B30466.1.

Cowan, D., 1994. Alternative hypotheses for the mid-Cretaceous paleogeography of the western Cordillera. GSA Today 4, 181–186.

Coxall, H.K., Wilson, P.A., Pälike, H., Lear, C.H., Backman, J., 2005. Rapid stepwise onset of Antarctic glaciation and deeper calcite compensation in the Pacific Ocean. Nature 433, 53. https://doi.org/10.1038/nature03135.

Cunningham, W.D., Klepeis, K.A., Gose, W.A., Dalziel, I.W.D., 1991. The Patagonian Orocline: New paleomagnetic data from the Andean magmatic arc in Tierra del Fuego, Chile. J. Geophys. Res. 96, 16061. https://doi.org/10.1029/91JB01498.

Currie, B.S., Polissar, P.J., Rowley, D.B., Ingalls, M., Li, S., Olack, G., Freeman, K.H., 2016. Multiproxy paleoaltimetry of the Late Oligocene-Pliocene Oiyug Basin, southern Tibet. Am. J. Sci. 316, 401–436. https://doi.org/10.2475/05.2016.01.

Cyr, A.J., Currie, B.S., Rowley, D.B., 2005. Geochemical evaluation of Fenghuoshan Group Lacustrine Carbonates, North-Central Tibet: implications for the Paleoaltimetry of the Eocene Tibetan Plateau. J. Geol. 113, 517–533. https://doi.org/10.1086/431907.

Dai, J., Fox, M., Shuster, D.L., Hourigan, J., Han, X., Li, Y., Wang, C., 2019. Burial and exhumation of the Hoh Xil Basin, northern Tibetan Plateau: constraints from detrital (U-Th)/He ages. Basin Res. Bre 12405. https://doi.org/10.1111/bre.12405.

Dalziel, I., Kligfield, R., Lowrie, W., Opdyke, N., 1973. Paleomagnetic data from the southernmost Andes and the Antarctandes. In: Tarling, D.H., Runcorn, S.K. (Eds.), Implications of Continental Drift to the Earth Sciences. Academic, New York, pp. 87–101.

Dalziel, I.W., Lawver, L.A., Norton, I.O., Gahagan, L.M., 2013. The Scotia Arc: genesis, evolution, global significance. Annu. Rev. Earth Planet. Sci. 41 https://doi.org/10.1146/annurev-earth-050212-124155.

Dauteuil, O., Bouffette, J., Toteu, F., de Lamotte, D.F., Bracken, A., 2009. The Changing Faces of Africa: Elements of African Geology (Commission for the Geological Map of the World).

DeCelles, P.G., 2004. Late Jurassic to Eocene evolution of the Cordilleran thrust belt and foreland basin system, western U.S.A. Am. J. Sci. 304, 105–168. https://doi.org/10.2475/ajs.304.2.105.

DeCelles, P.G., Kapp, P., Gehrels, G.E., Ding, L., 2014. Paleocene-Eocene foreland basin evolution in the Himalaya of southern Tibet and Nepal: implications for the age of initial India-Asia collision: Paleogene Himalayan foreland basin. Tectonics 33, 824–849. https://doi.org/10.1002/2014TC003522.

DeCelles, P.G., Castañeda, I.S., Carrapa, B., Liu, J., Quade, J., Leary, R., Zhang, L., 2018. Oligocene-Miocene Great Lakes in the India-Asia Collision Zone. Basin Res. 30, 228–247. https://doi.org/10.1111/bre.12217.

DeConto, R.M., Pollard, D., 2003. Rapid Cenozoic glaciation of Antarctica induced by declining atmospheric CO2. Nature 421, 245–249. https://doi.org/10.1038/nature01290.

DeConto, R.M., Pollard, D., Wilson, P.A., Pälike, H., Lear, C.H., Pagani, M., 2008. Thresholds for Cenozoic bipolar glaciation. Nature 455, 652. https://doi.org/10.1038/nature07337.

Dedow, R., Franz, M., Szulc, A., Schneider, J.W., Brückner, J., Ratschbacher, L., Gągała, Ł., Ringenbach, J.-C., Rajabov, N., Gadoev, M., Oimahmadov, I., 2020. Tajik Basin and Southwestern Tian Shan, Northwestern India-Asia Collision Zone: 3. Pre- to Syn-orogenic Retro-foreland Basin evolution in the Eastern Tajik Depression and Linkage to the Pamir Hinterland. Tectonics. https://doi.org/10.1029/2019TC005874 e2019TC005874.

Deng, T., Wang, X., Wu, F., Wang, Y., Li, Q., Wang, S., Hou, S., 2019. Review: implications of vertebrate fossils for paleo-elevations of the Tibetan Plateau. Glob. Planet. Chang. 174, 58–69. https://doi.org/10.1016/j.gloplacha.2019.01.005.

Densmore, M.S., Ehlers, T.A., Woodsworth, G.J., 2007. Effect of Alpine glaciation on thermochronometer age-elevation profiles. Geophys. Res. Lett. 34, L02502 https://doi.org/10.1029/2006GL028371.

Dercourt, J., Gaetani, M., Vrielynck, B., Barrier, E., Biju-Duval, B., Brunet, M., Cadet, J., Crasquin, S., Sandulescu, M., 2000. Peri-Tethys Atlas. CCGM/CGMW, Paris: 24 Maps and Explanatory Notes (269 pp).

Dewey, J.F., Helman, M.L., Knott, S.D., Turco, E., Hutton, D.H.W., 1989. Kinematics of the western Mediterranean. Geol. Soc. Lond., Spec. Publ. 45, 265–283. https://doi.org/10.1144/GSL.SP.1989.045.01.15.

Dickinson, W.R., Snyder, W.S., 1978. Plate tectonics of the Laramide orogeny. In: Geological Society of America Memoirs. Geological Society of America, pp. 355–366. https://doi.org/10.1130/MEM151-p355.

Ding, L., Xu, Q., Yue, Y., Wang, H., Cai, F., Li, S., 2014. The Andean-type Gangdese Mountains: paleoelevation record from the Paleocene–Eocene Linzhou Basin. Earth Planet. Sci. Lett. 392, 250–264. https://doi.org/10.1016/j.epsl.2014.01.045.

Ding, L., Spicer, R.A., Yang, J., Xu, Q., Cai, F., Li, S., Lai, Q., Wang, H., Spicer, T.E.V., Yue, Y., Shukla, A., Srivastava, G., Khan, M.A., Bera, S., Mehrotra, R., 2017. Quantifying the rise of the Himalaya orogen and implications for the South Asian monsoon. Geology 45, 215–218. https://doi.org/10.1130/G38583.1.

Domeier, M., Shephard, G.E., Jakob, J., Gaina, C., Doubrovine, P.V., Torsvik, T.H., 2017. Intraoceanic subduction spanned the Pacific in the Late Cretaceous–Paleocene. Sci. Adv. 3 https://doi.org/10.1126/sciadv.aao2303 eaao2303.

Doubrovine, P.V., Steinberger, B., Torsvik, T.H., 2012. Absolute plate motions in a reference frame defined by moving hot spots in the Pacific, Atlantic, and Indian oceans. J. Geophys. Res. 117 https://doi.org/10.1029/2011JB009072.

Dupont-Nivet, G., Krijgsman, W., Langereis, C.G., Abels, H.A., Dai, S., Fang, X., 2007. Tibetan plateau aridification linked to global cooling at the Eocene–Oligocene transition. Nature 445, 635–638. https://doi.org/10.1038/nature05516.

Dupont-Nivet, G., Lippert, P.C., Van Hinsbergen, D.J.J., Meijers, M.J.M., Kapp, P., 2010. Palaeolatitude and age of the Indo-Asia collision: palaeomagnetic constraints. Geophys. J. Int. 182, 1189–1198. https://doi.org/10.1111/j.1365-246X.2010.04697.x.

Eagles, G., Jokat, W., 2014. Tectonic reconstructions for paleobathymetry in Drake Passage. Tectonophysics 611, 28–50. https://doi.org/10.1016/j.tecto.2013.11.021.

Echaurren, A., Folguera, A., Gianni, G., Orts, D., Tassara, A., Encinas, A., Giménez, M., Valencia, V., 2016. Tectonic evolution of the North Patagonian Andes (41°–44° S) through recognition of syntectonic strata. Tectonophysics 677–678, 99–114. https://doi.org/10.1016/j.tecto.2016.04.009.

Ehlers, T.A., Poulsen, C.J., 2009. Influence of Andean uplift on climate and paleoaltimetry estimates. Earth Planet. Sci. Lett. 281, 238–248.

Eichelberger, N., McQuarrie, N., 2015. Kinematic reconstruction of the Bolivian orocline. Geosphere 11, 445–462. https://doi.org/10.1130/GES01064.1.

English, J.M., Johnston, S.T., 2004. The Laramide Orogeny: what were the driving forces? Int. Geol. Rev. 46, 833–838. https://doi.org/10.2747/0020-6814.46.9.833.

English, K.L., Redfern, J., Bertotti, G., English, J.M., Yahia Cherif, R., 2017. Intraplate uplift: new constraints on the Hoggar dome from the Illizi basin (Algeria). Basin Res. 29, 377–393. https://doi.org/10.1111/bre.12182.

Enkin, R.J., Johnston, S.T., Larson, K.P., Baker, J., Haggart, J., Monger, J., 2006. Paleomagnetism of the 70 Ma Carmacks Group at Solitary Mountain, Yukon, confirms and extends controversial results: Further evidence for the Baja British Columbia model. Geol. Assoc. Can. Spec. Pap. 46, 221–232.

Fan, M., Dettman, D.L., 2009. Late Paleocene high Laramide ranges in northeast Wyoming: oxygen isotope study of ancient river water. Earth Planet. Sci. Lett. 286, 110–121. https://doi.org/10.1016/j.epsl.2009.06.024.

Fenneman, N.M., 1931. Physiography of Western United States. McGraw-Hill, New York, New York, USA.

Fernández-Blanco, D., Bertotti, G., Aksu, A., Hall, J., 2019. Monoclinal flexure of an orogenic plateau margin during subduction, south Turkey. Basin Res. 31, 709–727. https://doi.org/10.1111/bre.12341.

Fitzgerald, P., 2002. Tectonics and landscape evolution of the Antarctic plate since the breakup of Gondwana, with an emphasis on the West Antarctic Rift System and the Transantarctic Mountains. Royal Soc. New Zealand Bull. 35, 453–469.

Flowers, R., Wernicke, B., Farley, K., 2008. Unroofing, incision, and uplift history of the southwestern Colorado Plateau from apatite (U-Th)/He thermochronometry. Geol. Soc. Am. Bull. 120, 571–587. https://doi.org/10.1130/B26231.1.

Fluteau, F., Ramstein, G., Besse, J., 1999. Simulating the evolution of the Asian and African monsoons during the past 30 Myr using an atmospheric general circulation model. J. Geophys. Res. 104, 11995–12018. https://doi.org/10.1029/1999JD900048.

Folguera, A., Bottesi, G., Duddy, I., Martín-González, F., Orts, D., Sagripanti, L., Rojas Vera, E., Ramos, V.A., 2015. Exhumation of the Neuquén Basin in the southern Central Andes (Malargüe fold and thrust belt) from field data and low-temperature thermochronology. J. S. Am. Earth Sci. 64, 381–398. https://doi.org/10.1016/j.jsames.2015.08.003.

Fosdick, J.C., Romans, B.W., Fildani, A., Bernhardt, A., Calderon, M., Graham, S.A., 2011. Kinematic evolution of the Patagonian retroarc fold-and-thrust belt and Magallanes foreland basin, Chile and Argentina, 51 30'S. Geol. Soc. Am. Bull. 123, 1679–1698. https://doi.org/10.1130/B30242.1.

France-Lanord, C., Derry, L.A., 1997. Organic carbon burial forcing of the carbon cycle from Himalayan erosion. Nature 390, 65–67. https://doi.org/10.1038/36324.

Frigola, A., Prange, M., Schulz, M., 2018. Boundary conditions for the middle Miocene climate transition (MMCT v1. 0). Geosci. Model Dev. 11, 1607–1626. https://doi.org/10.5194/gmd-11-1607-2018.

Frizon de Lamotte, D., Saint Bezar, B., Bracène, R., Mercier, E., 2000. The two main steps of the Atlas building and geodynamics of the western Mediterranean. Tectonics 19, 740–761. https://doi.org/10.1029/2000TC900003.

Frizon de Lamotte, D.F., Leturmy, P., Missenard, Y., Khomsi, S., Ruiz, G., Saddiqi, O., Guillocheau, F., Michard, A., 2009. Mesozoic and Cenozoic vertical movements in the Atlas system (Algeria, Morocco, Tunisia): An overview. Tectonophysics 475, 9–28. https://doi.org/10.1016/j.tecto.2008.10.024.

Furlong, K.P., Schwartz, S.Y., 2004. Influence of the Mendocino triple junction on the tectonics of coastal California. Annu. Rev. Earth Planet. Sci. 32, 403–433. https://doi.org/10.1146/annurev.earth.32.101802.120252.

Gabet, E.J., 2014. Late Cenozoic uplift of the Sierra Nevada, California? A critical analysis of the geomorphic evidence. Am. J. Sci. 314, 1224–1257. https://doi.org/10.2475/08.2014.03.

Gabrielse, H., Murphy, D.C., Mortensen, J.K., Haggart, J., Enkin, R., Monger, J., 2006. Cretaceous and Cenozoic dextral orogen-parallel displacements, magmatism, and paleogeography, north-central Canadian Cordillera. In: Geological Association of Canada Special Paper, 46, pp. 255–276, 255–276 46.

Galindo-Zaldívar, J., Puga, E., Bohoyo, F., González, F.J., Maldonado, A., Martos, Y.M., Pérez, L.F., Ruano, P., Schreider, A.A., Somoza, L., Suriñach, E., de Antonio, D.F., 2014. Reprint of "Magmatism, structure and age of Dove Basin (Antarctica): a key to understanding South Scotia Arc development.". Glob. Planet. Chang. 123, 249–268. https://doi.org/10.1016/j.gloplacha.2014.11.002.

Gallagher, K., Brown, R., 1999. Denudation and uplift at passive margins: the record on the Atlantic Margin of southern Africa. Philosophical Transactions of the Royal Society of London. Series A: Mathematical, Phys. Eng. Sci. 357, 835–859. https://doi.org/10.1098/rsta.1999.0354.

Galy, V., France-Lanord, C., Beyssac, O., Faure, P., Kudrass, H., Palhol, F., 2007. Efficient organic carbon burial in the Bengal fan sustained by the Himalayan erosional system. Nature 450, 407. https://doi.org/10.1038/nature06273.

Galy, V., Peucker-Ehrenbrink, B., Eglinton, T., 2015. Global carbon export from the terrestrial biosphere controlled by erosion. Nature 521, 204–207. https://doi.org/10.1038/nature14400.

Garver, J.I., Davidson, C.M., 2015. Southwestern Laurentian zircons in Upper Cretaceous flysch of the Chugach-Prince William terrane in Alaska. Am. J. Sci. 315, 537–556. https://doi.org/10.2475/06.2015.02.

Garzanti, E., 2019. The Himalayan Foreland Basin from collision onset to the present: a sedimentary–petrology perspective. Geol. Soc. Lond., Spec. Publ. 483, 65–122. https://doi.org/10.1144/SP483.17.

Garzanti, E., Limonta, M., Vezzoli, G., An, W., Wang, J., Hu, X., 2018. Petrology and multimineral fingerprinting of modern sand generated from a dissected magmatic arc (Lhasa River, Tibet). In: Ingersoll, R.V., Lawton, T.F., Graham, S.A. (Eds.), Tectonics, Sedimentary Basins, and Provenance: A Celebration of William R. Dickinson's Career. Geological Society of America, Special Papers, 540, pp. 197–221. https://doi.org/10.1130/2018.2540(09).

Garzione, C.N., Molnar, P., Libarkin, J.C., MacFadden, B.J., 2006. Rapid late Miocene rise of the Bolivian Altiplano: Evidence for removal of mantle lithosphere. Earth Planet. Sci. Lett. 241, 543–556. https://doi.org/10.1016/j.epsl.2005.11.026.

Garzione, C.N., Auerbach, D.J., Jin-Sook Smith, J., Rosario, J.J., Passey, B.H., Jordan, T. E., Eiler, J.M., 2014. Clumped isotope evidence for diachronous surface cooling of the Altiplano and pulsed surface uplift of the Central Andes. Earth Planet. Sci. Lett. 393, 173–181. https://doi.org/10.1016/j.epsl.2014.02.029.

Genik, G.J., 1993. Petroleum geology of Cretaceous-Tertiary Rift Basins in Niger, Chad, and Central African Republic. Bulletin 77. https://doi.org/10.1306/BDFF8EAC-1718-11D7-8645000102C1865D.

Ghosh, P., 2006. Rapid uplift of the Altiplano revealed through 13C-18O bonds in paleosol carbonates. Science 311, 511–515. https://doi.org/10.1126/science.1119365.

Gibbons, A.D., Zahirovic, S., Müller, R.D., Whittaker, J.M., Yatheesh, V., 2015. A tectonic model reconciling evidence for the collisions between India, Eurasia and intra-oceanic arcs of the central-eastern Tethys. Gondwana Res. 28, 451–492. https://doi.org/10.1016/j.gr.2015.01.001.

Gill, A.E., Bryan, K., 1971. Effects of geometry on the circulation of a three-dimensional southern-hemisphere ocean model. Deep-Sea Res. Oceanogr. Abstr. 18, 685–721. https://doi.org/10.1016/0011-7471(71)90086-6.

Goddéris, Y., Donnadieu, Y., Le Hir, G., Lefebvre, V., Nardin, E., 2014. The role of palaeogeography in the Phanerozoic history of atmospheric CO2 and climate. Earth Sci. Rev. 128, 122–138. https://doi.org/10.1016/j.earscirev.2013.11.004.

Goddéris, Y., Donnadieu, Y., Carretier, S., Aretz, M., Dera, G., Macouin, M., Regard, V., 2017. Onset and ending of the late Palaeozoic ice age triggered by tectonically paced rock weathering. Nat. Geosci. 10, 382–386. https://doi.org/10.1038/ngeo2931.

Göğüş, O.H., Pysklywec, R.N., Şengör, A.M.C., Gün, E., 2017. Drip tectonics and the enigmatic uplift of the Central Anatolian Plateau. Nat. Commun. 8, 1538. https://doi.org/10.1038/s41467-017-01611-3.

Golonka, J., Krobicki, M., Pajak, J., Van Giang, N., Zuchiewicz, Z., 2006. Global plate tectonics and paleogeography of Southeast Asia. In: Fac. of Geology, Geophysics and Environmental Protection. AGH Univ. of Science and Technology, Krakow.

Gombosi, D.J., Barbeau Jr., D.L., Garver, J.I., 2009. New thermochronometric constraints on the rapid Palaeogene exhumation of the Cordillera Darwin complex and related thrust sheets in the Fuegian Andes. Terra Nova 21, 507–515. https://doi.org/10.1111/j.1365-3121.2009.00908.x.

Gómez, J., Montes, N.E., Nivia, Á., Diedrix, H., 2015. Atlas Geológico de Colombia, scale 1:1,000,000. Colombian Geological Survay, Bogotá.

Gregory-Wodzicki, K.M., 2000. Relationships between leaf morphology and climate, Bolivia: implications for estimating paleoclimate from fossil floras. Paleobiology 26, 668–688. https://doi.org/10.1666/0094-8373(2000)026<0668:RBLMAC>2.0.CO;2.

Guillocheau, F., Chelalou, R., Linol, B., Dauteuil, O., Robin, C., Mvondo, F., Callec, Y., Colin, J.-P., 2015. Cenozoic landscape evolution in and around the Congo Basin: constraints from sediments and planation surfaces. In: Geology and Resource Potential of the Congo Basin. Springer, pp. 271–313. https://doi.org/10.1007/978-3-642-29482-2_14.

Guillocheau, F., Simon, B., Baby, G., Bessin, P., Robin, C., Dauteuil, O., 2018. Planation surfaces as a record of mantle dynamics: the case example of Africa. Gondwana Res. 53, 82–98. https://doi.org/10.1016/j.gr.2017.05.015.

Guillot, S., Garzanti, E., Baratoux, D., Marquer, D., Mahéo, G., de Sigoyer, J., 2003. Reconstructing the total shortening history of the NW Himalaya. Geochem. Geophys. Geosyst. 4 https://doi.org/10.1029/2002GC000484.

Guilmette, C., Hébert, R., Dostal, J., Indares, A., Ullrich, T., Bédard, É., Wang, C., 2012. Discovery of a dismembered metamorphic sole in the Saga ophiolitic mélange, South Tibet: Assessing an Early Cretaceous disruption of the Neo-Tethyan supra-subduction zone and consequences on basin closing. Gondwana Res. 22, 398–414. https://doi.org/10.1016/j.gr.2011.10.012.

Gürer, D., Van Hinsbergen, D.J.J., 2019. Diachronous demise of the Neotethys Ocean as a driver for non-cylindrical orogenesis in Anatolia. Tectonophysics 760, 95–106. https://doi.org/10.1016/j.tecto.2018.06.005.

Gurnis, M., 1990. Bounds on global dynamic topography from Phanerozoic flooding of continental platforms. Nature 344, 754–756. https://doi.org/10.1038/344754a0.

Gurnis, M., Yang, T., Cannon, J., Turner, M., Williams, S., Flament, N., Müller, R.D., 2018. Global tectonic reconstructions with continuously deforming and evolving rigid plates. Computers & Geosciences 116, 32–41. https://doi.org/10.1016/j.cageo.2018.04.007.

Hartley, A., 2003. Andean uplift and climate change. J. Geol. Soc. 160, 7–10. https://doi.org/10.1144/0016-764902-083.

Haschke, M., Günther, A., Melnick, D., Echtler, H., Reutter, K.-J., Scheuber, E., Oncken, O., 2006. Central and Southern Andean tectonic evolution inferred from arc magmatism. In: Oncken, O., Chong, G., Franz, G., Giese, P., Götze, H.-J., Ramos, V. A., Strecker, M.R., Wigger, P. (Eds.), The Andes, Frontiers in Earth Sciences. Springer, Berlin Heidelberg, pp. 337–353. https://doi.org/10.1007/978-3-540-48684-8_16.

Haxel, G.B., Tosdal, R.M., May, D.J., Wright, J.E., 1984. Latest Cretaceous and early Tertiary orogenesis in south-central Arizona: thrust faulting, regional metamorphism, and granitic plutonism. Geol. Soc. Am. Bull. 95, 631–653. https://doi.org/10.1130/0016-7606(1984)95<631:LCAETO>2.0.CO;2.

Hay, W.W., Wold, C.N., 1998. The role of mountains and plateaus in a Triassic climate model. In: Crowley, T.J., Burke, K.C. (Eds.), Tectonic Boundary Conditions for Climate Reconstructions, 39. Oxford University Press, Oxford, pp. 116–146.

Hay, W., Soeding, E., DeConto, R., Wold, C., 2002. The Late Cenozoic uplift - climate change paradox. Int. J. Earth Sci. 91, 746–774. https://doi.org/10.1007/s00531-002-0263-1.

He, P., Song, C., Wang, Y., Chen, L., Chang, P., Wang, Q., Ren, B., 2017. Cenozoic exhumation in the Qilian Shan, northeastern Tibetan Plateau: evidence from detrital fission track thermochronology in the Jiuquan Basin: Cenozoic Exhumation in the Qilian Shan. J. Geophys. Res. Solid Earth 122, 6910–6927. https://doi.org/10.1002/2017JB014216.

Hébert, R., Bezard, R., Guilmette, C., Dostal, J., Wang, C.S., Liu, Z.F., 2012. The Indus–Yarlung Zangbo ophiolites from Nanga Parbat to Namche Barwa syntaxes, southern Tibet: first synthesis of petrology, geochemistry, and geochronology with incidences on geodynamic reconstructions of Neo-Tethys. Gondwana Res. 22, 377–397. https://doi.org/10.1016/j.gr.2011.10.013.

Heine, C., Yeo, L.G., Müller, R.D., 2015. Evaluating global paleoshoreline models for the Cretaceous and Cenozoic. Aust. J. Earth Sci. 1–13. https://doi.org/10.1080/08120099.2015.1018321.

Henderson, M.A., Mihalynuk, M.G., Sigloch, K., Johnston, S.T., Shephard, G.A., 2014. Jurassic to Recent tectonic evolution of North America: a preliminary model using GPlates software. BC Geol. Surv. Geofile (2014–11).

Henríquez, S., DeCelles, P.G., Carrapa, B., 2018. Cretaceous to Middle Cenozoic Exhumation History of the Cordillera de Domeyko and Salar de Atacama Basin, Northern Chile. Tectonics 38, 395–416. https://doi.org/10.1029/2018TC005203.

Herman, F., Seward, D., Valla, P.G., Carter, A., Kohn, B., Willett, S.D., Ehlers, T.A., 2013. Worldwide acceleration of mountain erosion under a cooling climate. Nature 504, 423–426. https://doi.org/10.1038/nature12877.

Herold, N., Buzan, J., Seton, M., Goldner, A., Green, J.A.M., Müller, R.D., Markwick, P., Huber, M., 2014. A suite of early Eocene (~ 55 Ma) climate model boundary conditions. Geosci. Model Dev. 7, 2077–2090. https://doi.org/10.5194/gmd-7-2077-2014.

Herrera, S., Pinto, L., Deckart, K., Cortés, J., Valenzuela, J., 2017. Cenozoic Tectonostratigraphic Evolution and Architecture of the Central Andes in Northern Chile based on the Aquine Region, Western Cordillera (19°-19o30' S). Andgeo 44, 87. https://doi.org/10.5027/andgeoV44n2-a01.

Hervé, F., Pankhurst, R.J., Fanning, C.M., Calderón, M., Yaxley, G.M., 2007. The South Patagonian batholith: 150 my of granite magmatism on a plate margin. Lithos 97, 373–394. https://doi.org/10.1016/j.lithos.2007.01.007.

Heureux, A.M., Rickaby, R.E., 2015. Refining our estimate of atmospheric CO2 across the Eocene–Oligocene climatic transition. Earth Planet. Sci. Lett. 409, 329–338. https://doi.org/10.1016/j.epsl.2014.10.036.

Hoareau, G., Bomou, B., Van Hinsbergen, D., Carry, N., Marquer, D., Donnadieu, Y., Le Hir, G., Vrielynck, B., Walter-Simonnet, A.-V., 2015. Did high Neo-Tethys subduction rates contribute to early Cenozoic warming? Clim. Past 11, 1751–1767. https://doi.org/10.5194/cp-11-1751-2015.

Hochmuth, K., Gohl, K., Leitchenkov, G., Sauermilch, I., Whittaker, J.M., Uenzelmann-Neben, G., Davy, B., De Santis, L., 2020. The evolving paleobathymetry of the Circum-Antarctic Southern Ocean Since 34 Ma: a key to understanding past cryosphere-ocean developments. Geochem. Geophys. Geosyst. 21 https://doi.org/10.1029/2020GC009122.

Hoorn, C., Straathof, J., Abels, H.A., Xu, Y., Utescher, T., Dupont-Nivet, G., 2012. A late Eocene palynological record of climate change and Tibetan Plateau uplift (Xining

Basin, China). Palaeogeogr. Palaeoclimatol. Palaeoecol. 344–345, 16–38. https://doi.org/10.1016/j.palaeo.2012.05.011.
Hu, X., An, W., Wang, J., Garzanti, E., Guo, R., 2014. Himalayan detrital chromian spinels and timing of Indus-Yarlung ophiolite erosion. Tectonophysics 621, 60–68. https://doi.org/10.1016/j.tecto.2014.02.003.
Huang, W., Van Hinsbergen, D.J.J., Maffione, M., Orme, D.A., Dupont-Nivet, G., Guilmette, C., Ding, L., Guo, Z., Kapp, P., 2015. Lower Cretaceous Xigaze ophiolites formed in the Gangdese forearc: evidence from paleomagnetism, sediment provenance, and stratigraphy. Earth Planet. Sci. Lett. 415, 142–153. https://doi.org/10.1016/j.epsl.2015.01.032.
Huber, M., Sloan, L.C., 2001. Heat transport, deep waters, and thermal gradients: Coupled simulation of an Eocene greenhouse climate. Geophys. Res. Lett. 28, 3481–3484. https://doi.org/10.1029/2001GL012943.
Ingalls, M., Rowley, D.B., Currie, B., Colman, A.S., 2016. Large-scale subduction of continental crust implied by India–Asia mass-balance calculation. Nat. Geosci. 9, 848–853. https://doi.org/10.1038/ngeo2806.
Irving, E., Archibald, D., 1990. Bathozonal tilt corrections to paleomagnetic data from Mid-Cretaceous plutonic rocks: examples from the Omineca Belt, British Columbia. J. Geophys. Res. Solid Earth 95, 4579–4585, 10.1029/JB095iB04p04579.
Irving, E., Woodsworth, G.J., Wynne, P.J., Morrison, A., 1985. Paleomagnetic evidence for displacement from the south of the Coast Plutonic Complex, British Columbia. Can. J. Earth Sci. 22, 584–598, 10.1139/e85-058.
Isacks, B.L., 1988. Uplift of the central Andean plateau and bending of the Bolivian orocline. J. Geophys. Res. Solid Earth 93, 3211–3231, 10.1029/JB093iB04p03211.
Jagoutz, O., Macdonald, F.A., Royden, L., 2016. Low-latitude arc–continent collision as a driver for global cooling. Proc. Natl. Acad. Sci. 113, 4935–4940, 10.1073/pnas.1523667113.
Jagoutz, O., Royden, L., Holt, A.F., Becker, T.W., 2015. Anomalously fast convergence of India and Eurasia caused by double subduction. Nat. Geosci. 8, 475–478. https://doi.org/10.1038/ngeo2418.
Japsen, P., Bonow, J.M., Green, P.F., Cobbold, P.R., Chiossi, D., Lilletveit, R., Magnavita, L.P., Pedreira, A., 2012a. Episodic burial and exhumation in NE Brazil after opening of the South Atlantic. Geol. Soc. Am. Bull. 124, 800–816. https://doi.org/10.1130/B30515.1.
Japsen, P., Chalmers, J.A., Green, P.F., Bonow, J.M., 2012b. Elevated, passive continental margins: Not rift shoulders, but expressions of episodic, post-rift burial and exhumation. Glob. Planet. Chang. 90, 73–86. https://doi.org/10.1016/j.gloplacha.2011.05.004.
Jolivet, M., Boulvais, P., Barrier, L., Robin, C., Heilbronn, G., Ledoyen, J., Ventroux, Q., Jia, Y., Guo, Z., Bataleva, E., 2018. Oxygen and carbon stable isotope composition of cretaceous to pliocene calcareous paleosols in the Tian Shan Region (Central Asia): controlling factors and paleogeographic implications. Geosciences 8, 330. https://doi.org/10.3390/geosciences8090330.
Kapp, P., DeCelles, P.G., 2019. Mesozoic–Cenozoic geological evolution of the Himalayan-Tibetan orogen and working tectonic hypotheses. Am. J. Sci. 319, 159–254. https://doi.org/10.2475/03.2019.01.
Kapp, P., Yin, A., Harrison, T.M., Ding, L., 2005. Cretaceous-Tertiary shortening, basin development, and volcanism in central Tibet. Geol. Soc. Am. Bull. 117, 865. https://doi.org/10.1130/B25595.1.
Kapp, P., DeCelles, P.G., Leier, A.L., Fabijanic, J.M., He, S., Pullen, A., Gehrels, G.E., Ding, L., 2007. The Gangdese retroarc thrust belt revealed. GSA Today 17, 4. https://doi.org/10.1130/GSAT01707A.1.
Karl, T.R., Trenberth, K.E., 2003. Modern global climate change. Science 302, 1719–1723. https://doi.org/10.1126/science.1090228.
Karl, M., Glasmacher, U.A., Kollenz, S., Franco-Magalhaes, A.O.B., Stockli, D.F., Hackspacher, P.C., 2013. Evolution of the South Atlantic passive continental margin in southern Brazil derived from zircon and apatite (U–Th–Sm)/He and fission-track data. Tectonophysics 604, 224–244. https://doi.org/10.1016/j.tecto.2013.06.017.
Kaya, M.Y., Dupont-Nivet, G., Proust, J., Roperch, P., Bougeois, L., Meijer, N., Frieling, J., Fioroni, C., Özkan Altıner, S., Vardar, E., Barbolini, N., Stoica, M., Aminov, J., Mamtimin, M., Zhaojie, G., 2019. Paleogene evolution and demise of the proto-Paratethys Sea in Central Asia (Tarim and Tajik basins): role of intensified tectonic activity at ca. 41 Ma. Basin Res. 31, 461–486. https://doi.org/10.1111/bre.12330.
Kennett, J.P., Houtz, R.E., et al., 1975. Initial Reports of the Deep Sea Drilling Project, 29, Initial Reports of the Deep Sea Drilling. Government Printing Office, Project. U.S. https://doi.org/10.2973/dsdp.proc.29.1975.
Kent, D.V., Irving, E., 2010. Influence of inclination error in sedimentary rocks on the Triassic and Jurassic apparent pole wander path for North America and implications for Cordilleran tectonics. J. Geophys. Res. 115, B10103 https://doi.org/10.1029/2009JB007205.
Kent, D.V., Muttoni, G., 2008. Equatorial convergence of India and early Cenozoic climate trends. Proc. Natl. Acad. Sci. 105, 16065–16070. https://doi.org/10.1073/pnas.0805382105.
Kent, D.V., Muttoni, G., 2013. Modulation of Late Cretaceous and Cenozoic climate by variable drawdown of atmospheric p CO 2 from weathering of basaltic provinces on continents drifting through the equatorial humid belt. Clim. Past 9, 525–546. https://doi.org/10.5194/cp-9-525-2013.
Klepeis, K., Betka, P., Clarke, G., Fanning, M., Hervé, F., Rojas, L., Mpodozis, C., Thomson, S., 2010. Continental underthrusting and obduction during the Cretaceous closure of the Rocas Verdes rift basin, Cordillera Darwin, Patagonian Andes. Tectonics 29. https://doi.org/10.1029/2009TC002610.
Kohn, M.J., Spear, F.S., Dalziel, I.W.D., 1993. Metamorphic P–T paths from Cordillera Darwin, a core complex in Tierra del Fuego, Chile. J. Petrol. 34, 519–542. https://doi.org/10.1093/petrology/34.3.519.
Krissansen-Totton, J., Catling, D.C., 2017. Constraining climate sensitivity and continental versus seafloor weathering using an inverse geological carbon cycle model. Nat. Commun. 8, 15423. https://doi.org/10.1038/ncomms15423.
Kuscu, I., Kuscu, G.G., Tosdal, R.M., Ulrich, T.D., Friedman, R., 2010. Magmatism in the southeastern Anatolian orogenic belt: transition from arc to post-collisional setting in an evolving orogen. Geol. Soc. Lond., Spec. Publ. 340, 437–460. https://doi.org/10.1144/SP340.19.
Ladant, J.-B., Donnadieu, Y., Dumas, C., 2014. Links between CO 2 , glaciation and water flow: reconciling the Cenozoic history of the Antarctic Circumpolar Current. Clim. Past 10, 1957–1966. https://doi.org/10.5194/cp-10-1957-2014.
Ladant, J.-B., Poulsen, C.J., Fluteau, F., Tabor, C.R., MacLeod, K.G., Martin, E.E., Haynes, S.J., Rostami, M.A., 2020. Paleogeographic controls on the evolution of Late Cretaceous ocean circulation. Clim. Past 16, 973–1006. https://doi.org/10.5194/cp-16-973-2020.
Lagabrielle, Y., Goddéris, Y., Donnadieu, Y., Malavieille, J., Suarez, M., 2009. The tectonic history of Drake Passage and its possible impacts on global climate. Earth Planet. Sci. Lett. 279, 197–211. https://doi.org/10.1016/j.epsl.2008.12.037.
Larsen, I.J., Montgomery, D.R., Greenberg, H.M., 2014. The contribution of mountains to global denudation. Geology 42, 527–530. https://doi.org/10.1130/G35136.1.
Lasaga, A.C., Berner, R.A., Garrels, R.M., 1985. An improved geochemical model of atmospheric CO2 fluctuations over the past 100 million years. In: The Carbon Cycle and Atmospheric CO2: Natural Variations Archean to Present, 32, pp. 397–411. https://doi.org/10.1029/GM032p0397.
Laskowski, A.K., Orme, D.A., Cai, F., Ding, L., 2019. The Ancestral Lhasa River: a Late Cretaceous trans-arc river that drained the proto–Tibetan Plateau. Geology 47, 1029–1033. https://doi.org/10.1130/G46823.1.
Lazarus, D., Caulet, J.P., 1993. Cenozoic Southern Ocean reconstructions. Antarctic Res. Ser. 60, 145–174.
Lear, C.H., Bailey, T.R., Pearson, P.N., Coxall, H.K., Rosenthal, Y., 2008. Cooling and ice growth across the Eocene-Oligocene transition. Geol 36, 251. https://doi.org/10.1130/G24584A.1.
Leary, R.J., Quade, J., DeCelles, P.G., Reynolds, A., 2017. Evidence from paleosols for low to moderate elevation of the India-Asia suture zone during mid-Cenozoic time. Geology 45, 399–402. https://doi.org/10.1130/G38830.1.
Leary, R.J., Quade, J., DeCelles, P.G., 2018. Evidence from Paleosols for low to moderate elevation of the India-Asia suture zone during mid-Cenozoic time: REPLY. Geology 46, e435. https://doi.org/10.1130/G39G39946Y.1.
Lechler, A.R., Niemi, N.A., Hren, M.T., Lohmann, K.C., 2013. Paleoelevation estimates for the northern and central proto-Basin and Range from carbonate clumped isotope thermometry. Tectonics 32, 295–316. https://doi.org/10.1002/tect.20016.
Lefebvre, V., Donnadieu, Y., Goddéris, Y., Fluteau, F., Hubert-Théou, L., 2013. Was the Antarctic glaciation delayed by a high degassing rate during the early Cenozoic? Earth Planet. Sci. Lett. 371–372, 203–211. https://doi.org/10.1016/j.epsl.2013.03.049.
Leier, A., McQuarrie, N., Garzione, C., Eiler, J., 2013. Stable isotope evidence for multiple pulses of rapid surface uplift in the Central Andes, Bolivia. Earth Planet. Sci. Lett. 371–372, 49–58. https://doi.org/10.1016/j.epsl.2013.04.025.
Li, G., Elderfield, H., 2013. Evolution of carbon cycle over the past 100 million years. Geochim. Cosmochim. Acta 103, 11–25. https://doi.org/10.1016/j.gca.2012.10.014.
Li, S., Zhao, S., Liu, X., Cao, H., Yu, Shan, Li, X., Somerville, I., Yu, Shengyao, Suo, Y., 2018. Closure of the Proto-Tethys Ocean and Early Paleozoic amalgamation of microcontinental blocks in East Asia. Earth Sci. Rev. 186, 37–75. https://doi.org/10.1016/j.earscirev.2017.01.011.
Li, L., Fan, M., Davila, N., Jesmok, G., Mitsunaga, B., Tripati, A., Orme, D., 2019. Carbonate stable and clumped isotopic evidence for late Eocene moderate to high elevation of the east-central Tibetan Plateau and its geodynamic implications. GSA Bull. 131, 831–844. https://doi.org/10.1130/B32060.1.
Licht, A., Quade, J., Kowler, A., De Los Santos, M., Hudson, A., Schauer, A., Huntington, K., Copeland, P., Lawton, T., 2017. Impact of the North American monsoon on isotope paleoaltimeters: Implications for the paleoaltimetry of the American southwest. Am. J. Sci. 317, 1–33. https://doi.org/10.2475/01.2017.01.
Lieberman, B.S., 2003. Paleobiogeography: The Relevance of Fossils to Biogeography. Annu. Rev. Ecol. Evol. Syst. 34, 51–69. https://doi.org/10.1146/annurev.ecolsys.34.121101.153549.
Lisker, F., Ventura, B., Glasmacher, U.A., 2009. Apatite thermochronology in modern geology. Geol. Soc. Lond., Spec. Publ. 324, 1–23. https://doi.org/10.1144/SP324.1.
Lithgow-Bertelloni, C., Silver, P.G., 1998. Dynamic topography, plate driving forces and the African superswell. Nature 395, 269–272. https://doi.org/10.1038/26212.
Liu, Z., Pagani, M., Zinniker, D., DeConto, R., Huber, M., Brinkhuis, H., Shah, S.R., Leckie, R.M., Pearson, A., 2009. Global cooling during the Eocene-Oligocene climate transition. Science 323, 1187–1190. https://doi.org/10.1126/science.1166368.
Lunt, D.J., Valdes, P.J., Haywood, A., Rutt, I.C., 2008. Closure of the Panama Seaway during the Pliocene: implications for climate and Northern Hemisphere glaciation. Clim. Dyn. 30, 1–18. https://doi.org/10.1007/s00382-007-0265-6.
Lunt, D.J., Huber, M., Anagnostou, E., Baatsen, M.L.J., Caballero, R., DeConto, R., Dijkstra, H.A., Donnadieu, Y., Evans, D., Feng, R., Foster, G.L., Gasson, E., von der Heydt, A.S., Hollis, C.J., Inglis, G.N., Jones, S.M., Kiehl, J., Kirtland Turner, S., Korty, R.L., Kozdon, R., Krishnan, S., Ladant, J.-B., Langebroek, P., Lear, C.H., LeGrande, A.N., Littler, K., Markwick, P., Otto-Bliesner, B., Pearson, P., Poulsen, C.J., Salzmann, U., Shields, C., Snell, K., Stärz, M., Super, J., Tabor, C., Tierney, J.E., Tourte, G.J.L., Tripati, A., Upchurch, G.R., Wade, B.S., Wing, S.L., Winguth, A.M.E., Wright, N.M., Zachos, J.C., Zeebe, R.E., 2017. The DeepMIP contribution to PMIP4: experimental design for model simulations of the EECO, PETM, and pre-PETM (version 1.0). Geosci. Model Dev. 10, 889–901. https://doi.org/10.5194/gmd-10-889-2017.

Macdonald, F.A., Swanson-Hysell, N.L., Park, Y., Lisiecki, L., Jagoutz, O., 2019. Arc-continent collisions in the tropics set Earth's climate state. Science. https://doi.org/10.1126/science.aav5300 eaav5300.
Maffre, P., Ladant, J.-B., Moquet, J.-S., Carretier, S., Labat, D., Goddéris, Y., 2018. Mountain ranges, climate and weathering. Do orogens strengthen or weaken the silicate weathering carbon sink? Earth Planet. Sci. Lett. 493, 174–185. https://doi.org/10.1016/j.epsl.2018.04.034.
Maloney, K.T., Clarke, G.L., Klepeis, K.A., Fanning, C.M., Wang, W., 2011. Crustal growth during back-arc closure: cretaceous exhumation history of Cordillera Darwin, southern Patagonia. J. Metamorph. Geol. 29, 649–672. https://doi.org/10.1111/j.1525-1314.2011.00934.x.
Malumián, N., Ramos, V.A., 1984. Magmatic intervals, transgression-regression cycles and oceanic events in the Cretaceous and Tertiary of southern South America. Earth Planet. Sci. Lett. 67, 228–237. https://doi.org/10.1016/0012-821X(84)90118-3.
Mansilla, H.G., De Valais, S., Stinnesbeck, W., Varela, N.A., Leppe, M.A., 2012. New Avian tracks from the lower to middle Eocene at Fossil Hill, King George Island, Antarctica. Antarct. Sci. 24, 500–506. https://doi.org/10.1017/S0954102012000260.
Markwick, P., Valdes, P., 2004. Palaeo-digital elevation models for use as boundary conditions in coupled ocean–atmosphere GCM experiments: a Maastrichtian (late Cretaceous) example. Palaeogeogr. Palaeoclimatol. Palaeoecol. 213, 37–63. https://doi.org/10.1016/S0031-0182(04)00330-X.
Martínez, F., Arriagada, C., Peña, M., Del Real, I., Deckart, K., 2013. The structure of the Chañarcillo Basin: an example of tectonic inversion in the Atacama region, northern Chile. J. S. Am. Earth Sci. 42, 1–16. https://doi.org/10.1016/j.jsames.2012.07.001.
Martínez, F., Kania, J., Muñoz, B., Riquelme, R., López, C., 2020. Geometry and development of a hybrid thrust belt in an inner forearc setting: insights from the Potrerillos Belt in the Central Andes, northern Chile. J. S. Am. Earth Sci. 98, 102439. https://doi.org/10.1016/j.jsames.2019.102439.
Mathews, W., 1986. Physiographic Map of the Canadian Cordillera 1: 5 000 000. Geological Survey of Canada.
Mathews, W., 1991. In: Gabrielse, H., Yorath, C.J. (Eds.), Physiographic evolution of the Canadian Cordillera. Geology of the Cordilleran Orogen in Canada, 4. Geological Survey of Canada, Geology of Canada, pp. 403–418.
Matthews, K.J., Maloney, K.T., Zahirovic, S., Williams, S.E., Seton, M., Müller, R.D., 2016. Global plate boundary evolution and kinematics since the late Paleozoic. Glob. Planet. Chang. 146, 226–250. https://doi.org/10.1016/j.gloplacha.2016.10.002.
McKay, R., Barrett, P., Levy, R., Naish, T., Golledge, N., Pyne, A., 2016. Antarctic Cenozoic climate history from sedimentary records: ANDRILL and beyond. Philos. Trans. R. Soc. A Math. Phys. Eng. Sci. 374, 20140301. https://doi.org/10.1098/rsta.2014.0301.
McPhee, P.J., Van Hinsbergen, D.J.J., Thomson, S.N., 2019. Thermal history of the western Central Taurides fold-thrust belt: implications for Cenozoic vertical motions of southern Central Anatolia. Geosphere 15, 1927–1942. https://doi.org/10.1130/GES02164.1.
McQuarrie, N., 2004. Crustal scale geometry of the Zagros fold–thrust belt, Iran. J. Struct. Geol. 26, 519–535. https://doi.org/10.1016/j.jsg.2003.08.009.
McQuarrie, N., Van Hinsbergen, D.J.J., 2013. Retrodeforming the Arabia-Eurasia collision zone: age of collision versus magnitude of continental subduction. Geology 41, 315–318. https://doi.org/10.1130/G33591.1.
McQuarrie, N., Wernicke, B.P., 2005. An animated tectonic reconstruction of southwestern North America since 36 Ma. Geosphere 1, 147–172. https://doi.org/10.1130/GES00016.1.
McQuarrie, N., Barnes, J.B., Ehlers, T.A., 2008. Geometric, kinematic, and erosional history of the central Andean Plateau, Bolivia (15-17°S). Tectonics 27. https://doi.org/10.1029/2006TC002054.
Mebrouk, F., Mahboubi, M., Bessedik, M., Feist, M., 1997. L'apport des charophytes à la stratigraphie des formations continentales paléogènes de l'Algérie. Geobios 30, 171–177. https://doi.org/10.1016/S0016-6995(97)80221-5.
Medvedev, S., Hartz, E.H., Faleide, J.I., 2018. Erosion-driven vertical motions of the circum Arctic: comparative analysis of modern topography. J. Geodyn. 119, 62–81. https://doi.org/10.1016/j.jog.2018.04.003.
Merzeraud, G., Essid, E.M., Marzougui, W., Khayati Ammar, H., Adnet, S., Marivaux, L., Tabuce, R., Vianey-Liaud, M., 2016. Stratigraphie et sédimentologie des dépôts marins et continentaux d'âge éocène moyen à miocène en Tunisie centrale (région du Djebel el Kébar). Bulletin de la Société Géologique de France 187, 11–25. https://doi.org/10.2113/gssgfbull.187.1.11.
Meschede, M., Frisch, W., 1998. A plate-tectonic model for the Mesozoic and Early Cenozoic history of the Caribbean plate. Tectonophysics 296, 269–291. https://doi.org/10.1016/S0040-1951(98)00157-7.
Miao, Y., Wu, F., Chang, H., Fang, X., Deng, T., Sun, J., Jin, C., 2016. A Late-Eocene palynological record from the Hoh Xil Basin, northern Tibetan Plateau, and its implications for stratigraphic age, paleoclimate and paleoelevation. Gondwana Res. 31, 241–252. https://doi.org/10.1016/j.gr.2015.01.007.
Mihlbachler, M.C., Lucas, S.G., Emry, R.J., Bayshashov, B., 2004. A new brontothere (Brontotheriidae, Perissodactyla, Mammalia) from the Eocene of the Ily Basin of Kazakstan and a phylogeny of Asian "horned" brontotheres. Am. Mus. Novit. 2004, 1–43. https://doi.org/10.1206/0003-0082(2004)439<0001:ANBBPM>2.0.CO;2.
Missenard, Y., Saddiqi, O., Barbarand, J., Leturmy, P., Ruiz, G., El Haimer, F.-Z., Frizon de Lamotte, D., 2008. Cenozoic denudation in the Marrakech High Atlas, Morocco: insight from apatite fission-track thermochronology. Terra Nova 20, 221–228. https://doi.org/10.1111/j.1365-3121.2008.00810.x.
Mix, H.T., Ibarra, D.E., Mulch, A., Graham, S.A., Chamberlain, C.P., 2016. A hot and high Eocene Sierra Nevada. Geol. Soc. Am. Bull. 128, 531–542. https://doi.org/10.1130/B31294.1.
Molnar, P., Tapponnier, P., 1975. Cenozoic Tectonics of Asia: Effects of a Continental Collision: Features of recent continental tectonics in Asia can be interpreted as results of the India-Eurasia collision. Science 189, 419–426. https://doi.org/10.1126/science.189.4201.419.
Montes, C., Cardona, A., Jaramillo, C., Pardo, A., Silva, J.C., Valencia, V., Ayala, C., Perez-Angel, L.C., Rodriguez-Parra, L.A., Ramirez, V., Nino, H., 2015. Middle Miocene closure of the Central American Seaway. Science 348, 226–229. https://doi.org/10.1126/science.aaa2815.
Moody, R., 1997. The iullemmeden basin. In: Selley, R.C. (Ed.), African Basins. Sedimentary Basins of the World, 3. Elsevier, Amsterdam, pp. 89–103. https://doi.org/10.1016/S1874-5997(97)80008-1, 89–103. 3.
Mora, A., Reyes-Harker, A., Rodriguez, G., Tesón, E., Ramirez-Arias, J.C., Parra, M., Caballero, V., Mora, J.P., Quintero, I., Valencia, V., Ibañez, M., Horton, B.K., Stockli, D.F., 2013. Inversion tectonics under increasing rates of shortening and sedimentation: Cenozoic example from the Eastern Cordillera of Colombia. Geol. Soc. Lond., Spec. Publ. 377, 411–442. https://doi.org/10.1144/SP377.6.
Morin, J., Jolivet, M., Barrier, L., Laborde, A., Li, H., Dauteuil, O., 2019. Planation surfaces of the Tian Shan Range (Central Asia): Insight on several 100 million years of topographic evolution. J. Asian Earth Sci. 177, 52–65. https://doi.org/10.1016/j.jseaes.2019.03.011.
Mouthereau, F., Lacombe, O., Vergés, J., 2012. Building the Zagros collisional orogen: timing, strain distribution and the dynamics of Arabia/Eurasia plate convergence. Tectonophysics 532–535, 27–60. https://doi.org/10.1016/j.tecto.2012.01.022.
Mpodozis, C., Arriagada, C., Basso, M., Roperch, P., Cobbold, P., Reich, M., 2005. Late Mesozoic to Paleogene stratigraphy of the Salar de Atacama Basin, Antofagasta, Northern Chile: implications for the tectonic evolution of the Central Andes. Tectonophysics 399, 125–154. https://doi.org/10.1016/j.tecto.2004.12.019.
Mulch, A., Graham, S.A., Chamberlain, C.P., 2006. Hydrogen isotopes in Eocene river gravels and paleoelevation of the Sierra Nevada. Science 313, 87–89. https://doi.org/10.1126/science.1125986.
Mulch, A., Teyssier, C., Cosca, M.A., Chamberlain, C.P., 2007. Stable isotope paleoaltimetry of Eocene core complexes in the North American Cordillera. Tectonics 26. https://doi.org/10.1029/2006TC001995.
Müller, R.D., Royer, J.-Y., Cande, S.C., Roest, W.R., Maschenkov, S., 1999. Chapter 2 New constraints on the late cretaceous/tertiary plate tectonic evolution of the caribbean. In: Sedimentary Basins of the World. Elsevier, pp. 33–59. https://doi.org/10.1016/S1874-5997(99)80036-7.
Müller, R.D., Sdrolias, M., Gaina, C., Roest, W.R., 2008a. Age, spreading rates, and spreading asymmetry of the world's ocean crust. Geochem. Geophys. Geosyst. 9 https://doi.org/10.1029/2007GC001743.
Müller, R.D., Sdrolias, M., Gaina, C., Steinberger, B., Heine, C., 2008b. Long-term sea-level fluctuations driven by ocean Basin dynamics. Science 319, 1357–1362. https://doi.org/10.1126/science.1151540.
Müller, R.D., Seton, M., Zahirovic, S., Williams, S.E., Matthews, K.J., Wright, N.M., Shephard, G.E., Maloney, K.T., Barnett-Moore, N., Hosseinpour, M., Bower, D.J., Cannon, J., 2016. Ocean basin evolution and global-scale plate reorganization events since pangea breakup. Annu. Rev. Earth Planet. Sci. 44, 107–138. https://doi.org/10.1146/annurev-earth-060115-012211.
Müller, R.D., Zahirovic, S., Williams, S.E., Cannon, J., Seton, M., Bower, D.J., Tetley, M. G., Heine, C., Le Breton, E., Liu, S., Russell, S.H.J., Yang, T., Leonard, J., Gurnis, M., 2019. A global plate model including lithospheric deformation along major rifts and orogens since the triassic. Tectonics 38, 1884–1907. https://doi.org/10.1029/2018TC005462.
Munday, D., Johnson, H., Marshall, D., 2015. The role of ocean gateways in the dynamics and sensitivity to wind stress of the early Antarctic Circumpolar Current. Paleoceanography 30, 284–302. https://doi.org/10.1002/2014PA002675.
Murphy, M.A., Yin, A., Harrison, T.M., Dürr, S.B., 1997. Did the Indo-Asian collision alone create the Tibetan plateau? 4. https://doi.org/10.1130/0091-7613(1997)025<0719:DTIACA>2.3.CO;2.
Nelson, E., 1982. Post-tectonic uplift of the Cordillera Darwin orogenic core complex: evidence from fission track geochronology and closing temperature–time relationships. J. Geol. Soc. 139, 755–761. https://doi.org/10.1144/gsjgs.139.6.0755.
Öğretmen, N., Cipollari, P., Frezza, V., Faranda, C., Karanika, K., Gliozzi, E., Radeff, G., Cosentino, D., 2018. Evidence for 1.5 km of Uplift of the Central Anatolian Plateau's Southern Margin in the Last 450 kyr and implications for its multiphased uplift history. Tectonics 37, 359–390. https://doi.org/10.1002/2017TC004805.
Olivero, E.B., Malumián, N., 2008. Mesozoic-Cenozoic stratigraphy of the Fuegian Andes. Arg. Geol. Acta 14. https://doi.org/10.1344/105.000000238.
Olivetti, V., Balestrieri, M.L., Rossetti, F., Talarico, F.M., 2013. Tectonic and climatic signals from apatite detrital fission track analysis of the Cape Roberts Project core records, South Victoria Land, Antarctica. Tectonophysics 594, 80–90. https://doi.org/10.1016/j.tecto.2013.03.017.
Ollier, C., Pain, C., 1997. Equating the basal unconformity with the palaeoplain: a model for passive margins. Geomorphology 19, 1–15. https://doi.org/10.1016/S0169-555X(96)00048-7.
O'Neill, C., Müller, D., Steinberger, B., 2005. On the uncertainties in hot spot reconstructions and the significance of moving hot spot reference frames. Geochem. Geophys. Geosyst. 6 https://doi.org/10.1029/2004GC000784.
Ordonez, E., 1936. Principal physiographic provinces of Mexico. AAPG Bull. 20, 1277–1307.
Otto-Bliesner, B.L., Brady, E.C., Shields, C., 2002. Late Cretaceous ocean: coupled simulations with the national center for atmospheric research climate system model. J. Geophys. Res.-Atmos. 107 https://doi.org/10.1029/2001JD000821. ACL 11–1.
Parra, M., Mora, A., Jaramillo, C., Strecker, M.R., Sobel, E.R., Quiroz, L., Rueda, M., Torres, V., 2009. Orogenic wedge advance in the northern Andes: evidence from the

Oligocene-Miocene sedimentary record of the Medina Basin, Eastern Cordillera, Colombia. Geol. Soc. Am. Bull. 121, 780–800. https://doi.org/10.1130/B26257.1.
Parra, M., Mora, A., Lopez, C., Ernesto Rojas, L., Horton, B.K., 2012. Detecting earliest shortening and deformation advance in thrust belt hinterlands: example from the Colombian Andes. Geology 40, 175–178. https://doi.org/10.1130/G32519.1.
Paxman, G.J.G., Jamieson, S.S.R., Hochmuth, K., Gohl, K., Bentley, M.J., Leitchenkov, G., Ferraccioli, F., 2019. Reconstructions of Antarctic topography since the Eocene–Oligocene boundary. Palaeogeogr. Palaeoclimatol. Palaeoecol. 535, 109346. https://doi.org/10.1016/j.palaeo.2019.109346.
Pelayo, A.M., Wiens, D.A., 1989. Seismotectonics and relative plate motions in the Scotia Sea region. J. Geophys. Res. 94, 7293, 10.1029/JB094iB06p07293.
Peyton, S.L., Carrapa, B., 2013. An introduction to low-temperature thermochronologic techniques, methodology, and applications. AAPG 65, 15–36. https://doi.org/10.1306/13381688St653578.
Pindell, J., Dewey, J.F., 1982. Permo-Triassic reconstruction of western Pangea and the evolution of the Gulf of Mexico/Caribbean region. Tectonics 1, 179–211. https://doi.org/10.1029/TC001i002p00179.
Pindell, J., Kennan, L., 2001. Processes & events in the terrane assembly of Trinidad and E. Venezuela. In: Presented at the GCSSEPM Foundation 21st Annual Research Conference Transactions, Petroleum Systems of Deep-Water Basins, pp. 159–192.
Pindell, J.L., Kennan, L., 2009. Tectonic evolution of the Gulf of Mexico, Caribbean and northern South America in the mantle reference frame: an update. Geol. Soc. Lond., Spec. Publ. 328, 1–55. https://doi.org/10.1144/SP328.1.
Pindell, J.L., Tabbutt, K.D., 1995. Mesozoic-Cenozoic Andean paleogeography and regional controls on hydrocarbon systems. In: Tankard, A.J., Suarez-Soruco, R., Welsink, H.J. (Eds.), Petroleum basins of South America, 62. American Association of Petroleum Geologists, Memoir, Tulsa, pp. 101–128.
Poage, M., Chamberlain, C., 2002. Stable isotopic evidence for a Pre-Middle Miocene rain shadow in the western Basin and Range: implications for the paleotopography of the Sierra Nevada. Tectonics 21. https://doi.org/10.1029/2001TC001303, 16–1.
Poblete, F., Arriagada, C., Roperch, P., Astudillo, N., Hervé, F., Kraus, S., Le Roux, J.P., 2011. Paleomagnetism and tectonics of the South Shetland Islands and the northern Antarctic Peninsula. Earth Planet. Sci. Lett. 302, 299–313. https://doi.org/10.1016/j.epsl.2010.12.019.
Poblete, F., Roperch, P., Hervé, F., Diraison, M., Espinoza, M., Arriagada, C., 2014. The curved Magallanes fold and thrust belt: Tectonic insights from a paleomagnetic and anisotropy of magnetic susceptibility study: tectonic Rotations Magallanes. Tectonics 33, 2526–2551. https://doi.org/10.1002/2014TC003555.
Poblete, F., Roperch, P., Arriagada, C., Ruffet, G., Ramírez de Arellano, C., Hervé, F., Poujol, M., 2016. Late Cretaceous–early Eocene counterclockwise rotation of the Fueguian Andes and evolution of the Patagonia–Antarctic Peninsula system. Tectonophysics 668–669, 15–34. https://doi.org/10.1016/j.tecto.2015.11.025.
Polissar, P.J., Freeman, K.H., Rowley, D.B., McInerney, F.A., Currie, B.S., 2009. Paleoaltimetry of the Tibetan Plateau from D/H ratios of lipid biomarkers. Earth Planet. Sci. Lett. 287, 64–76. https://doi.org/10.1016/j.epsl.2009.07.037.
Popov, S.V., Rögl, F., Rozanov, A.Y., Steininger, F.F., Shcherba, I.G., Kovac, M., 2004. Lithological-paleogeographic maps of Paratethys-10 maps late Eocene to pliocene. In: Courier Forschungsinstitut Senckenberg, 250, pp. 1–42.
Portner, D.E., Delph, J.R., Biryol, C.B., Beck, S.L., Zandt, G., Özacar, A.A., Sandvol, E., Türkelli, N., 2018. Subduction termination through progressive slab deformation across Eastern Mediterranean subduction zones from updated P-wave tomography beneath Anatolia. Geosphere 14, 907–925. https://doi.org/10.1130/GES01617.1.
Pueyo, E.L., Pocoví, A., Millán, H., Sussman, A.J., 2004. Map-view models for correcting and calculating shortening estimates in rotated thrust fronts using paleomagnetic data. In: Special Paper 383: Orogenic Curvature: Integrating Paleomagnetic and Structural Analyses. Geological Society of America, pp. 57–71. https://doi.org/10.1130/0–8137–2383-3(2004)383[57:MMFCAC]2.0.CO;2.
Quade, J., Breecker, D.O., Daeron, M., Eiler, J., 2011. The paleoaltimetry of Tibet: an isotopic perspective. Am. J. Sci. 311, 77–115. https://doi.org/10.2475/02.2011.01.
Quade, J., Dettinger, M.P., Carrapa, B., DeCelles, P., Murray, K.E., Huntington, K.W., Cartwright, A., Canavan, R.R., Gehrels, G., Clementz, M., 2015. The growth of the central Andes, 22°S–26°S. In: Geodynamics of a Cordilleran Orogenic System: The Central Andes of Argentina and Northern Chile. Geological Society of America. https://doi.org/10.1130/2015.1212(15.
Quade, J., Leary, R., Dettinger, M., Orme, D., Krupa, A., DeCelles, P., Kano, A., Kato, H., Waldrip, R., Huang, W., 2020. Resetting Southern Tibet: The serious challenge of obtaining primary records of Paleoaltimetry. Glob. Planet. Chang. 103194 https://doi.org/10.1016/j.gloplacha.2020.103194.
Ramos, V.A., 2009. Anatomy and global context of the Andes: Main geologic features and the Andean orogenic cycle. In: Backbone of the Americas: Shallow Subduction, Plateau Uplift, and Ridge and Terrane Collision. Geological Society of America. https://doi.org/10.1130/2009.1204(02.
Rapalini, A.E., 2007. A paleomagnetic analysis of the Patagonian Orocline. Geol. Acta 5, 287–294. https://doi.org/10.1344/105.000000289.
Rapalini, A.E., Peroni, J., Luppo, T., Tassone, A., Elena Cerredo, M., Esteban, F., Lippai, H., Franciscovilas, J., 2016. Palaeomagnetism of Mesozoic magmatic bodies of the Fuegian Cordillera: implications for the formation of the Patagonian Orocline. Geol. Soc. Lond., Spec. Publ. 425, 65–80. https://doi.org/10.1144/SP425.3.
Ravikant, V., Wu, F.-Y., Ji, W.-Q., 2009. Zircon U–Pb and Hf isotopic constraints on petrogenesis of the Cretaceous–Tertiary granites in eastern Karakoram and Ladakh, India. Lithos 110, 153–166. https://doi.org/10.1016/j.lithos.2008.12.013.
Raymo, M.E., Ruddiman, W.F., 1992. Tectonic forcing of late Cenozoic climate. Nature 359, 117–122. https://doi.org/10.1038/359117a0.
Reilinger, R., McClusky, S., Vernant, P., Lawrence, S., Ergintav, S., Cakmak, R., Ozener, H., Kadirov, F., Guliev, I., Stepanyan, R., Nadariya, M., Hahubia, G., Mahmoud, S., Sakr, K., ArRajehi, A., Paradissis, D., Al-Aydrus, A., Prilepin, M., Guseva, T., Evren, E., Dmitrotsa, A., Filikov, S.V., Gomez, F., Al-Ghazzi, R., Karam, G., 2006. GPS constraints on continental deformation in the Africa-Arabia-Eurasia continental collision zone and implications for the dynamics of plate interactions. J. Geophys. Res. 111 https://doi.org/10.1029/2005JB004051.
Reiners, P.W., Brandon, M.T., 2006. Using thermochronology to understand orogenic erosion. Annu. Rev. Earth Planet. Sci. 34, 419–466. https://doi.org/10.1146/annurev.earth.34.031405.125202.
Replumaz, A., Tapponnier, P., 2003. Reconstruction of the deformed collision zone Between India and Asia by backward motion of lithospheric blocks. J. Geophys. Res. 108 https://doi.org/10.1029/2001JB000661.
Roberts, G.G., White, N., 2010. Estimating uplift rate histories from river profiles using African examples. J. Geophys. Res. Solid Earth 115. https://doi.org/10.1029/2009JB006692.
Rognon, P., Gourinard, Y., Bandet, Y., Koeniguer, J.C., Delteil-Desneux, F., 1983. Precisions chronologiques sur l'evolution volcanotectonique et geomorphologique de l'Atakor (Hoggar); apports des donnees radiometriques (K/Ar) et paleobotaniques (bois fossiles). In: Bulletin de la Societe Geologique de France S7-XXV, pp. 973–980. https://doi.org/10.2113/gssgfbull.S7-XXV.6.973.
Rohrmann, A., Kapp, P., Carrapa, B., Reiners, P.W., Guynn, J., Ding, L., Heizler, M., 2012. Thermochronologic evidence for plateau formation in central Tibet by 45 Ma. Geology 40, 187–190. https://doi.org/10.1130/G32530.1.
Roperch, P., Mégard, F., Laj, C., Mourier, T., Clube, T.M., Noblet, C., 1987. Rotated oceanic blocks in western Ecuador. Geophys. Res. Lett. 14, 558–561. https://doi.org/10.1029/GL014i005p00558.
Roperch, P., Sempere, T., Macedo, O., Arriagada, C., Fornari, M., Tapia, C., García, M., Laj, C., 2006. Counterclockwise rotation of late Eocene-Oligocene fore-arc deposits in southern Peru and its significance for oroclinal bending in the central Andes. Tectonics 25. https://doi.org/10.1029/2005TC001882 n/a-n/a.
Rougier, S., Missenard, Y., Gautheron, C., Barbarand, J., Zeyen, H., Pinna, R., Liégeois, J.-P., Bonin, B., Ouabadi, A., Derder, M.E.-M., de Lamotte, D.F., 2013. Eocene exhumation of the Tuareg Shield (Sahara Desert, Africa). Geology 41, 615–618. https://doi.org/10.1130/G33731.1.
Rowley, D.B., Currie, B.S., 2006. Palaeo-altimetry of the late Eocene to Miocene Lunpola basin, central Tibet. Nature 439, 677–681. https://doi.org/10.1038/nature04506.
Rowley, D.B., Garzione, C.N., 2007. Stable isotope-based paleoaltimetry. Annu. Rev. Earth Planet. Sci. 35, 463–508. https://doi.org/10.1146/annurev.earth.35.031306.140155.
Rowley, D.B., Pierrehumbert, R.T., Currie, B.S., 2001. A new approach to stable isotope-based paleoaltimetry: implications for paleoaltimetry and paleohypsometry of the High Himalaya since the Late Miocene. Earth Planet. Sci. Lett. 188, 253–268. https://doi.org/10.1016/S0012-821X(01)00324-7.
Royer, D.L., Berner, R.A., Montañez, I.P., Tabor, N.J., Beerling, D.J., 2004. CO2 as a primary driver of phanerozoic climate. GSA Today 14, 4–10. https://doi.org/10.1130/1052-5173(2004)014<4:CAAPDO>2.0.CO;2.
Ruiz, G.M.H., Sebti, S., Negro, F., Saddiqi, O., Frizon de Lamotte, D., Stockli, D., Foeken, J., Stuart, F., Barbarand, J., Schaer, J.-P., 2011. From central Atlantic continental rift to Neogene uplift - western Anti-Atlas (Morocco): From central Atlantic continental rift to Neogene uplift. Terra Nova 23, 35–41. https://doi.org/10.1111/j.1365-3121.2010.00980.x.
Ruiz, D., Dupont-Nivet, G., Aminov, J., Poblete, F., Van Der Linden, T., Van Hinsbergen, D., 2020. "Terra Antiqua" : a paleogeographic reconstruction plugin for QGIS (other). Oral. https://doi.org/10.5194/egusphere-egu2020-20362.
Ruiz-Villanueva, V., Mazzorana, B., Bladé, E., Bürkli, L., Iribarren-Anacona, P., Mao, L., Nakamura, F., Ravazzolo, D., Rickenmann, D., Sanz-Ramos, M., Stoffel, M., Wohl, E., 2019. Characterization of wood-laden flows in rivers: wood-laden flows. Earth Surf. Process. Landf. 44, 1694–1709. https://doi.org/10.1002/esp.4603.
Sahagian, D., Proussevitch, A., Carlson, W., 2002. Timing of Colorado Plateau uplift: Initial constraints from vesicular basalt-derived paleoelevations. Geology 30, 807–810. https://doi.org/10.1130/0091-7613(2002)030<0807:TOCPUI>2.0.CO;2.
Schepers, G., Van Hinsbergen, D.J.J., Spakman, W., Kosters, M.E., Boschman, L.M., McQuarrie, N., 2017. South-American plate advance and forced Andean trench retreat as drivers for transient flat subduction episodes. Nat. Commun. 8, 15249. https://doi.org/10.1038/ncomms15249.
Scher, H.D., Whittaker, J.M., Williams, S.E., Latimer, J.C., Kordesch, W.E., Delaney, M.L., 2015. Onset of Antarctic circumpolar current 30 million years ago as Tasmanian Gateway aligned with westerlies. Nature 523, 580–583. https://doi.org/10.1038/nature14598.
Schettino, A., Turco, E., 2006. Plate kinematics of the Western Mediterranean region during the Oligocene and Early Miocene. Geophys. J. Int. 166, 1398–1423. https://doi.org/10.1111/j.1365-246X.2006.02997.x.
Schildgen, T.F., Van Der Beek, P.A., Sinclair, H.D., Thiede, R.C., 2018. Spatial correlation bias in late-Cenozoic erosion histories derived from thermochronology. Nature 559, 89–93.
Schmid, S.M., Pfiffner, O.-A., Froitzheim, N., Schönborn, G., Kissling, E., 1996. Geophysical-geological transect and tectonic evolution of the Swiss-Italian Alps. Tectonics 15, 1036–1064. https://doi.org/10.1029/96TC00433.
Schull, T., 1988. Rift basins of interior Sudan: petroleum exploration and discovery. Bulletin 72. https://doi.org/10.1306/703C9965-1707-11D7-8645000102C1865D.
Scotese, C.R., 2001. Atlas of Earth History (PALEOMAP Project).
Scotese, C.R., Golonka, J., 1997. Paleogeographic Atlas. PALEOMAP Project. University of Texas at Arlington Arlington.
Scotese, C.R., McKerrow, W.S., 1990. Revised world maps and introduction. Geol. Soc. Lond. Mem. 12, 1–21.
Scotese, C.R., Wright, N., 2018. PALEOMAP Paleodigital Elevation Models (PaleoDEMS) for the Phanerozoic. URL: https://www. earthbyte. org/paleodem-resource-scotese-and-wright-2018.

Scotese, C.R., Gahagan, L.M., Larson, R.L., 1988. Plate tectonic reconstructions of the Cretaceous and Cenozoic ocean basins. Tectonophysics 155, 27–48.
Searle, M.P., Robb, L.J., Gardiner, N.J., 2016. Tectonic Processes and Metallogeny along the Tethyan Mountain Ranges of the Middle East and South Asia (Oman, Himalaya, Karakoram, Tibet, Myanmar, Thailand, Malaysia), 19. Society of Economic Geologists, Inc. Special Publication, pp. 301–327.
Sempere, T., Butler, R.F., Richards, D.R., Marshall, L.G., Sharp, W., Swisher, C.C., 1997. Stratigraphy and chronology of Upper Cretaceous–lower Paleogene strata in Bolivia and northwest Argentina. Geol. Soc. Am. Bull. 109, 709–727. https://doi.org/10.1130/0016-7606(1997)109<0709:SACOUC>2.3.CO;2.
SERNAGEOMIN, 2003. Mapa Geológico de Chile, Carta Geol. In: Chile, Versión Digital, No 4, scale 1:1,000,000. Serv. Nac. de Geol. y Minería, Santiago.
Seton, M., Müller, R.D., Zahirovic, S., Gaina, C., Torsvik, T., Shephard, G., Talsma, A., Gurnis, M., Turner, M., Maus, S., Chandler, M., 2012. Global continental and ocean basin reconstructions since 200Ma. Earth Sci. Rev. 113, 212–270. https://doi.org/10.1016/j.earscirev.2012.03.002.
Sewall, J.O., Sloan, L.C., 2006. Come a little bit closer: a high-resolution climate study of the early Paleogene Laramide foreland. Geology 34, 81. https://doi.org/10.1130/G22177.1.
Sewall, J.O., Sloan, L.C., Huber, M., Wing, S., 2000. Climate sensitivity to changes in land surface characteristics. Glob. Planet. Chang. 26, 445–465. https://doi.org/10.1016/S0921-8181(00)00056-4.
Shields, G.A., Mills, B.J., 2017. Tectonic controls on the long-term carbon isotope mass balance. Proc. Natl. Acad. Sci. 114, 4318–4323. https://doi.org/10.1073/pnas.1614506114.
Si, D., Ding, Y., 2013. Decadal change in the correlation pattern between the Tibetan Plateau winter snow and the East Asian summer precipitation during 1979–2011. J. Clim. 26, 7622–7634.
Silberling, N.J., Jones, D.L., Monger, J., Coney, P., 1992. Lithotectonic Terrane Map of the North American Cordillera (No. 2176). IMAP. https://doi.org/10.3133/i2176.
Silver, E.A., 1971. Tectonics of the Mendocino triple junction. Geol. Soc. Am. Bull. 82, 2965–2978. https://doi.org/10.1130/0016-7606(1971)82[2965:TOTMTJ]2.0.CO;2.
Sjostrom, D.J., Hren, M.T., Horton, T.W., Waldbauer, J.R., Chamberlain, C.P., 2006. Stable isotopic evidence for a pre–late Miocene elevation gradient in the Great Plains–Rocky Mountain region, USA. In: Tectonics, Climate, and Landscape Evolution. Geological Society of America. https://doi.org/10.1130/2006.2398(19.
Slattery, J.S., Cobban, W.A., McKinney, K.C., Harries, P.J., Sandness, A.L., 2015. Early Cretaceous to Paleocene paleogeography of the Western Interior Seaway: the interaction of eustasy and tectonism. Wyoming Geol. Assoc. Guidebook 2015, 22–60.
Sloan, L.C., Barron, E.J., 1992. A comparison of Eocene climate model results to quantified paleoclimatic interpretations. Palaeogeogr. Palaeoclimatol. Palaeoecol. 93, 183–202. https://doi.org/10.1016/0031-0182(92)90096-N.
Smellie, J.L., Pankhurst, R., Thomson, M., Davies, R., 1984. The geology of the South Shetland Islands: VI. In: Stratigraphy, Geochemistry and Evolution. Br. Antarct. Surv. Sci. Rep.
Smith, A.G., Smith, D.G., Funnell, B.M., 2004. Atlas of Mesozoic and Cenozoic coastlines. Cambridge University Press, Cambridge, United Kingdom (112 p).
Sobel, E.R., Chen, J., Schoenbohm, L.M., Thiede, R., Stockli, D.F., Sudo, M., Strecker, M. R., 2013. Oceanic-style subduction controls late Cenozoic deformation of the Northern Pamir orogen. Earth Planet. Sci. Lett. 363, 204–218. https://doi.org/10.1016/j.epsl.2012.12.009.
Solari, M.A., Hervé, F., Martinod, J., Le Roux, J.P., Ramírez, L.E., Palacios, C., 2008. Geotectonic evolution of the Bransfield Basin, Antarctic Peninsula: insights from analogue models. Antarct. Sci. 20, 185–196. https://doi.org/10.1017/S095410200800093X.
Song, B., Zhang, K., Zhang, L., Ji, J., Hong, H., Wei, Y., Xu, Y., Algeo, T.J., Wang, C., 2018. Qaidam Basin paleosols reflect climate and weathering intensity on the northeastern Tibetan Plateau during the Early Eocene Climatic Optimum. Palaeogeogr. Palaeoclimatol. Palaeoecol. 512, 6–22. https://doi.org/10.1016/j.palaeo.2018.03.027.
Spakman, W., Hall, R., 2010. Surface deformation and slab–mantle interaction during Banda arc subduction rollback. Nat. Geosci. 3, 562–566. https://doi.org/10.1038/ngeo917.
Spicer, R.A., 2018. Phytopaleoaltimetry: using plant fossils to measure past land surface elevation. In: Mountains, Climate and Biodiversity. Wiley, Oxford, pp. 95–109.
Spikings, R.A., Crowhurst, P.V., Winkler, W., Villagomez, D., 2010. Syn- and post-accretionary cooling history of the Ecuadorian Andes constrained by their in-situ and detrital thermochronometric record. J. S. Am. Earth Sci. 30, 121–133. https://doi.org/10.1016/j.jsames.2010.04.002.
Staisch, L.M., Niemi, N.A., Hong, C., Clark, M.K., Rowley, D.B., Currie, B., 2014. A Cretaceous-Eocene depositional age for the Fenghuoshan Group, Hoh Xil Basin: implications for the tectonic evolution of the northern Tibet Plateau. Tectonics 33, 281–301. https://doi.org/10.1002/2013TC003367.
Staisch, L.M., Niemi, N.A., Clark, M.K., Chang, H., 2016. Eocene to late Oligocene history of crustal shortening within the Hoh Xil Basin and implications for the uplift history of the northern Tibetan Plateau. Tectonics 35, 862–895. https://doi.org/10.1002/2015TC003972.
Stamps, D.S., Saria, E., Kreemer, C., 2018. A geodetic strain rate model for the East African rift system. Sci. Rep. 8, 732. https://doi.org/10.1038/s41598-017-19097-w.
Stephens, G.L., Li, J., Wild, M., Clayson, C.A., Loeb, N., Kato, S., L'ecuyer, T., Stackhouse, P.W., Lebsock, M., Andrews, T., 2012. An update on Earth's energy balance in light of the latest global observations. Nat. Geosci. 5, 691–696. https://doi.org/10.1038/ngeo1580.
Sternai, P., Jolivet, L., Menant, A., Gerya, T., 2014. Driving the upper plate surface deformation by slab rollback and mantle flow. Earth Planet. Sci. Lett. 405, 110–118. https://doi.org/10.1016/j.epsl.2014.08.023.
Sternai, P., Caricchi, L., Pasquero, C., Garzanti, E., Hinsbergen, D.J.J., Castelltort, S., 2020. Magmatic forcing of Cenozoic Climate? J. Geophys. Res. Solid Earth 125. https://doi.org/10.1029/2018JB016460.
Straume, E.O., Gaina, C., Medvedev, S., Nisancioglu, K.H., 2020. Global Cenozoic Paleobathymetry with a focus on the Northern Hemisphere Oceanic Gateways. Gondwana Res. 86, 126–143. https://doi.org/10.1016/j.gr.2020.05.011.
Su, T., Farnsworth, A., Spicer, R., Huang, J., Wu, F.-X., Liu, J., Li, S.-F., Xing, Y.-W., Huang, Y.-J., Deng, W.-Y.-D., 2019. No high Tibetan Plateau until the Neogene. Sci. Adv. 5 https://doi.org/10.1126/sciadv.aav2189 eaav2189.
Swezey, C.S., 2009. Cenozoic stratigraphy of the Sahara, Northern Africa. J. Afr. Earth Sci. 53, 89–121. https://doi.org/10.1016/j.jafrearsci.2008.08.001.
Tassara, A., Yáñez, G., 2003. Relación entre el espesor elástico de la litosfera y la segmentación tectónica del margen andino (15-47 S). Rev. Geol. Chile 30, 159–186. https://doi.org/10.4067/S0716-02082003000200002.
Tate, G.W., McQuarrie, N., Van Hinsbergen, D.J.J., Bakker, R.R., Harris, R., Jiang, H., 2015. Australia going down under: quantifying continental subduction during arc-continent accretion in Timor-Leste. Geosphere 11, 1860–1883. https://doi.org/10.1130/GES01144.1.
Tate, G.W., McQuarrie, N., Tiranda, H., Van Hinsbergen, D.J.J., Harris, R., Zachariasse, W.J., Fellin, M.G., Reiners, P.W., Willett, S.D., 2017. Reconciling regional continuity with local variability in structure, uplift and exhumation of the Timor orogen. Gondwana Res. 49, 364–386. https://doi.org/10.1016/j.gr.2017.06.008.
Thiéblemont, D., Liégeois, J., Fernandez-Alonso, M., Ouabadi, A., Le Gall, B., Maury, R., Jalludin, M., Vidal, M., Ouattara Gbélé, C., Tchaméni, R., 2016. Geological Map of Africa at 1: 10M scale. Geological Map. CGMW-BRGM.
Tinker, J., de Wit, M., Brown, R., 2008. Linking source and sink: evaluating the balance between onshore erosion and offshore sediment accumulation since Gondwana break-up, South Africa. Tectonophysics 455, 94–103. https://doi.org/10.1016/j.tecto.2007.11.040.
Torres, T., 1984. Nothofagoxylon antarcticus n. sp., medera fósil del Terciario de la isla Rey Jorge, Islas Shetland del Sur, Antártica. Serie Cientifica Instituto Ántartico Chileno 31, 39–52.
Torres Carbonell, P.J., Olivero, E.B., 2019. Tectonic control on the evolution of depositional systems in a fossil, marine foreland basin: example from the SE Austral Basin, Tierra del Fuego, Argentina. Mar. Pet. Geol. 104, 40–60. https://doi.org/10.1016/j.marpetgeo.2019.03.022.
Torres Carbonell, P.J., Dimieri, L.V., Olivero, E.B., Bohoyo, F., Galindo-Zaldívar, J., 2014. Structure and tectonic evolution of the Fuegian Andes (southernmost South America) in the framework of the Scotia Arc development. Glob. Planet. Chang. 123, 174–188. https://doi.org/10.1016/j.gloplacha.2014.07.019.
Torres Carbonell, P.J., Guzmán, C., Yagupsky, D., Dimieri, L.V., 2016. Tectonic models for the Patagonian orogenic curve (southernmost Andes): an appraisal based on analog experiments from the Fuegian thrust–fold belt. Tectonophysics 671, 76–94. https://doi.org/10.1016/j.tecto.2016.01.020.
Torres García, M.F., Calderón, M., Ramírez de Arellano, C., Hervé, F., Opitz, J., Theye, T., Fanning, C.M., Pankhurst, R.J., González-Guillot, M., Fuentes, F., Babinski, M., 2020. Trace element composition of amphibole and petrogenesis of hornblendites and plutonic suites of Cretaceous magmatic arcs developed in the Fuegian Andes, southernmost South America. Lithos 372–373, 105656. https://doi.org/10.1016/j.lithos.2020.105656.
Torsvik, T.H., Müller, R.D., Van Der Voo, R., Steinberger, B., Gaina, C., 2008. Global plate motion frames: toward a unified model. Rev. Geophys. 46, RG3004 https://doi.org/10.1029/2007RG000227.
Torsvik, T.H., Van Der Voo, R., Preeden, U., Mac Niocaill, C., Steinberger, B., Doubrovine, P.V., Van Hinsbergen, D.J.J., Domeier, M., Gaina, C., Tohver, E., Meert, J.G., McCausland, P.J.A., Cocks, L.R.M., 2012. Phanerozoic polar wander, palaeogeography and dynamics. Earth Sci. Rev. 114, 325–368. https://doi.org/10.1016/j.earscirev.2012.06.007.
Trenberth, K.E., Fasullo, J.T., Kiehl, J., 2009. Earth's global energy budget. Bull. Amer. Meteor. Soc. 90, 311–324. https://doi.org/10.1175/2008BAMS2634.1.
Trumbull, R.B., Riller, U., Oncken, O., Scheuber, E., Munier, K., Hongn, F., 2006. The time-space distribution of Cenozoic Volcanism in the South-Central Andes: A new data compilation and some tectonic implications. In: Oncken, O., Chong, G., Franz, G., Giese, P., Götze, H.-J., Ramos, V.A., Strecker, M.R., Wigger, P. (Eds.), The Andes, Frontiers in Earth Sciences. Springer, Berlin Heidelberg, pp. 29–43. https://doi.org/10.1007/978-3-540-48684-8_2.
Umhoefer, P.J., 1987. Northward translation of "BAJA British Columbia" along the Late Cretaceous to Paleocene margin of western North America. Tectonics 6, 377–394. https://doi.org/10.1029/TC006i004p00377.
Underwood, C.J., King, C., Steurbaut, E., 2013. Eocene initiation of Nile drainage due to East African uplift. Palaeogeogr. Palaeoclimatol. Palaeoecol. 392, 138–145. https://doi.org/10.1016/j.palaeo.2013.09.014.
Utescher, T., Bruch, A., Erdei, B., François, L., Ivanov, D., Jacques, F., Kern, A., Mosbrugger, V., Spicer, R., 2014. The Coexistence Approach—theoretical background and practical considerations of using plant fossils for climate quantification. Palaeogeogr. Palaeoclimatol. Palaeoecol. 410, 58–73. https://doi.org/10.1016/j.palaeo.2014.05.031.
Vaes, B., Van Hinsbergen, D.J.J., Boschman, L.M., 2019. Reconstruction of subduction and back-arc spreading in the NW Pacific and Aleutian Basin: clues to causes of Cretaceous and Eocene Plate Reorganizations. Tectonics 38, 1367–1413. https://doi.org/10.1029/2018TC005164.
Van de Lagemaat, S.H.A., Van Hinsbergen, D.J.J., Boschman, L.M., Kamp, P.J.J., Spakman, W., 2018. Southwest pacific absolute plate kinematic reconstruction reveals major Cenozoic Tonga-Kermadec slab dragging. Tectonics 37, 2647–2674, 10.1029/2017TC004901.

Van Der Beek, P., Van Melle, J., Guillot, S., Pêcher, A., Reiners, P.W., Nicolescu, S., Latif, M., 2009. Eocene Tibetan plateau remnants preserved in the northwest Himalaya. Nat. Geosci. 2, 364–368. https://doi.org/10.1038/ngeo503.

Van Der Linden, T., Dupont-Nivet, G., Van Hinsbergen, D., 2020. Towards a quantitative paleogeography calculator (other). Oral. https://doi.org/10.5194/egusphere-egu2020-2402.

Van Der Meer, D.G., Spakman, W., Van Hinsbergen, D.J.J., Amaru, M.L., Torsvik, T.H., 2010. Towards absolute plate motions constrained by lower-mantle slab remnants. Nat. Geosci. 3, 36–40. https://doi.org/10.1038/ngeo708.

Van Der Meer, D.G., Zeebe, R.E., Van Hinsbergen, D.J., Sluijs, A., Spakman, W., Torsvik, T.H., 2014. Plate tectonic controls on atmospheric CO2 levels since the Triassic. Proc. Natl. Acad. Sci. 111, 4380–4385. https://doi.org/10.1073/pnas.1315657111.

Van Hinsbergen, D.J.J., Schmid, S.M., 2012. Map view restoration of Aegean-West Anatolian accretion and extension since the Eocene. Tectonics 31. https://doi.org/10.1029/2012TC003132 n/a-n/a.

Van Hinsbergen, D.J.J., Kapp, P., Dupont-Nivet, G., Lippert, P.C., DeCelles, P.G., Torsvik, T.H., 2011. Restoration of Cenozoic deformation in Asia and the size of Greater India. Tectonics 30. https://doi.org/10.1029/2011TC002908 n/a-n/a.

Van Hinsbergen, D.J.J., Lippert, P.C., Dupont-Nivet, G., McQuarrie, N., Doubrovine, P.V., Spakman, W., Torsvik, T.H., 2012. Greater India Basin hypothesis and a two-stage Cenozoic collision between India and Asia. Proc. Natl. Acad. Sci. 109, 7659–7664. https://doi.org/10.1073/pnas.1117262109.

Van Hinsbergen, D.J.J., Vissers, R.L.M., Spakman, W., 2014. Origin and consequences of western Mediterranean subduction, rollback, and slab segmentation: western Mediterranean subduction. Tectonics 33, 393–419. https://doi.org/10.1002/2013TC003349.

Van Hinsbergen, D.J.J., Cunningham, D., Straathof, G.B., Ganerød, M., Hendriks, B.W.H., Dijkstra, A.H., 2015a. Triassic to Cenozoic multi-stage intra-plate deformation focused near the Bogd Fault system, Gobi Altai, Mongolia. Geosci. Front. 6, 723–740. https://doi.org/10.1016/j.gsf.2014.12.002.

Van Hinsbergen, D.J.J., de Groot, L.V., Van Schaik, S.J., Spakman, W., Bijl, P.K., Sluijs, A., Langereis, C.G., Brinkhuis, H., 2015b. A paleolatitude calculator for paleoclimate studies. PLoS One 10. https://doi.org/10.5281/zenodo.16166.

Van Hinsbergen, D.J.J., Lippert, P.C., Li, S., Huang, W., Advokaat, E.L., Spakman, W., 2019. Reconstructing Greater India: paleogeographic, kinematic, and geodynamic perspectives. Tectonophysics 760, 69–94. https://doi.org/10.1016/j.tecto.2018.04.006.

Van Hinsbergen, D.J., Torsvik, T.H., Schmid, S.M., Maţenco, L.C., Maffione, M., Vissers, R.L., Gürer, D., Spakman, W., 2020. Orogenic architecture of the Mediterranean region and kinematic reconstruction of its tectonic evolution since the Triassic. Gondwana Res. 81, 79–229. https://doi.org/10.1016/j.gr.2019.07.009.

Villagómez, D., Spikings, R., 2013. Thermochronology and tectonics of the Central and Western Cordilleras of Colombia: early Cretaceous–Tertiary evolution of the Northern Andes. Lithos 160–161, 228–249. https://doi.org/10.1016/j.lithos.2012.12.008.

Vissers, R.L.M., Meijer, P.Th., 2012. Iberian plate kinematics and Alpine collision in the Pyrenees. Earth Sci. Rev. 114, 61–83. https://doi.org/10.1016/j.earscirev.2012.05.001.

Volkmer, J.E., Kapp, P., Horton, B.K., Gehrels, G.E., Minervini, J.M., Ding, L., 2014. Northern Lhasa thrust belt of central Tibet: Evidence of Cretaceous–early Cenozoic shortening within a passive roof thrust system?. In: Toward an Improved Understanding of Uplift Mechanisms and the Elevation History of the Tibetan Plateau. Geological Society of America. https://doi.org/10.1130/2014.2507(03.

Wang, C., Zhao, X., Liu, Z., Lippert, P.C., Graham, S.A., Coe, R.S., Yi, H., Zhu, L., Liu, S., Li, Y., 2008. Constraints on the early uplift history of the Tibetan Plateau. PNAS 105, 4987–4992. https://doi.org/10.1073/pnas.0703595105.

Wang, Y., Xu, Y., Khawaja, S., Passey, B.H., Zhang, C., Wang, X., Li, Q., Tseng, Z.J., Takeuchi, G.T., Deng, T., Xie, G., 2013. Diet and environment of a mid-Pliocene fauna from southwestern Himalaya: Paleo-elevation implications. Earth Planet. Sci. Lett. 376, 43–53. https://doi.org/10.1016/j.epsl.2013.06.014.

Wang, C., Dai, J., Zhao, X., Li, Y., Graham, S.A., He, D., Ran, B., Meng, J., 2014. Outward-growth of the Tibetan Plateau during the Cenozoic: a review. Tectonophysics 621, 1–43. https://doi.org/10.1016/j.tecto.2014.01.036.

Wang, F., Shi, W., Zhang, W., Wu, L., Yang, L., Wang, Y., Zhu, R., 2017. Differential growth of the northern Tibetan margin: evidence for oblique stepwise rise of the Tibetan Plateau. Sci. Rep. 7, 1–9. https://doi.org/10.1038/srep41164.

Wegener, A., 1929. The origin of continents and oceans, 4th ed. Dover Publications, New York.

Weissel, J.K., Karner, G.D., 1989. Flexural uplift of rift flanks due to mechanical unloading of the lithosphere during extension. J. Geophys. Res. Solid Earth 94, 13919–13950, 10.1029/JB094iB10p13919.

Wen, D., Liu, D., Chung, S., Chu, M., Ji, J., Zhang, Q., Song, B., Lee, T., Yeh, M., Lo, C., 2008. Zircon SHRIMP U–Pb ages of the Gangdese Batholith and implications for Neotethyan subduction in southern Tibet. Chem. Geol. 252, 191–201. https://doi.org/10.1016/j.chemgeo.2008.03.003.

Wessel, P., Smith, W.H.F., Scharroo, R., Luis, J., Wobbe, F., 2013. Generic mapping tools: improved version released. Eos Trans. AGU 94, 409–410. https://doi.org/10.1002/2013EO450001.

Westerweel, J., Roperch, P., Licht, A., Dupont-Nivet, G., Win, Z., Poblete, F., Ruffet, G., Swe, H.H., Thi, M.K., Aung, D.W., 2019. Burma Terrane part of the Trans-Tethyan arc during collision with India according to palaeomagnetic data. Nat. Geosci. 12, 863–868. https://doi.org/10.1038/s41561-019-0443-2.

Wheeler, L.B., Galewsky, J., Herold, N., Huber, M., 2016. Late Cenozoic surface uplift of the southern Sierra Nevada (California, USA): a paleoclimate perspective on lee-side stable isotope paleoaltimetry. Geology 44, 451–454. https://doi.org/10.1130/G37718.1.

Wildman, M., Brown, R., Persano, C., Beucher, R., Stuart, F.M., Mackintosh, V., Gallagher, K., Schwanethal, J., Carter, A., 2017. Contrasting Mesozoic evolution across the boundary between on and off craton regions of the South African plateau inferred from apatite fission track and (U-Th-Sm)/He thermochronology: mesozoic Evolution of Southern Africa. J. Geophys. Res. Solid Earth 122, 1517–1547. https://doi.org/10.1002/2016JB013478.

Williams, S.E., Whittaker, J.M., Halpin, J.A., Müller, R.D., 2019. Australian-Antarctic breakup and seafloor spreading: balancing geological and geophysical constraints. Earth Sci. Rev. 188, 41–58. https://doi.org/10.1016/j.earscirev.2018.10.011.

Wilson, D.S., Luyendyk, B.P., 2009. West Antarctic paleotopography estimated at the Eocene-Oligocene climate transition. Geophys. Res. Lett. 36, L16302 https://doi.org/10.1029/2009GL039297.

Wilson, D.S., Jamieson, S.S.R., Barrett, P.J., Leitchenkov, G., Gohl, K., Larter, R.D., 2012. Antarctic topography at the Eocene–Oligocene boundary. Palaeogeogr. Palaeoclimatol. Palaeoecol. 335–336, 24–34. https://doi.org/10.1016/j.palaeo.2011.05.028.

Xu, Q., Ding, L., Spicer, R.A., Liu, X., Li, S., Wang, H., 2018. Stable isotopes reveal southward growth of the Himalayan-Tibetan Plateau since the Paleocene. Gondwana Res. 54, 50–61. https://doi.org/10.1016/j.gr.2017.10.005.

Ye, J., Chardon, D., Rouby, D., Guillocheau, F., Dall'asta, M., Ferry, J.-N., Broucke, O., 2017. Paleogeographic and structural evolution of northwestern Africa and its Atlantic margins since the early Mesozoic. Geosphere 13, 1254–1284. https://doi.org/10.1130/GES01426.1.

Yin, A., Harrison, T.M., 2000. Geologic evolution of the Himalayan-Tibetan Orogen. Annu. Rev. Earth Planet. Sci. 28, 211–280. https://doi.org/10.1146/annurev.earth.28.1.211.

Yuan, X., Braun, J., Guerit, L., Simon, B., Bovy, B., Rouby, D., Robin, C., Jiao, R., 2019. Linking continental erosion to marine sediment transport and deposition: A new implicit and O (N) method for inverse analysis. Earth Planet. Sci. Lett. 524, 115728. https://doi.org/10.1016/j.epsl.2019.115728.

Zachos, J., Kump, L., 2005. Carbon cycle feedbacks and the initiation of Antarctic glaciation in the earliest Oligocene. Glob. Planet. Chang. 47, 51–66. https://doi.org/10.1016/j.gloplacha.2005.01.001.

Zachos, J., Pagani, M., Sloan, L., Thomas, E., Billups, K., 2001. Trends, rhythms, and aberrations in global climate 65 Ma to present. Science 292, 686–693. https://doi.org/10.1126/science.1059412.

Zattin, M., Talarico, F.M., Sandroni, S., 2010. Integrated provenance and detrital thermochronology studies on the ANDRILL AND-2A drill core: Late Oligocene-Early Miocene exhumation of the Transantarctic Mountains (southern Victoria Land, Antarctica): Provenance and thermochronology on the AND-2A drill core. Terra Nova 22, 361–368. https://doi.org/10.1111/j.1365-3121.2010.00958.x.

Zattin, M., Pace, D., Andreucci, B., Rossetti, F., Talarico, F.M., 2014. Cenozoic erosion of the Transantarctic Mountains: a source-to-sink thermochronological study. Tectonophysics 630, 158–165. https://doi.org/10.1016/j.tecto.2014.05.022.

Zhu, D.-C., Zhao, Z.-D., Niu, Y., Mo, X.-X., Chung, S.-L., Hou, Z.-Q., Wang, L.-Q., Wu, F.-Y., 2011. The Lhasa Terrane: record of a microcontinent and its histories of drift and growth. Earth Planet. Sci. Lett. 301, 241–255. https://doi.org/10.1016/j.epsl.2010.11.005.

Ziegler, P., 1987. Late Cretaceous and Cenozoic intra-plate compressional deformations in the Alpine foreland—a geodynamic model. Tectonophysics 137, 389–420. https://doi.org/10.1016/0040-1951(87)90330-1.

Ziegler, A., Rowley, D.B., Lottes, A.L., Sahagian, D.L., Hulver, M.L., Gierlowski, T.C., 1985. Paleogeographic interpretation: with an example from the mid-Cretaceous. Annu. Rev. Earth Planet. Sci. 13, 385–428. https://doi.org/10.1146/annurev.ea.13.050185.002125.

Zuza, A.V., Cheng, X., Yin, A., 2016. Testing models of Tibetan Plateau formation with Cenozoic shortening estimates across the Qilian Shan–Nan Shan thrust belt. Geosphere 12, 501–532. https://doi.org/10.1130/GES01254.1.